UTS UNIVERSITY OF TECHNOLOGY SYDNEY

Modelling and Simulation of Multiple Galloping Quadrupedal Dynamics

by Md Imam Hossain

Thesis submitted in fulfilment of the requirements for the degree of

Master of Engineering (Research)

under the supervision of David Eager and Paul David Walker

University of Technology Sydney
Faculty of Engineering and IT

February 2020

Project Title
Modelling and simulation of multiple galloping quadrupedal dynamics

Student
Md Imam Hossain
Email: MDImam.Hossain@uts.edu.au

Supervisor
Professor David Eager
Email: David.Eager@uts.edu.au

Co-Supervisor
Dr Paul Walker
Email: Paul.Walker@uts.edu.au

Address
School of Mechanical and Mechatronic Engineering
University of Technology Sydney, 81 Broadway, Ultimo NSW 2007, Australia

Certificate of originality

This is to confirm that to the best of my knowledge and belief, the content of this dissertation is my work and has not been previously submitted for a degree, nor it has been submitted as a part of the requirements for another degree.

I hereby declare that the material of this thesis is the product of my own work, except where appropriately referenced. I certify that all information sources and literature are properly quoted in the thesis.

Finally, this research is supported by the Australian Government Research Training Program.

Signature of Student:

Production Note:
Signature removed prior to publication.

Date: 24-07-2020

ABSTRACT

MODELLING AND SIMULATION OF MULTIPLE GALLOPING QUADRUPEDAL DYNAMICS

by

Md Imam Hossain

The work presented in this dissertation is comprised of three distinct parts. Namely data modelling and analysis for galloping quadruped dynamics, numerically modelling race track path design, and numerically simulating multiple galloping quadrupeds race dynamics. Fundamentally, all the parts are interlinked to one another at the level of searching for dynamics stability of galloping quadrupeds. A holistic approach was taken for information synthesising, ranging from data acquisition to modelling and simulation. The dissertation presents an overview of the current progress in the field, approaches the problem by linking information from modelling, then derives numerical solutions to come to conclusions.

Data modelling demonstrated greyhound galloping gait performance and existing race track design conditions. The techniques utilised for data gathering and analysis allowed effective retrieval of diverse information. Racing greyhound galloping gait performance was verified including speed, acceleration, yaw rate, stride frequency, stride length and paw dynamics. Also, reviewing of existing tracks revealed track designs limitations.

Data modelling showed that trajectory dynamics could significantly influence race dynamics stability. Thus, methods were derived for modelling and designing galloping greyhound ideal path trajectory between a straight and curve track path segments. To do this, clothoid and algebraic curved segments were numerically generated using a sequential vector transformation method that allows the inclusion of greyhound kinematic parameters. And an equation was derived to model suitable clothoid segments which represents greyhound kinematic parameters and boundary conditions of a track. Finally, results from race data modelling and past injury data are also provided to support transition curve segments improving the dynamics and safety of racing greyhounds while reducing injuries.

A race simulation platform was created which emulates greyhound racing. The race simulation explained various aspects of race dynamics affecting overall dynamical outcomes. Results were derived for yaw rate, speed, and the congestion pattern through numerical modelling race simulations. The simulation results presented are also correlated to actual race data to validate modelling performance and reliability. The fundamental tasks carried out include the development of a numerical model for greyhound veering and race-related supporting models. The results from race simu-

lations showed circumstances causing unstable conditions and relationships between various race factors.

Finally, this project is useful as it is being applied to optimising quadrupeds racing track design. It could also be used in various other fields such as analysing and numerical modelling and simulation of games, animations and multi-body dynamical physical systems.

This dissertation was supervised by Professor David Eager and Dr Paul Walker within the School of Mechanical and Mechatronic Engineering.

Keywords: Quadruped Racing, Quadruped Kinematics, Galloping Dynamics, Numerical Simulation, Numerical Modelling, Rigid Body Dynamics, Path Smoothing, Injury Prevention, Animal Welfare.

Dedication

To my parents Hajji Md Hossain (late) and Hajji Salma Begum. I remember my dad always used to call me Mr. engineer whenever he could and buy different hardware to play with. Once he bought me a small dynamo from a shipyard after seeing I was very much involved in knowing electrical power generation from motors. He very much encouraged me to get into engineering from a very early age. Essentially, he created a passion for engineering in me. My mom always pushed me to study and she would always remind me of studying for learning different subject matters which I can apply rather than just passing and completing courses from the school with a high grade. So, I used to do things like reading books from science subjects outside of my school syllabus. I am grateful to have both of them in my life.

Acknowledgements

Special thanks to my supervisors Professor David Eager and Dr Paul Walker, for introducing and allowing me to work on this project. I sincerely appreciate how Professor David Eager and Dr Paul Walker graciously answered an endless stream of questions and given me all kinds of directions while working on this project. I also would like to take the opportunity to express my deepest gratitude toward Professor David Eager to provide me with sound advice, brilliant insights and encouragement throughout my candidature, which fostered my development in numerous dynamical aspects. Furthermore, his knowledge, engineering attitude and research ethics encouraged me to work consistently towards my research goals.

Many thanks go to the great team of people at Greyhound Research UTS team for their outstanding help and collaboration with data and race injury insights during my candidature period.

I also wish to gratefully acknowledge the financial support from the University of Technology, Sydney (UTS).

Finally, I would like to thank my parents, my siblings, and my friends, for their tremendous support throughout my research.

Md Imam Hossain
Sydney, Australia, 2020

Journals, conferences and reports

The contents of this thesis are based on the following papers and reports which have been published, or accepted to peer-reviewed journals, conferences, and the industry as well as institutional repositories.

Journal publications

J-1. **Hossain, M.I.**, Eager, D. and Walker, P. (2020). Greyhound racing ideal trajectory path generation for straight to bend based on jerk rate minimization. Scientific Reports.

Conference papers

C-1. **Hossain, M.I.**, Eager, D. and Walker, P. (2019). Simulation of racing greyhound kinematics. In Proceedings of the 9th International Conference on Simulation and Modeling Methodologies, Technologies and Applications, pages 47–56. SCITEPRESS-Science and Technology Publications.

C-2. Mahdavi, F., **Hossain, M.I.**, Hayati, H., Eager, D. and Kennedy, P. (2018). Track shape, resulting dynamics and injury rates ofgreyhounds. In ASME 2018 International Mechanical Engineering Congress and Exposition. American Society of Mechanical Engineers Digital Collection.

Industry reports

R-1. Eager, D. and **Hossain, M.I.** (2019). Traralgon: Preliminary review of the track path dynamics for 60 m 1-turn, 57 m 2-turn and 70 m 1-turn designs.

R-2. Eager, D. and **Hossain, M.I.** (2019). Design analysis for the proposed Goulbourn track (drawing no. 5143).

R-3. Eager, D. and **Hossain, M.I.** (2019). Cranbourne: Preliminary review of the path dynamics for a 57 m 1-turn and 2-turn track designs.

R-4. Eager, D. and **Hossain, M.I.** (2018). Mt. Gambier track design analysis of drawing 5135 (UTS2018-0003).

R-5. Eager, D. and **Hossain, M.I.** (2018). Grafton track analysis.

R-6. Eager, D. and **Hossain, M.I.** (2018). Cranbourne track comparison.

R-7. Eager, D., Hayati, H., Mahdavi, F., **Hossain, M.I.**, Stephenson, R. and Thomas, N. (2018). Identifying optimal greyhound track design for greyhound safety and welfare Phase II – Progress Report 1 January 2016 to 31 December 2017. Retrieved from Sydney: https://opus.lib.uts.edu.au/handle/10453/126775

R-8. **Hossain, M.I.** and Eager, D. (2018). Wentworth park track review.

R-9. Eager, D., Mahdavi, F. and **Hossain, M.I.** (2018). The Meadows new start distance analysis report.

R-10. Eager, D., Hayati, H. and **Hossain, M.I.** (2018). Mt Gambier track injury analysis and preliminary design report.

R-11. Eager, D. and **Hossain, M.I.** (2017). The Gardens track starting boxes alignment analysis.

R-12. Eager, D., Hayati, H. and **Hossain, M.I.** (2017). A preliminary investigation into the Cranbourne Track for GRV.

R-13. Eager, D. and **Hossain, M.I.** (2017). Alternative track designs for Tweed Heads (options A – D). Retrieved from Sydney: https://opus.lib.uts.edu.au/handle/10453/121928

R-14. Eager, D., Hayati, H. and **Hossain, M.I.** (2017). Identifying optimal greyhound track design for greyhound safety and welfare Phase I Report Jan 2016 to 31 Dec 2016. Retrieved from Sydney: https://opus.lib.uts.edu.au/handle/10453/136854

R-15. **Hossain, M.I.**, Hayati, H. and Eager, D. (2016). A comparison of the track shape for Wentworth Park and proposed Murray Bridge. Retrieved from Sydney: https://opus.lib.uts.edu.au/handle/10453/122021

Contents

List of figures

List of tables

Abbreviations

2D	two-dimensional
3D	three-dimensional
AOA	angle of attack
CAD	computer aided design
CBF	callback function
CF	centrifugal force
CJ	centrifugal acceleration jerk
CG	centre of gravity
CS	continuous simulation
CSV	comma-separated values
DES	discrete-event simulation
DFT	discrete Fourier transform
DTS	deterministic simulation
EM	Euler method
FDM	finite difference method
fps	frames per second
GR	greyhound racing
GRNSW	Greyhound Racing New South Wales
GRS	greyhound racing sport
GRV	Greyhound Racing Victoria
HFR	high frame rate
IMU	inertial measurement unit
LRP	lure rail path
ML	machine learning
OOP	object-oriented programming
PY	Python programming language
RLT	real-time location tracking
ROC	rate of change
ROR	Rate of rotation
SD	survey data
SP	superposition principle
SCS	stochastic simulation

TM	transformation matrix
UML	unified modeling language
UTS	University of Technology Sydney

Nomenclature

Units

km	kilometer
mm	millimeter
m	meter
s	second
N	Newton
kg	kilogram
g	g-force
Hz	Hertz
rad	radian
deg	degree

Chapter 1

Introduction

1.1 Background

In November 2015 Greyhound Racing New South Wales (GRNSW) established a working group to investigate, develop and provide recommendations on achieving strategic direction for greyhound racing in New South Wales. An outcome of this was for GRNSW to support research into the optimisation of greyhound track design.

On the 4^{th} of April 2016, the University of Technology Sydney (UTS) entered into a 12 months contract with GRNSW to provide research and technical support through reports on optimum track design. This resulted in the formation of a research team at UTS lead by Professor David Eager. I was appointed as a Graduate Engineer by UTS to conduct technical activities for greyhound race simulation and modelling tasks which provided a unique window and opportunity to be involved with something that had real-world applications to science and engineering. There were two significant aspects considered to be vital for the UTS greyhound racing research, incidents and injury hazards at the tracks, and animal biomechanics research. Both aspects required a scientific approach to problem-solving, including modelling and simulation of greyhound racing dynamics.

Injury in the sports industry is an important consideration for many parties. This causes significant damages to the people who are involved directly or indirectly. The design of dynamically safe racing tracks for fast quadrupeds like greyhounds is paramount as this would allow the industry to move forward. Furthermore, in recent times the quadrupeds racing industry skyrocketed in terms of industry reach and

workforce. This brings up the need for an urgent reworking of the race safety factors and their classifications. Which in turn makes injury prevention more relevant within the industry. Now, there is a growing interest in the racing industry to resolve and minimise race-related injuries. Researchers indicated that racing injuries could be controlled or minimised to some extent by solely making alternations in racing environments despite various external factors. However, it was found that existing literature lacks a direct focus on what the industry is aiming to reach. This research provides simulation, modelling techniques and results for galloping quadrupeds to optimise various track design and racing parameters, with the aim of aiding the construction of dynamically safe racing specifications.

In animal locomotion, the gallop is the gait deployed by fast quadrupeds. Galloping quadrupeds such as cheetahs and greyhounds can travel with a maximum speed averaging above 70 km/h on land. The dynamics of these quadrupeds contain valuable information that is highly regarded in the various engineering fields, including bio-inspired engineering and bio-mechanics because of locomotion efficiency and cost of transport. A better understanding of the dynamics exhibited by these quadrupeds would help many parties including industries that rely on quadrupeds such as greyhound and horse racing industries in the United States, United Kingdom, France, Italy, Czech Republic, Japan, Hong Kong, United Arab Emirates, Australia, New Zealand and Ireland. On the other hand, a dynamically optimum race track design for fast quadrupeds such as greyhounds would provide a solid ground and verification platform for proving fast quadrupeds' dynamics.

Fastest moving quadrupeds such as greyhounds and cheetahs deploy a gait mechanism known as rotatory gallop which has unique dynamics of its own. While greyhounds gallop inside a race track, understanding galloping dynamics at various track points becomes vital for creating a safe racing environment for the greyhounds. As a result, the potential of a greyhound getting injured at the race track increases

significantly if the hazardous dynamical conditions of greyhounds are not considered while designing racing tracks as well as racing elements. To set the boundaries of what racing environment is acceptable to fast quadrupeds such as greyhound, first various dynamics exerted by the racing greyhounds need to be fully understood. This can be done by looking into existing studies on quadrupedal dynamics and track design factors and fusing these factors to generate relationships with the feedbacks from actual race incidents data as well as modelling and simulations of various parameters to arrive at a refined solution.

Limited studies have been conducted in the past strongly relating to galloping quadrupeds dynamics, especially in the area of canine and equine kinematics and dynamics analysis of race injuries causes. There are also studies from fields such as motorsports, which emphasises finding an optimum racing line for a given track which would minimise lap time, discomfort and exertion for the drivers. These studies shed some light on the mechanism of dynamics employed by quadrupeds and their limits. However, existing studies lack focus on race track dynamical performance for fast quadrupeds as well as the design of dynamically optimum race track based on rigid-body, multi-body, and analytical dynamics variables other than statistical methods. Besides, existing studies can not establish a relationship between different dynamics variables performance of quadrupeds such as centrifugal acceleration, horizontal acceleration, turn radius, heading turn and leaning rate, race surface reaction force to injury rates of quadrupeds.

1.2 Research project motivation and aim

The principal objective of this research was to analyse, model, and simulate race track geometric and race operating conditions to verify whether these conditions improve the dynamics stability of quadrupeds racing subjects. The prime motivation of this research was to explore new knowledge and meet the criterion set by the

industry moving forward. The secondary purpose and incentive of this research was the application of knowledge from various disciplines to solve track design and race-related dynamics problems which are existing in the industry. Below are the main requirements for the research as set by the aims and objectives.

1.2.1 Introduction of safe application practices

It was one of the primary industry goals to benefit from safe practices within the industry as there are no verified or standardised guidelines to conduct safe racing which reduces racing greyhound hazards to the minimum. Specifically, race track designs and race operating conditions and factors need special attention and care. Moreover, there are discussion and concern in the literature about the safety and welfare of racing greyhounds and other galloping quadrupeds. This is because galloping quadrupeds racing at the tracks was not well explored and understood in terms of applications. The biomechanics of galloping quadrupeds is different from other racing subjects such as a racing car that has well-round development practices. This provided an outstanding opportunity to inquire about the biomechanics of galloping quadrupeds such as greyhound for arriving at safe track design and racing operating conditions practices.

1.2.2 Understanding quadruped biomechanics

Biomechanics present in animal locomotion is gradually becoming an essential area of scientific discoveries and applications. As robots are becoming more inexpensive to manufacture and build with the widespread availability of sensors and actuators, investigation of the natural dynamics of animals is of enormous interest among researchers for providing optimal solutions. One such research area which is finding its way in robotic research is identifying ideal controllers for robot actuator which would perform specific tasks more efficiently. However, without a proper in-depth understanding of the requirement dynamics as found in animals' gaits and locomo-

tion deriving such controllers are somewhat complicated. Plenty of research has been done on quadrupeds' locomotion as quadrupedal robots provide decent trade-offs between speed and balancing. Furthermore, current researches are still trying to solve a quadrupedal gait known as galloping as this gait has essential details of fast and cost-effective terrain navigation where the terrain is not flat or has regular geometry. Likewise, only a small number of animal species are capable of maintaining a fast speed phase exceeding 65 km/h while having unique locomotion such as galloping gait. Consequently, this research aimed to shed more light on galloping biomechanics dynamic properties which would validate fast quadruped dynamics as evolved in nature for various application fields.

1.3 Scope of Thesis

The scope of this thesis was pertinent to the application and collaboration of data from various fields, such as biomechanics, civil design, and computer simulation and modelling science. The development in these areas aids formulating a direct relationship between quadrupeds' dynamics and racing track design and racing variables.

1.3.1 Areas that are addressed

The following areas are within the scope of this thesis:

- Analysing and relating to galloping quadruped's rigid-body dynamics factors such as speed, acceleration, and forces affecting race incidents
- Identifying track geometric properties best suitable for galloping quadruped dynamic optimisations of the mass center
- Development of numerical and mathematical models necessary for analysing and optimising racing dynamics outcomes of quadrupeds' mass centres motions
- Providing quadruped track design and dynamic operating recommendations

- Analysing galloping quadruped's rigid-body dynamics conditions at the existing tracks

1.3.2 Areas that are not addressed

The following areas are beyond the scope of this thesis:

- Analysing and relating track surface effects on the galloping quadrupeds gait dynamics performance
- Modelling and analysing galloping gait multi-body mechanism functioning
- Analysis, simulation, and modelling of non-dynamical variables affecting racing outcomes such as quadruped psychology, training, breeding, racing history, etc

1.4 Thesis contributions to the body of knowledge

This research has various levels of contributions relating to objective track design requirements for galloping quadrupeds and their dynamics. A large body of work from this research tried to identify, confirm, and validate variables related to racing dynamics and corresponding results. Furthermore, a review of existing track design geometric features can be found in this dissertation.

1.4.1 Identifying non-optimal track design and racing variables

An optimum track design is something which is tailored for certain circumstances and produces expected results under various given situations. The first step into optimising track designs is confirming and locating the variables which need to be included in the design considerations. Not only that, while searching for the variables to be optimised, it is important that they are compatible with the goals of the design. Likewise, optimising variables of interest should be measurable and accountable

for certain outcomes while meeting the design aims. This research started with a focus of identifying major factors affecting galloping quadruped dynamics at the tracks, which in result pointed to the various track design factors requiring analysing and modelling. However, it was evident from observations and race injury data that solely modelling track geometric features were not enough to optimise race dynamics conditions. It made sense that there could be issues which can be only learned by simulating galloping quadrupeds motions at the tracks. The simulation of racing showed that race dynamic variables outside of the track design variables were affecting racing conditions as well. By comparing the effects of race simulation variables to actual race dynamics, the non-optimal track design and racing variables were identified.

1.4.2 Methods and techniques to measure the effects and design of the geometrically safe racing track

This research involved utilising information from real-world data which was not a smooth fit for analysing and producing results. Data that was available was not directly applicable and sufficient to model various dynamic aspects occurring at the tracks. Various layers of abstractions were necessary to predict the race dynamics causes as well as use the data available in the most efficient manner. There were missing links in the available field data as well as noises in the data which lead to a numeric approach to problem-solving. Moreover, the research required multi-variable scenarios investigations where each variable is independent of one another. Consequently, the research needed creating and the usage of numerical modelling and simulation methodologies besides only analytical approaches to derive the results. Numerical techniques are vast in numbers and frequently used in real-world designs and applications where this research showed the application of numerical development for generating outputs from the real-world data.

1.5 Methodologies

In the initial stage of this research, rigorous investigations took place into the research area, which allowed the definition of the exact questions that needed to be answered by the research. Besides, this research went through many phases like requirements analysis, setting acceptable thresholds for modelling and simulation, and creating performance evaluation models. However, most of these phases needed validation and verification from further research activities. By defining an appropriate framework at every level, the scope of the research was bounded to specific task groups.

Figure 1.1 portrays the fundamental working model of this research where it shows various levels of activities and flow of information from one level to the other. It was necessary to retrieve diverse data from both the literature and from the race events and environments, as indicated in the data acquisition stage. Data retrieval of quadruped galloping occurred in the form of injury records and dynamics data collections. Injury records of galloping quadrupeds at the tracks provided strong evidence of dynamics instabilities which were existing during the races. Data acquisition was followed up by information extraction for galloping quadruped physics understanding and validation through solving kinematics and kinetics equations. A concurrent engineering work strategy was adopted for simultaneous system modelling and design work from the feature analysis and validation activities results. The system design activities were needed for conducting quadrupeds dynamic race simulation, whereas system modelling activities came up with solutions for quadruped kinetic and kinematic aspects results. A validation platform was created (Design evaluation) by designing track designs to test the results from both system modelling and system simulation activities.

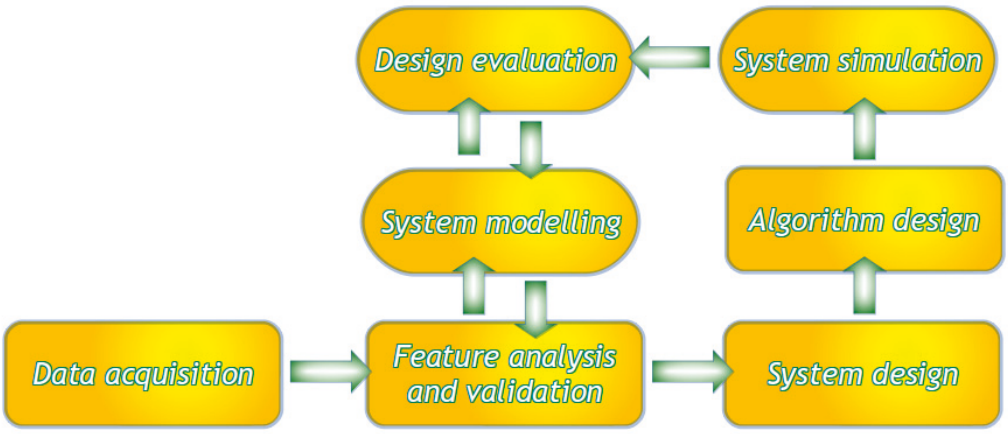

Figure 1.1: Workflow diagram for modelling and simulation of multiple galloping quadrupeds dynamics in racing.

1.6 Dissertation outline

The Chapters within this thesis are organised as follows:

Chapter 2 gives an overview and explores literature repositories and recent related work regarding fast quadruped racing dynamics, race track design and dynamics, and system modelling and simulation.

Chapter 3 concisely presents the work which was carried out to make data-based decisions for progressing into the design of effective and efficient modelling and simulation techniques. Also, it contains the different limitations exposed by the available data and data retrieval approaches.

Chapter 4 presents the steps and procedures that were taken for the development of race simulation and dynamics models. The reasoning for different applied techniques is explored. Different considerations and justifications of the considerations are given and also provides details on implementation-specific information.

Chapter 5 illustrates the various results derived from simulations and models' out-

puts and how they relate to actual field events and situations. Also, validation of results by second-order approximation through data verification. The significant discrepancies due to limitations exposed by the data and techniques are presented.

Chapter 6 summarises the work of this Masters dissertation and also presents potential future research.

Chapter 2

Literature review

2.1 Introduction

For the research work, information was synthesised from different sources and grouped as relevant key terms. For designing and researching a dynamically safe racing track for fast quadrupeds, research elements such as quadrupeds and racing track were thoroughly examined to find the critical research components. After critically synthesising a vast array of literature in the relevant fields as shown in Figure 2.1, the topics quadrupeds dynamics, race track design, race track dynamics, system modelling and system simulation were considered to be fundamental for carrying out the research.

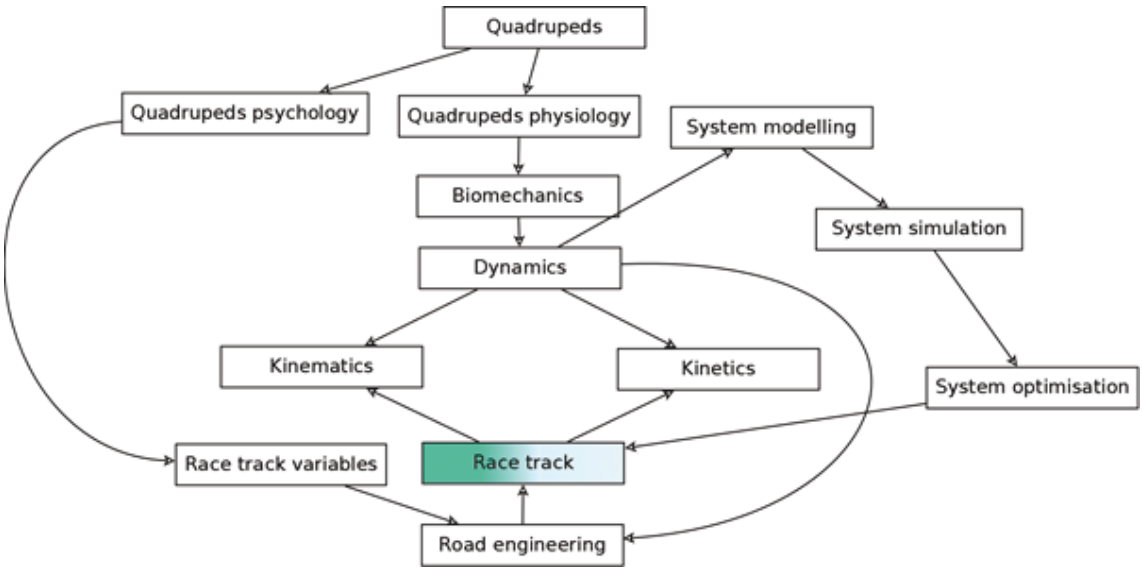

Figure 2.1: Research topic linking ideas.

2.2 Quadrupeds dynamics

Quadrupeds dynamics is one of the fundamental topics that need to be fully explored before designing a greyhound race track. Biomechanics found in gaits provides a good starting point for understanding quadrupeds dynamics. On the other hand, the evolution of clinical methods for gait analysis has been maturing for the past 40 years [3]. Methods such as kinematic analysis allow the observation of positions, velocities, accelerations, angles of anatomical points, segments and joints in space [3]. Kinematic analysis of gait can be performed by using a set of markers and using video capture technologies [3]. For instance, researchers collected the degree of coxofemoral joint abduction–adduction, mediolateral foot movement, the distance between hind feet, maximum hindfoot elevation, mediolateral pelvic movement, and coxofemoral joint angular acceleration by kinematic gait analysis [4]. However, kinematic analysis is still a daunting task for many because of the factors such as variance in canine morphological characteristics, gait symmetry, and skin movement where these variables may introduce undefined error into the reported data, which may lead to misinterpretation of the kinematic analysis [3].

Another technique for gait analysis is looking into the kinetic data of the gait which includes peak vertical and horizontal forces, vertical impulses, strain within various tissues, rate of loading, temporal gait characteristics and pressure distribution of the paw [3]. There are various techniques, and devices are available to aid with kinetic analysis, for example, force plates, using inverse dynamic analysis devices, and neuromuscular measurement systems [3].

When it comes to gait types, quadrupeds utilises different gaits at different speeds [5, 6]. The gaits are the way foot contact the ground [7]. For instance, when the locomotion speed is lowest quadrupeds use a walking gait and as the locomotion speed increases the gait changes to a trotting gait and finally for fastest locomotion speed

the galloping gait is used [6]. While moving very fast quadrupeds adopt a gait called galloping [8]. The gallop is also the preferred gait for most quadrupedal mammals in high-speed running [9]. The galloping gait exhibits distinct characteristics when it comes to locomotor nature [6]. This is because galloping gait is asymmetric in nature compared to walking and trotting gait when it comes to mass distribution [10, 11, 12]. This can be observed in left to right asymmetry gait factors including touchdown angle and relative phase of limb movements [6]. On the contrary, in the symmetrical gait, the left and right side of the quadruped has the same motion, but phase-lag occurs after half a stride [13]. Additionally, as the locomotion speed goes up further and a quadruped is in the galloping gait, the relative phase decreases and becomes closer to the in-phases found in bounding gait [14]. There are two major types of galloping, namely transverse gallop and rotary gallop. Rotary gallop is where quadrupeds foot contact the ground in a sequential rotating manner whereas in transverse gallop contra-lateral foot contact the ground simultaneously [15]. The limb phase as defined by Hildebrand* can be used to differentiate rotary gallop (limb phase <50%) from transverse gallop (limp phase >50%) [16]. Between transverse and rotary gallop, the rotary gallop is more common in cheetahs and racing dogs like greyhounds [16]. Moreover, the results from the study done by Biancardi and Minetti [16] show that mammals with a relatively shorter leg and longer body tend to use rotary gallop. The galloping requires quadrupeds to have a flexible spine which can act as a spring for storing and restoring energy [15]. Furthermore, the mechanism employed in the elastic spine in galloping quadrupeds allows the most economical gait at high speed [17]. In the paper, Biomechanics of terrestrial locomotion: asymmetric octopedal and quadrupedal gaits, Biancardi [15] demonstrated that rotary gallop as adopted by species like greyhounds has signifi-

*Limb phase defines the footfall pattern of any gait by comparing phase differences between a reference limb and other limbs.

cantly higher maximum angular excursion as indicated by Froude number.

The nature of gait can also be experimentally evaluated by looking into locomotion duty factor and phase shifts [16]. There are studies that talk about specific characteristics of quadruped galloping gaits, yet the mechanism of galloping gait is not quite clear [6]. A physical model of rigid bodies can be used to reproduce the galloping gait mechanism for galloping gait mechanism simulation which works when model parameters have certain combinations [6]. In the article Generating high-speed dynamic running gaits in a quadruped robot using an evolutionary search, authors state that dynamic similarity between artificially evolved robot using stochastic optimisation algorithm and biological gait supports high speed running simple mechanism robot possibility. Likewise, to investigate locomotion mechanism, a spring-loaded inverted pendulum models were used previously to understand locomotion dynamic nature [18, 19, 20, 21, 22, 23, 24, 25]. Besides that, legged locomotion is inherently hybrid dynamic systems; that is, systems which have aspects of continuous and discrete dynamics [13]. For instance, when a foot strikes or leaves the ground, the multi-body system which expresses continuous dynamics are interrupted and altered [13]. In the article, A galloping quadruped model using left-right asymmetry in touchdown angles, authors illustrate that at low speeds with small Froude number a model of galloping gait becomes unstable whereas significantly increased locomotion speed provides stable gaits. Additionally, the model also shows that in the rotary gallop gravitational energy utilisation between forelimb and hindlimb stance phases contributes to rotary gallop having two flight phases [6]. The duty factor is said to be inversely proportional to cursoriality and is also a measure of limb contact time [16]. For example, forelimb and hindlimb duty factor values can vary significantly depending on the nature of strides [16]. When it comes to pure gait analysis, it is possible to model quadrupeds gaits with two different phased biped gaits in a series [15].

Knowing the precise position of the centre of mass of quadrupeds is also valuable for dynamical analysis. It has been demonstrated through modelling that it is optimum for a galloping system to have a centre of mass closer to the shoulder than to the hips [16]. This configuration of the centre of mass results higher vertical thrust component where the resulting force vector is approximately vertical [26]. Likewise, understanding joint forces in quadrupeds at different surface slopes and conditions is essential for predicting quadrupeds dynamical performance. It has been shown by research that joint moment patterns are significantly different between slope and level surface quadrupeds movements [27]. The swing joint moments have identical patterns for different surface slope configurations where stance joint moment varies from slope to slope configurations [27]. This indicates that as long as quadrupeds are galloping the acting moments at the joints remains approximately similar for varying surface slopes. Similarly, locomotion neural control in quadrupeds found to have specific patterns defining neuro-muscular response for different surface slopes [28, 29]. On the other hand, quadrupeds dynamic factor such as ground reaction force is a good measure of actual limb force experienced by the quadrupeds. As for ground reaction forces on the quadrupeds limbs, the normal component of the ground reaction force is quite similar between slope and level walking except for significant variance in the peak magnitudes [27]. For downslope walking there is an increase in shock absorption in the early stance period while decreasing propulsion in the late stance period when compared to level walking [27]. Likewise, quadrupeds have higher impact loses at higher speeds where the impact force spikes occur after foot touches down due to damping effect [9].

On the other hand, stride frequency versus stride length analysis showed that stride frequency is scattered about a relatively flat trend line whereas stride length has a constant positive sharp slope while galloping speed is increased in quadrupeds [30, 9]. The experimental model also shows that the stride length increases almost linearly

with the speed where the slope is approximately ten per cent of biological counterpart [9]. This proves that the mechanism used in galloping for increasing speed is to increase stride length instead of stride frequency [9]. In the article titled optimal exploitation of natural dynamics in legged locomotion, Krasny and Orin suggested two main sources of energy drains in locomotion: firstly, the frictional and damping effects from the limb impacts; and secondly, deceleration of a leg at the end of the swing phase while supporting the weight. Acceleration is another important aspect of fast quadrupeds. In nature, fast quadrupeds such as the cheetah can accelerate from 0 to 97 km/h in just a mere 3 s whereas for greyhounds it is 0 to 72 km/h in approximately 2 s. This impressive acceleration ability of fast quadrupeds is because of their muscle power output across a speed range [31]. Besides that, during acceleration, fast quadrupeds have two aerial phases per stride where the work and energy output from the muscle can be determined from the kinematic data of fore and hind legs [31]. A study on ten racing greyhounds using high frame rate (HFR) videos shows that greyhounds have a peak horizontal acceleration of roughly 15 m/s^2 for the first two strides [31]. The study also showed the work done by both hind and forelegs during acceleration for the first seven strides were similar despite a large speed range citeWilliams2007. Finally, the same study calculates the muscles were working close to their maximum power production at approximately 40 J/kg stroke-1 during the acceleration phase [31].

2.3 Racing track design

There are several fundamental factors that need to be considered before designing a racing track which includes the path of a racing track, vertical and horizontal transitions, race surface condition, and race operational elements. The track design goal should also consider optimising lap time and mechanical cost of transport for each quadruped by taking into consideration of changing quadruped dynamics at

each point of the track. This can be solved partially by optimising racing line where the best racing line would provide the lowest lap time for quadrupeds [32]. When searching for the optimum racing line, it is also important to take fast quadrupeds rapid acceleration as another variable. In the article Acceleration in the racing greyhound, authors show that the mean horizontal acceleration of greyhounds in racing from the exit of the starting traps to near maximal speed was 9 m/s^2 for a maximum speed of roughly 17 m/s. Moreover, to enable quadrupeds to maintain their gaits in the racing track, the design must also follow the principles of ergonomics and highway engineering all around and particularly for curved track paths [33]. Due to real-estate restrictions, many tracks have round sections where the banking in the track becomes an intrinsic part of the curved track path, which has to be suitable to enable more compatible environments for quadrupeds in motion [34]. This is because banking is another way of reducing centrifugal force acting on the quadruped when it negotiates a turn [34]. The precise amount of banking depends on the track path curve radii and the speed with which quadruped enters the turn [35]. Similarly, transitions enabler for the semicircular and straight track path known as transition curves would reduce disturbances in quadrupeds gait symmetry [34]. This is because quadrupeds are subject to centrifugal force, an outward pull in the curved track path, which would cause quadrupeds to deviate from the original navigating path [33].

Fredricson (1975) proposed that centrifugal force in the turns attributes to an increased risk of injury. In the track, galloping quadrupeds decrease the speed as they enter the turns while increase radius of the turn to reduce acting centrifugal force [33]. A transition curve is a series of circular arcs where arcs have gradual decreasing radii [34]. Mathematically, a transition curve can be represented by a cubic parabola or by a spiral [34]. Transition curves are an essential element of curved track design as without them quadrupeds would be most likely to lose co-ordination

during entering and exiting a curved track path [34]. The transition curve also helps significantly if the track path curve is not adequately banked [35].

As with race surface contribution in the race track design consideration, the race surface mechanics as produced by material contribution, moisture content, surface temperature, surface maintenance procedures play an essential role [36]. The overall goal of race surface design is to support the musculoskeletal health of quadrupeds [36]. However, the relationship between surface mechanics and it's contributing factors is somewhat complicated and not explored adequately currently [36].

Again, the racing line is another variable that helps in identifying a suitable transition curve design as well as a race track path. This is because a racing line defines the path an object should follow to achieve the best lap time where the track curvature remains minimal [37]. On the other hand, the ideal racing line is fundamentally different from track shortest path as it is also a function of track running speed and track obstacles [38]. In the article, Searching for the optimal racing line using genetic algorithms, authors denoted that the best racing line can be modelled using a quadratic optimisation problem where optimal trade-off can be computed by minimum curvature path and shortest following path. The minimum curvature path is the path that would have the least curvature throughout [37]. This is important since centrifugal force as experienced by quadrupeds is directly proportional to the track path curvature [33]. The problem of finding the ideal racing line most of the time requires the application of different optimisation algorithms [38]. Furthermore, it also requires the application of dynamic programming, which is different from linear programming [38]. In dynamic programming system state changes with time where input from previous states combined with current state defines future system state [38]. Within the field of dynamic programming, discrete Markov decision processes are one of the major optimisation algorithms for finding an ideal racing line [38]. The idea of discrete Markov decision processes algorithm is taking into

account all the intermediate decisions during a race which would have some results [38]. The major step when applying discrete Markov decision processes is formulating the problem model, which demands to discretise the continuous variables [38]. For example, race object position in the track can be discretised by dividing track map into segments and identifying race object position by segments [38]. The velocity of the race object can also be discretised by using a discrete set of velocities, for example, integers from zero to maximum velocity [38]. Finally, an ideal racing line which would be race object state variables that minimises lap running time [38]. However, for finding optimal race object state variables application of value iteration algorithm is necessary [38].

2.4 Race track dynamics

Musculoskeletal injuries are a common happening in racing quadrupeds such as greyhounds when compared to non-racing quadrupeds [39]. In Wisconsin, USA, race track dynamic factors such as the grade of surface, track speed, and race distance have resulted in a significant effect on injury rates as found from investigating five tracks [40]. The same research found that variables such as time of year and the ambient temperature had little effect on injury rates [39]. Research by Sicard et al. (1999) also points out that temperature and time of year did not correlate with the greyhound injury rates. In the article, Greyhound Injuries, Poulter and David (2018), indicated that young greyhounds speeding into bend 80 – 100 meters from the starting boxes results in checking and colliding between greyhounds. Furthermore, when the races are run anti-clockwise, the front left and the hind legs are most susceptible to strains and stress during entering, negotiating, and leaving a bend in the fast quadrupeds such as greyhound [41]. In the paper, A survey of injuries at five greyhound racing tracks, Sicard et al. stated that the track with decreased initial straightaway, a decreased turning radius in the second turn and an increased

turn bank had substantially higher greyhound injury rates. Furthermore, it was found from the analysis that most greyhound injuries occurred at first and second turns of the tracks [39]. Likewise, race distance also appeared to have a significant consequence on greyhound injury rates [39]. When it comes to quadruped speed on the track, it was observed that greyhounds could reach higher speed if the track cross-fall is increased [39]. This is since an increased cross-fall in the bend may reduce the strain on the support of leg [39]. However, an increased surface grade like cross-fall was found to be more hazardous for greyhounds as this aids greyhounds to go faster and lose coordination, contributing to injury rates [39]. However, the article, Racetrack Design Performance, authors suggest adequate banking should help quadruped balance in the turns. Moreover, quantitative analysis of injury data pre- and post-track reconstruction was not sufficient to conclude banking effects on injury rates [35].

2.5 System modelling and simulation

Modelling is a technique to predict and understand a system's nature, whereas simulation recreates an event derived from various models. The modelling and simulation provide a way to experiment with various natural systems and situations efficiently, which can not be otherwise recreated feasibly in the lab or physically. One purpose of system simulation using means of software simulation to reduce hardware experiments and costly prototypes [42]. Also, computer simulations should be an integral part of the conceptual design as this always paves the way for the best possible system performance [42]. Traditionally, system modelling and simulation has been considered as a tool to create an abstract model of the real-world system where performance measurement of the system is carried out by computing the model [43]. Another application of system modelling and simulation is that to be used in the prototyping in the same manner CAD tool is useful to a product design

engineer [43]. Likewise, in the paper, Modelling, simulations, and optimisation of electric vehicles for analysis of transmission ratio selection, authors consider that model development is a significant step to move from concept analysis to prototyping and development which also allows flexibility conducting detailed studies.

There are various steps in simulation and modelling development. The first step into creating a viable model is to identify and address various system internal and external variables [44]. One step is to define initial conditions and experimentally find the values, as shown by the authors to model greyhound hind-leg single support to the ground [45]. Another step is to make fundamental assumptions to measure specific behaviours of the models and system. When it comes to numerical modelling and simulation, realistic constraints must be defined for the models such that numerical algorithms output converges [46]. This also allows extending dynamic system model conditions for given problems [47].

2.6 Summary

In the literature review, some of the ideas, research and theories are presented which are available currently from the different scientific, engineering, and relevant fields communities deemed to be suitable for the research. As drawn from the predominant literature, there is still considerable opportunity for research and development in the area of modelling and simulation of fast quadruped racing dynamics for optimising track designs safety performance. Furthermore, the literature review indicated the multi-disciplinary nature of the research and the importance of correlating results from different sources as well as the significance of this research for knowledge development.

Chapter 3

Information gathering for galloping quadruped race simulation and modelling

3.1 Introduction

Information gathering from the research was one of the core objectives for this research as there is a scarcity in the details of fast quadrupeds racing dynamics. Not only that, it soon became a significant part of this research project in terms of research resource allocations and contributions. To model and simulate various aspects of quadruped racing dynamics detailed knowledge on the model and simulation parameters was necessary to properly constrain and drive the models to generate results. Also, to formulate and conceive the structure and abstract for the models, in-depth information of various races, thorough investigations were required to progress the research. Moreover, to accurately recreate different scenarios through the models an in-depth theoretical knowledge on the research laid the foundation for various technical work. The information-gathering process happened concurrently while the fundamental analyses and modelling work carried out.

This chapter provides details of the major techniques, procedures and works carried out, as well as the final outputs of the information gathering tasks as conducted during this research.

3.2 Instrumental data collection for various parameters

Different measuring devices were used throughout this research. Every instrument used was specific for collecting a unique set of information about racing greyhound

biomechanics. High-frame-rate (HFR) videos of galloping greyhounds were recorded to understand the exact nature of the galloping gait and define the gait parameters, including stride length and stride frequency. Pawprint x-y positional data collected post-race was used to measure variations in the galloping gait performance in different track sections such as straight and bend sections. Data from the inertial measurement unit (IMU) placed on the greyhound's back as shown in Figure 3.1 were used to identify the nature of tri-axial acceleration acting on the greyhound's centre of gravity (CG). Full-length race videos were used to understand general racing dynamics. The real-time location coordinate tracking (RLT) data for individual racing greyhounds and lure for various races for a particular track were obtained to find trends in the racing including, but not limited to, acceleration and the maximum speed of the racing greyhound and, racing operational conditions such as lure separation from the leading greyhound. Finally, a radar gun was used for measuring peak greyhound speed at different tracks for different locations at the tracks.

Every instrumental setup resulted in some limitations about what could be retrieved and data accuracy tolerances. Most of the data collection limitations were inherent to device design limitations exposed by the hardware from the manufacturer. Some limitations came from the operating procedure and budget planning restrictions placed on conducting the research. For HFR video recording, the device used was a Sony DSC RX10 M3 camera, which was capable of recording a maximum of 500 frames per second (fps) at 1080p pixel resolution per frame. However, the camera can not record continuous HFR recording for more than one second, which played an important role while taking shots by the camera. The camera triggering needed to be in sync with the specific actions occurred at a track to collect measurable data. The non-continuous HFR recording by the camera also defaulted unfolding of full events for specific race actions happened at the track. The paw prints data came from one particular track for only one trail run by a dog that may not show all the race

dynamics. There could be any number of outcomes if a different dog was used for the trail run, and a different track was used for collecting the paw print data. A few different IMU devices were deployed (GPSports, MetaWear, and 3-Space) for getting acceleration data from the running greyhounds. All the IMU devices used could log greater than 100 data samples per second and also had onboard storage to save the data samples. As IMU devices are inherent to drifting errors where the reading from the IMU sensors are drifted from the actual value is accumulated according to the number of data samples recorded. As a lower data sampling rate would result in a less drifting error in the sensors reading compared to a higher sampling rate, also using a sample rate reading too low would result in a loss of detail, the precise greyhound actions could not be retrieved for the entire race duration other than instantaneous actions. Furthermore, data synchronising with the actual events at the track from visual feed-backs was a complex task as there was no direct link between the IMU and video recording clocks. This made the analysis of various detailed racing events cumbersome and not feasible. Also, the IMU devices were placed on the back of the greyhounds do not precisely represent the CG of the greyhounds. As a result, the collected data from the IMU devices inherently would have embedded noises from the local movements of different greyhound actions. This also implies that there would be local high-frequency vibrations data in the IMU acceleration data other than the acceleration data of the greyhound's CG. The full-length race videos analysed were taken from various vantage points at the tracks which do not always give a clear view of the different racing greyhounds when at various locations at the tracks. This restricted what could be concluded from the various race incidents. The greyhound real-time location tracking data was received at various signal towers located around the track which sometimes had communication signal interruptions due to the presence of ferromagnetic objects at the track such as the lure rail and fences. This resulted in corrupted data readings

in the RLT data collection. Consequently, the RLT data had limitations about analysing instantaneous changes and events at the track. Furthermore, due to a low sampling rate of <30 of RLT data it was a daunting task to analyse a full stride performance of greyhounds other than the overall performance of GR over a longer period. At last, the radar gun device used for measuring the greyhound speed had an accuracy of ±1.8 km/h (±0.5 m/s) for a racing dog approaching the gun near head-on. However, the measurements taken using the gun were from the track fence, which may have resulted in a lower speed reading in the gun than the actual speed of the galloping quadruped.

Figure 3.1: Placement of an IMU device inside the jacket of a racing greyhound.

3.3 Understanding quadrupedal racing incidents

Various quadrupedal racing-related incidents and issues were learned, observed and witnessed over the period from speaking with industry personnel, visiting the racing tracks and events, and by watching race videos as released after the races. The matters from the racing incidents gave a starting point for the research direction and brainstorming of subject matters. Observation has confirmed that a galloping

quadruped's motion is greatly influenced by the line-of-sight to a lure at a track as shown in race Video 1. Bumping and collisions were observed frequently at the bends because of proximity similar to that shown in race Video 2, where the white greyhound was deviated from its trajectory by the green greyhound immediately behind due to lack of heading clearance while accelerating ahead of the white greyhound. Also, when there is a lack of preemptive leaning action from a greyhound before entering the bend results in greyhound's path deviation or gait imbalance, as shown in race Video 3. Sharp deviation and convergence of greyhounds immediately after a race start was repeatedly seen from the race videos, as shown in race Video 4 and 5.

Additionally, the dispersing of greyhounds from the congestion has an effect on undesirable incidents at the bends (see race Videos 4 and 5). Races confirm that many greyhounds lagging significantly behind tend to chose a higher lane like shown in race Videos 6 and 7. During a race, after the initial boxes to the track transitional phase, greyhounds most likely would maintain their lane unless there is an approaching bend or while coming out from a bend or pressured by the greyhounds in proximity to maximise their galloping performance outputs to chase the lure as can be seen from race Video 8. It was common to observe that a greyhound tends to remain leaned for a short period after exiting a bend and leaning considerably before approaching a bend as shown in race Video 9. Greyhounds getting congested as well as changing to higher lanes upon entering the bend was also noticeable at race tracks. The paw prints of greyhounds for the boxes to track transition run revealed that greyhounds were turning towards the lure rail as well as away from the lure rail as they move closer to the lure, which hinted non-optimal boxes orientations at the tracks. All the distinct situations which were arising at the tracks seemed like compound effects from various influencing sources that needed direct measurements and optimisations.

Video 1: http://bit.ly/35Tqr0p

Video 2: http://bit.ly/2QY4Xv5

Video 3: http://bit.ly/2FSMOIz

Video 4: http://bit.ly/2RjUpW2

Video 5: http://bit.ly/2tcX8Zt

Video 6: http://bit.ly/2NuqTM8

Video 7: http://bit.ly/2Nw0HR9

Video 8: http://bit.ly/2Tz86D0

Video 9: http://bit.ly/2FQ0swf

3.4 Reviewing race track designs using survey data

A total of 28 oval-shaped tracks' civil survey data (SD) was provided by the GR industry, which was processed and analysed during the research. The data contained both GRNSW and GRV tracks. The SD was comprised of lure rail path (LRP), cross slopes of the track surface, race starting boxes locations and orientations relative to the track, locations of starting boxes gate opening sensors, location of the finish line, location of the catching pen, and track boundary fences. The information from the SD was essential as it provided the limit state racing environment and operating conditions the greyhounds were facing at the tracks.

3.5 Data processing and analysis

Data processing was essential for synthesising and extracting useful information from the various data. After the data had been extracted from the various sources, it was processed and analysed to create models for racing greyhound biomechanics outputs. Some of the major steps taken for data processing were, the selection of appropriate data sampling rate for a particular study to isolate components from the data, data smoothing from real-world data to discard unwanted noises in the data, and reformat

raw data to facilitate easier data extraction. Matching the data sampling rate to an actual event cycle was necessary as this would signify the results of the event of interest while reducing the results of unwanted events. For example, the HFR, IMU, and RLT data were re-sampled to retrieve a greyhounds gait performance more closely while minimising information lost from the data. While calculating higher derivatives, larger periods were considered rather than the period from the captured sampling rate, which allowed removal of local data fluctuations and noises from the analyses. Different noise filters and data fitting techniques were explored for the re-sampled data to smooth out the output results, which facilitated accurate dynamics calculation as well as model real-world behaviour from the noisy data. For instance, filters such as Butterworth and Hamming window filters were applied to the IMU data in MATLAB to discard higher noise frequencies from the data.

The curve fitting using least-squares polynomial fit was applied to get polynomial interpolation to actual data for dynamics analyses of one variable in relation to another variable. The rate of change (ROC) between one variable in relation to another variable was calculated to find a sudden change in the data, which was useful for identifying and discarding noisy samples from the data. Spline interpolation and moving average filters were applied to data calculations to draw accurate model where higher derivative calculations were required. Shape-preserving spline interpolation technique was used from MATLAB for accurate track shape curvature processing which maintained instantaneous spikes in the data while smoothing the interpolation between the samples to replicate real-world scenarios. As regular moving average filters have phase delay issues depending on the window size, a moving average filter was designed which maintained the phase while reducing the noises in the data. This was done by choosing past and future data samples for the average window and variable window sizes. The designed moving average filter also considers a smoothing factor that smoothed gradients' changes between the

data samples. The cosine similarity technique was applied to approximate matching and duplicated data samples and race dynamics states from the noisy data samples. Graphical analysis was required for certain data extractions such as data extraction from the SD of the racing tracks. The SD was formatted in 2D elements where the 3D geometric point description was laid out as 2D point and point elevation text. By analysing SD point to elevation text proximity in PY 3D points were generated for the tracks SD.

3.5.1 Track survey data

In the SD the LRP was defined by 3D coordinate points with roughly 3 m intervals and using arcs and polylines whereas the cross slopes of a track were defined by 3D point cloud with average distances between the points were roughly 6 m along the track length. And along the track width, the 3D point cloud was approximately 2 m. All the information provided in the track SD was formatted in 3D points, point clouds, polylines, and arcs primitives. The information provided in the SD was reconstructed as 3D mesh, surface and mathematical models using SolidWorks, AutoCAD, and Blender computer-aided design (CAD) software packages. The 3D mesh, surface, and mathematical model allowed retrieving of track geometric features such as catching pen transition, starting boxes transitions to the track, the track cross slopes and super-elevation, and track width at the arbitrary locations within the track. Table 3.1 shows various geometric features of the tracks as derived from the graphical analysis of the LRP and the point cloud in SolidWorks and AutoCAD CAD software. The procedure followed for the graphical analysis of a track path, as defined by the LRP, was using the optimal arc spline approximation method in SolidWorks software. The arc spline approximation method approximates a curve as defined by point sequences by arc segments with G1 continuity [48]. By choosing optimal discretisation factor for the curve to be approximated a highly accurate map

of the original point sequences can be achieved through the arc spline approximation method. In SolidWorks software, the point sequences of the LRP were approximated by the arc spline until a minimum offset threshold of 5 mm for fitted arc spline was reached. Using AutoCAD Civil CAD software package, the point cloud of different tracks were translated into AutoCAD surface primitives which gave accurate maps of the cross falls at arbitrary locations on the tracks. This process also allowed the generation of overall track surface elevations maps from the tracks SD for different tracks. Figure 3.2 shows the elevations of a track as generated using AutoCAD Civil CAD package after translating SD points cloud to a surface primitive which shows the highest and lowest points at the track as well as surface gradients with respect to an arbitrary datum point. As can be seen from Figure 3.2, the track elevation between the highest and lowest point of the track was greater than 2 m indicating that when quadrupeds would move around the track, they either climb up or climb down the track. Figure 3.3 depicts cross falls as slope arrows at various points on a track as modelled by AutoCAD Civil after translating points clouds to a surface primitive. As can be seen from Table 3.1, the maximum, minimum and average cross-slopes of the bend for the innermost region nearest to the rail among the tracks are 10.0%, 4.8%, and 7.7% respectively. All the values presented in Table 3.1 were calculated for the chainage path where a chainage path usually laid out roughly 1 m off the LRP. This measurement was important as greyhounds roughly follow the chainage path around a track. For the tracks which had a horizontal transition, the average transition length was 24 m. Almost all tracks analysed had shorter straights than bend sections as seen from the straight to bend section length ratio where the average length of the straight section was 60% less compared to the bend section. Using cluster analysis utilising k-means++ algorithm it was found that all the SD tracks can be divided into three bend radiuses groups where 10 tracks, 16 tracks, and 2 tracks fall into 61.7 m, 52.1 m, and 44.7 m bend radiuses groups respectively.

This shows that the majority of the tracks were designed with a 52 m radius bend followed up by a 62 m radius bend.

Table 3.1: Greyhound tracks geometric features as analysed from the survey data.

	Bend chainage cross-slope percentage	Straight chainage cross-slope percentage	Avg. length of straight section (m)	Avg. length of bend section (m)	Straight to bend section length ratio	Avg. radius of bend 1m off the rail (m)	Avg. horizontal transition length (m)	Chainage perimeter (m)
Maximum	10.0	5.0	123.2	214.1	0.7	68.1	35.0	644.7
Minimum	4.8	2.2	36.4	133.4	0.0	42.5	15.1	440.7
Average	7.7	4.0	71.7	172.8	0.4	55.0	24.0	519.3

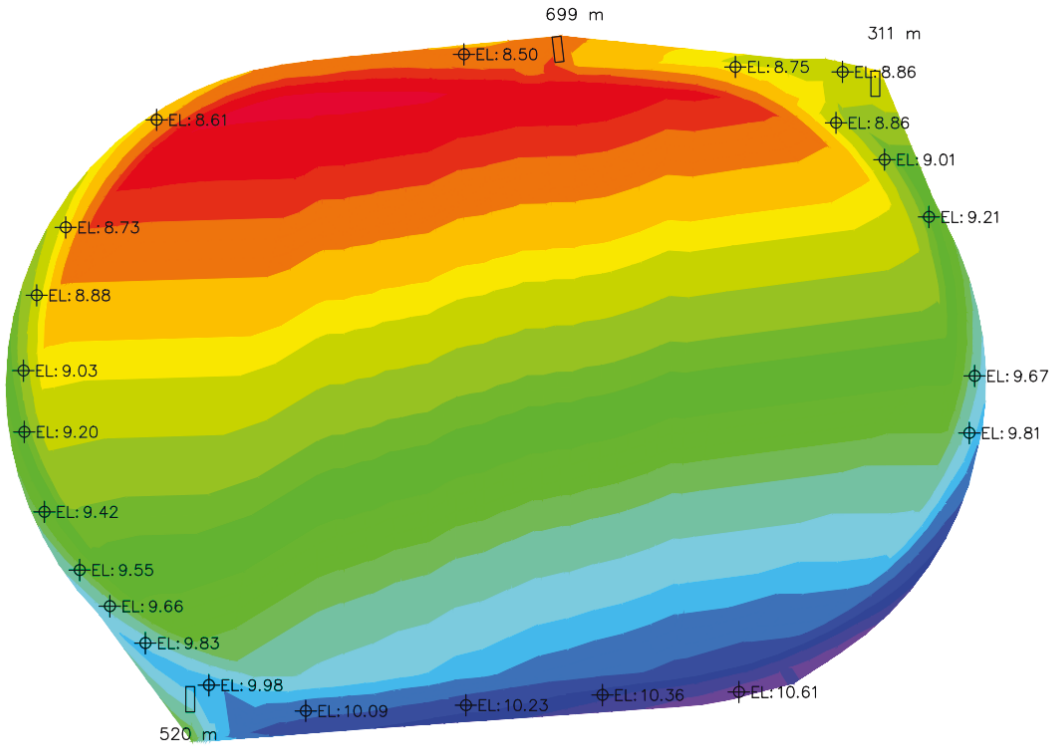

Figure 3.2: Surface elevation and gradient analysis of a greyhound track using AutoCAD Civil engineering CAD package.

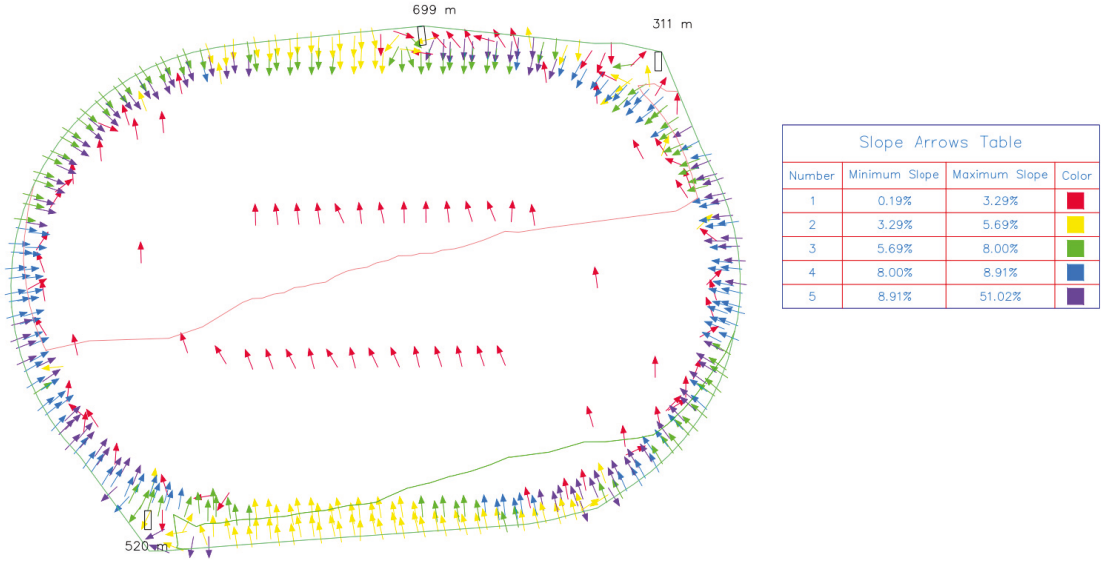

Figure 3.3: Cross-fall analysis of a greyhound track using AutoCAD Civil engineering CAD package.

3.5.2 High-frame-rate video data

The HFR videos of both GR side and front views were analysed in the video motion analysis and modelling software called Tracker and Kinovea. By tracking a greyhound's stride in the HFR videos as shown in Figure 3.4, the stride length and stride frequency of the racing greyhound were determined. Also, velocity and acceleration of various points of interests were calculated using FDM algorithms given in Equations 3.1 and 3.2. For example, Figure 3.4 shows HFR video analysis in Tracker software to determine the stride length (approx. 5.5 m) of a racing dog at a track's straight section where the distance between the rail post was approximately 3 m and HFR video single frame duration was 2 ms (500 fps). For this HFR analysis, there were a total of 138 video frames for one greyhound stride which equals a stride frequency of 3.6 strides per second. Moreover, all the conducted HFR analyses showed that a greyhound's paw striking with the track surface occurs either in the front-right, front-left, hind-left, and hind-right or the front-left, front-right,

hind-right, and hind-left order.

Figure 3.4: HFR video stride analysis using Tracker software for a 500 fps recording.

$$v_I[k] = (x[k+1] - x[k-1])/(2 \times dt) \tag{3.1}$$

$$a_I[k] = (v[k] - v[k-1])/dt \tag{3.2}$$

Where $v_I[k]$ and $a_I[k]$ are instantaneous velocity and acceleration at k sample respectively and dt is sample period.

Galloping stride paw ground contacting and aerial periods analysis

While galloping, a greyhound's stride has both paw landing phases as well as aerial phases where the greyhound body is in the air, as shown in Figure 3.5. By analysing a 500 fps video where a greyhound ran in the straight section the greyhound's paws ground contact periods and aerial phases periods were calculated. The HFR video analysed had a video frame interval of 2 ms. The left foreleg ground contact period was calculated to be 46 ms, as shown in Figure 3.5, which appeared after

around 22 video frames. Similarly, for the right fore-leg, the right hind-leg, the left hind-leg contact periods were approximately 40 ms, 48 ms and 44 ms, respectively. Likewise, there were two aerial phases where the greyhound fully contracted and fully extended, which lasted roughly 54 ms and 52 ms, respectively. This shows that the greyhound spent about 38% of its time in the air for the stride. Furthermore, the overall time spent on the hind-legs ground contacts was longer compared to fore-legs.

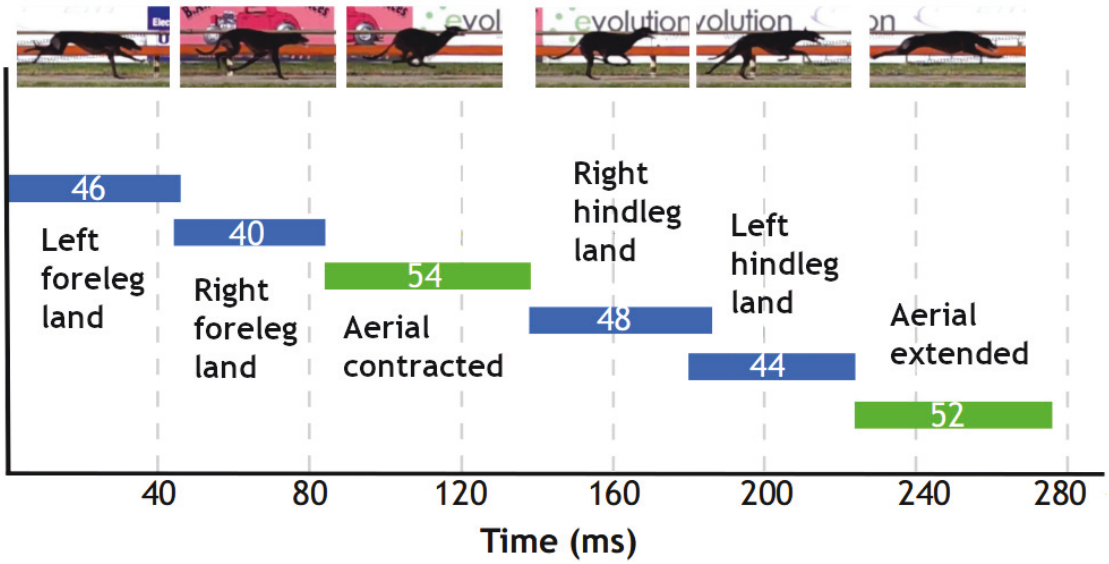

Figure 3.5: A greyhound's paw ground contact and aerial phase periods during a galloping stride in a straight run.

Galloping stride pose analysis

An HFR video recording at 500 fps was analysed in Tracker software for tracing different points on a greyhound's galloping stride gait. The points that were traced were selected so that they had the least movement due to any morphing effects by the greyhound's skin other than the actual physical structure change by the galloping gait. Furthermore, the points were traced with the touch down of the right foreleg. As the total horizontal displacements of the points can be known

from the greyhound's stride length and are identical for all the points, only the vertical displacement results are shown in this section. Four points were traced as shown in Figure 3.6, where the vertical motion of each point relative to the track ground was extracted to find the total vertical displacement of each point in a stride. Figure 3.7 illustrates the vertical displacement of the points from the track ground in a galloping stride gait as analysed by tracing the points. As can be seen, the motion of Points A, C and D were almost one full sine wave where the points were out of phase from each other. Table 3.2 shows the total vertical displacements of each point in the galloping gait, where the greyhound's stride length was just above 5.5 m.

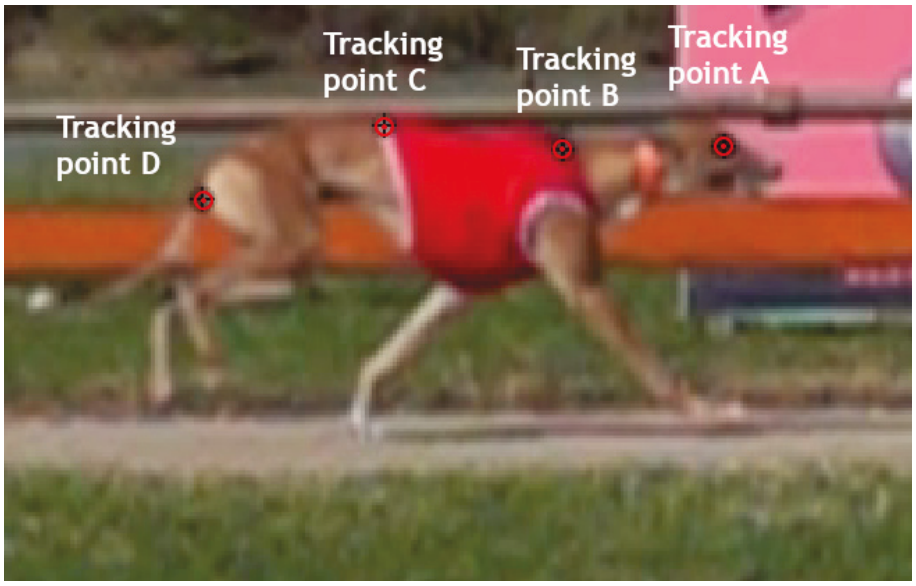

Figure 3.6: Location of tracking points lying on the greyhound's body.

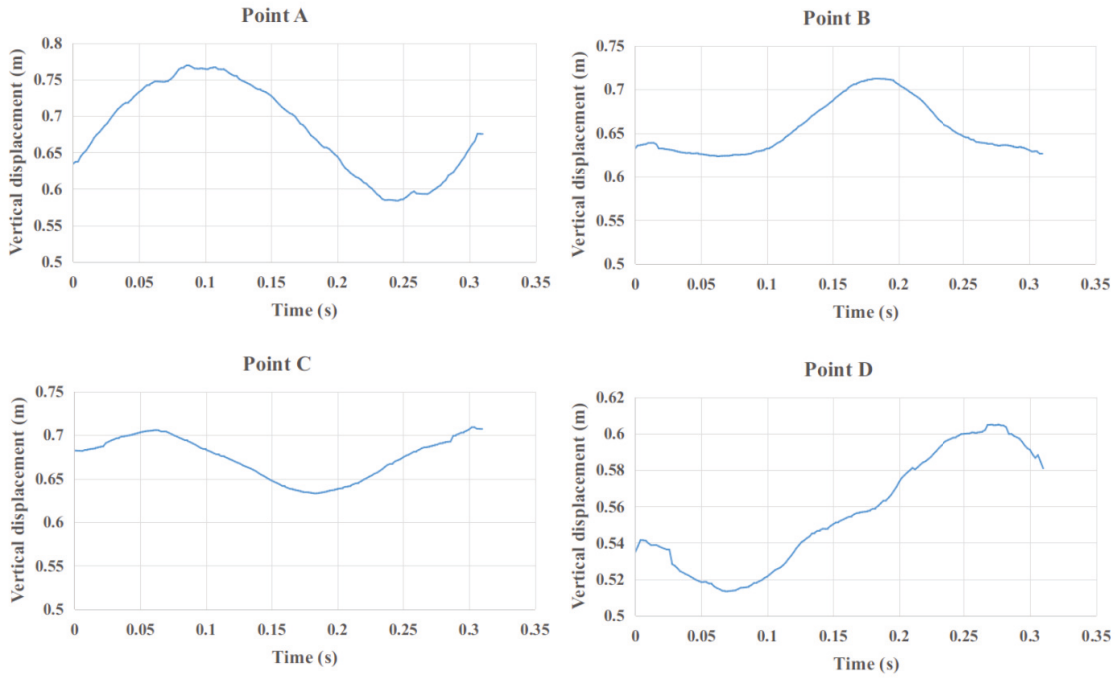

Figure 3.7: Pose analysis using different tracking points lying on the greyhound's body.

Table 3.2: Vertical displacements of different tracking points lying on the galloping greyhound's body.

Point	**mm**
A	186
B	89
C	76
D	92

As can be seen from Table 3.2, Point A, which indicates the movement of the head experiences maximum vertical displacement among the all traced points of about 186 mm in a stride. The least vertical movement occurred at Point C followed up

by Point B. As a greyhound would maintain the least amount of vertical movements of its CG, the total displacements of Points B and C indicated the location of CG to be between these two points and closer to Point C horizontally.

Centre of gravity estimation from non moving pixels analysis with respect to a local inertial frame of reference

For an object which is in motion, the CG defines the overall object's motion in an inertial frame. Locating the CG of a racing greyhound is a vital measurement for calculating and relating various dynamics such as centrifugal acceleration of the body, impact energy during a bumping and tracing the overall trajectory of a greyhound in the track. The CG location is such that all body parts move about CG while CG is in motion. For example, in the air, the body rotates about CG if there is a moment acting on the body. From the HFR videos, a greyhound's galloping gait was captured by Blender software video sequence editor and converted to 2D sequence frames to process moving regions in the greyhound's body. After this, a motion analysis was carried out on the pixels in the different frames by computing motion vectors of each pixel by using Mpegflow software package as can be seen from Figure 3.8. For image sequence frames which were following the galloping gait precisely by maintaining the greyhound's galloping gait speed, the motion vector computation gave an approximate calculation of individual region movements in the frames. Figure 3.8 shows motion vectors calculations for two different frames from two different HFR video captures where the regions with the least moving pixels are marked with the white circles. As a greyhound would naturally maintain the least amount of movements of its CG to increase galloping efficiency, the motion vector analysis on all HFR galloping gait frames showed the approximate location of the CG of a galloping greyhound. Furthermore, as a greyhound's body is roughly symmetrical along the body width, the location region of the CG as depicted by the

white circles in Figure 3.8 was enough to calculate the location of the CG effectively.

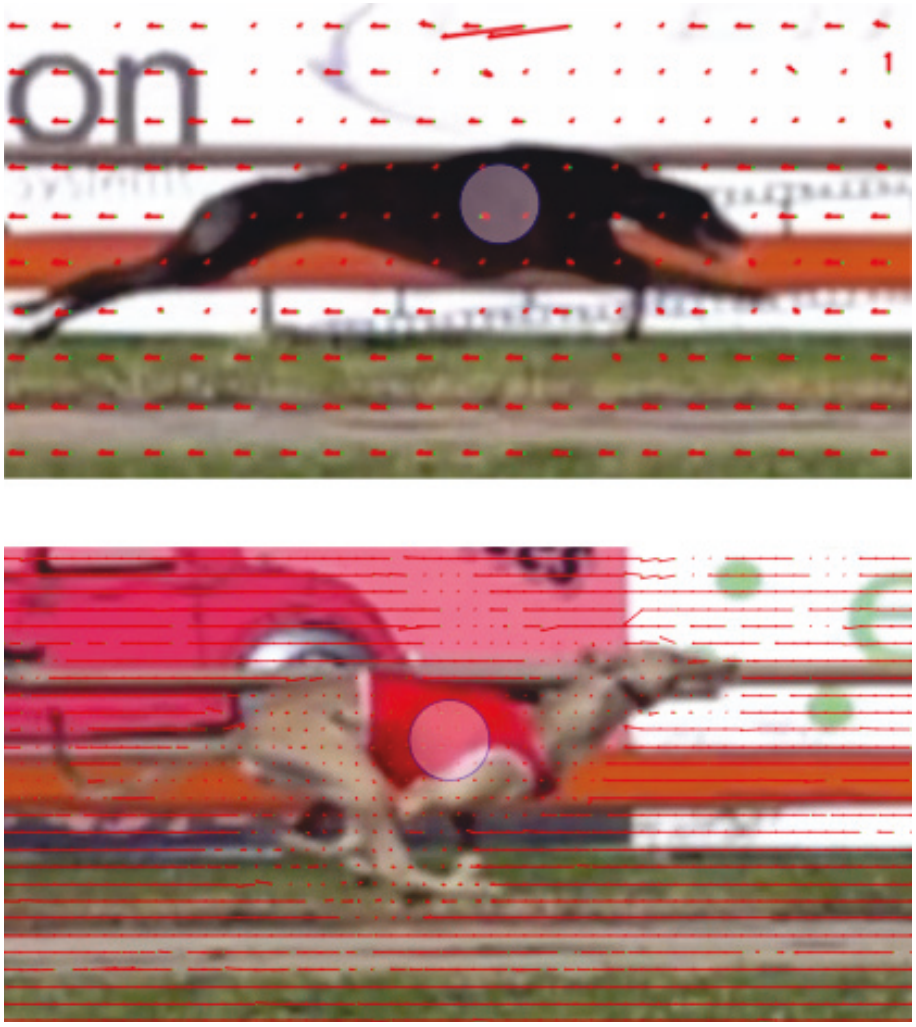

Figure 3.8: A greyhound's probable centre of gravity location region for galloping stride as determined from the motion vector analysis.

Limb work analysis from the rotating limb's paw acceleration with respect to a local inertial frame of reference

The motion of a galloping greyhound limb contains valuable information regarding the nature of work performed by the limb. This is because the kinetic energy of a limb is an indicator of the actual work carried out by the limb. From the HFR videos, the paws of the left front, right front, left hind and right hind limbs were traced in

Tracker software to understand the overall work performed by the individual limb which keeps a greyhound in motion. A local inertial frame as can be seen from Figure 3.9 was selected for performing the paw tracing analysis. The local inertial frame was chosen such that it is not far from the greyhound at any given point of the galloping gait and maintained a close distance from the greyhound's CG. This was done to ensure the capturing of detailed and comparable data for all paws' movements in a galloping gait. Figures 3.10, 3.11, 3.12, and 3.13 illustrate the motion tracing of a greyhound's paws in a complete galloping gait for the left front, right front, left hind and right hind paws respectively. The calculations of the displacements, speeds, and accelerations of the paws from the paws motions tracing with respect to the local inertial frame of reference like shown in Figure 3.9 is presented in Figures 3.14 to 3.17. In the graphs, the horizontal motion referred to the motion of paws in the direction of the X-axis of the local inertial frame, whereas the vertical motion referred to the Y-axis of the local inertial frame of reference. As can be seen from Table 3.3, which distills the motions of paws from Figures 3.14 to 3.17, the maximum horizontal speeds of hind paws were slightly higher than front paws. Another noticeable thing was that the left hind paw had the highest vertical velocity as well as the highest horizontal and vertical accelerations in a galloping gait. This indicated that the left hind paw provided most of the thrust in the galloping gait.

Similarly, the right front paw had the second-highest acceleration of all as can be seen from Table 3.3, which hinted that this paw was used for turning and decelerating of the greyhound's body, as can be seen from the motion graphs. This motion analysis of a greyhound's paws in a gallop provided critical information regarding the nature of work activities performed by each limb during a gallop. This analysis also helped verify the hypothesis found in the literature regarding the nature of work performed by the front and hind legs in a gallop.

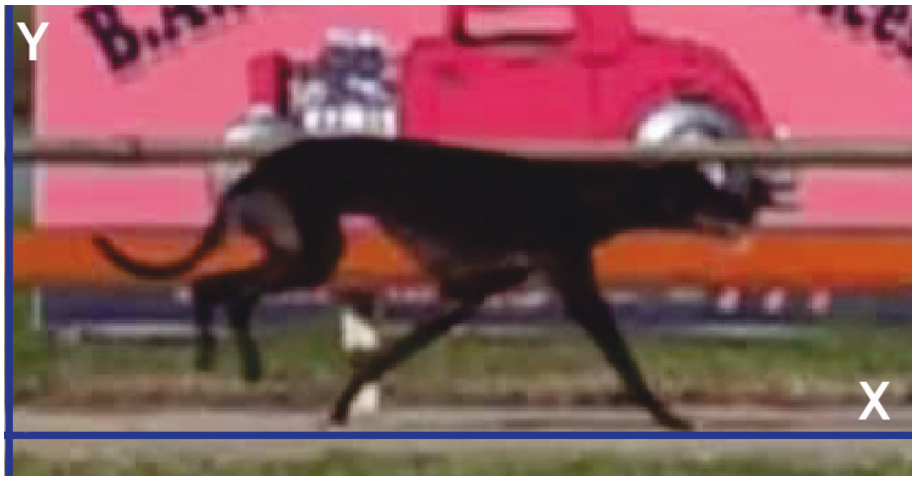

Figure 3.9: A local following inertial frame of reference for analysing different limbs' paws motions.

Figure 3.10: The motion tracing of the front left paw in a galloping stride with respect to a local frame.

Figure 3.11: The motion tracing of the front right paw in a galloping stride with respect to a local frame.

Figure 3.12: The motion tracing of the hind left paw in a galloping stride with respect to a local frame.

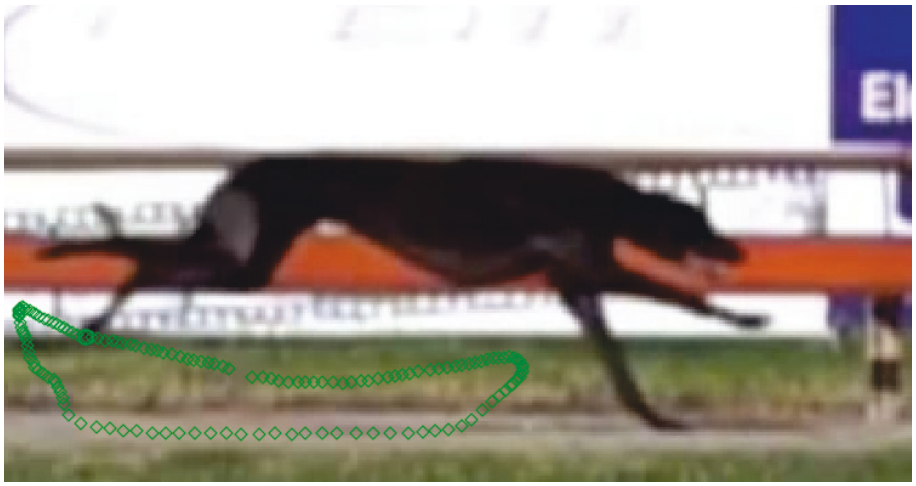

Figure 3.13: The motion tracing of the hind right paw in a galloping stride with respect to a local frame.

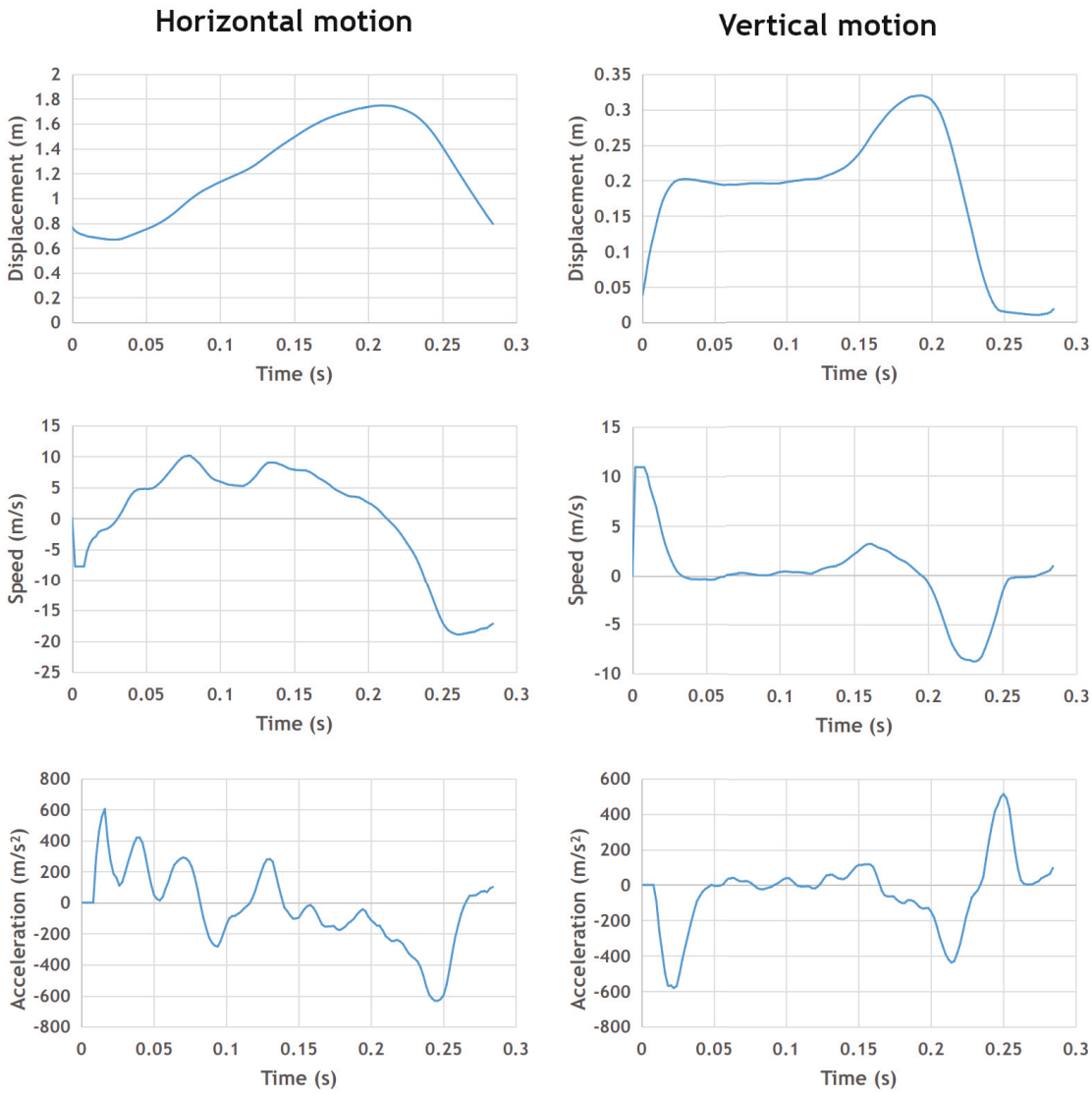

Figure 3.14: The motion of the front left paw in a galloping stride with respect to a local frame.

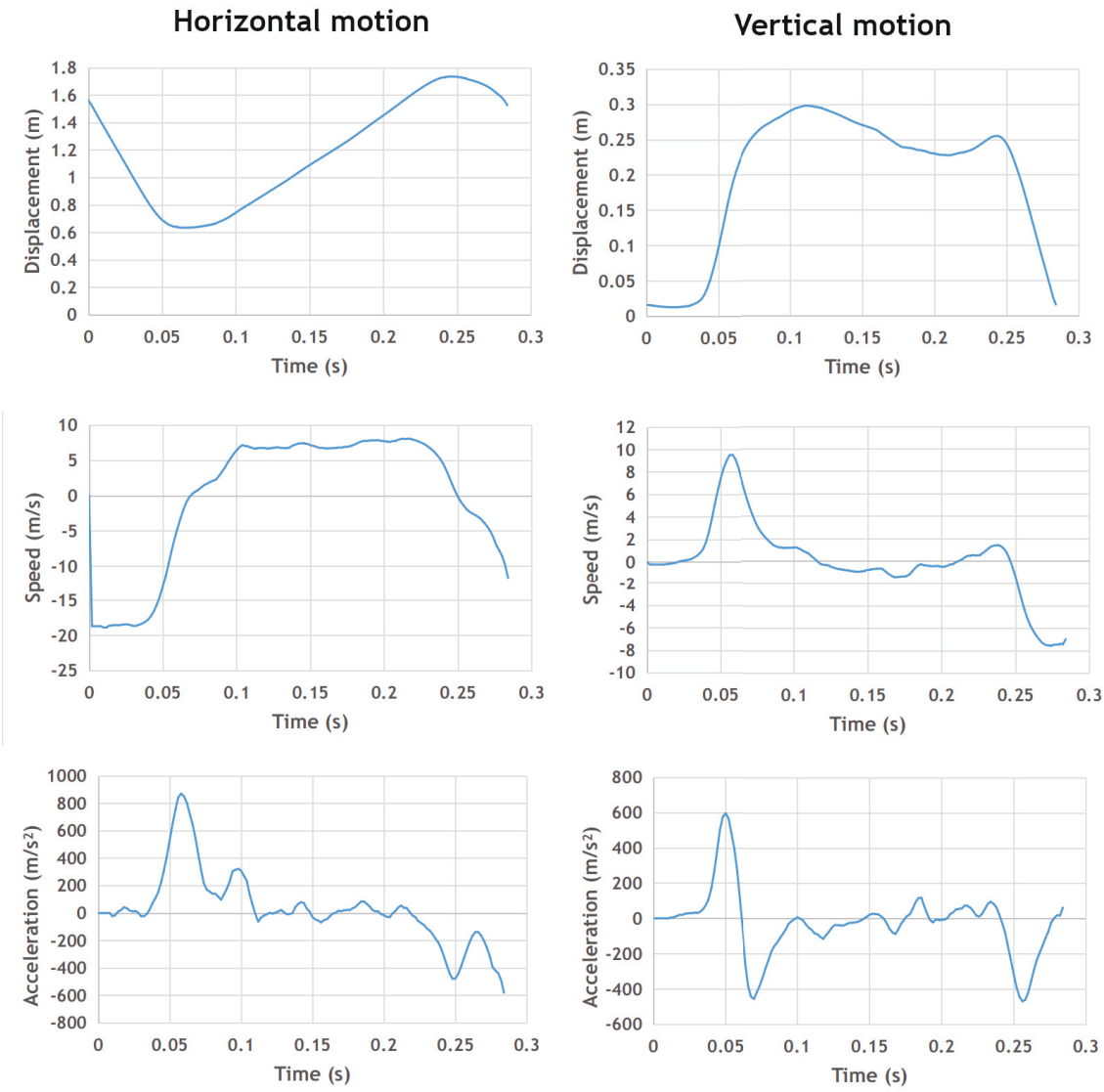

Figure 3.15: The motion of the front right paw in a galloping stride with respect to a local frame.

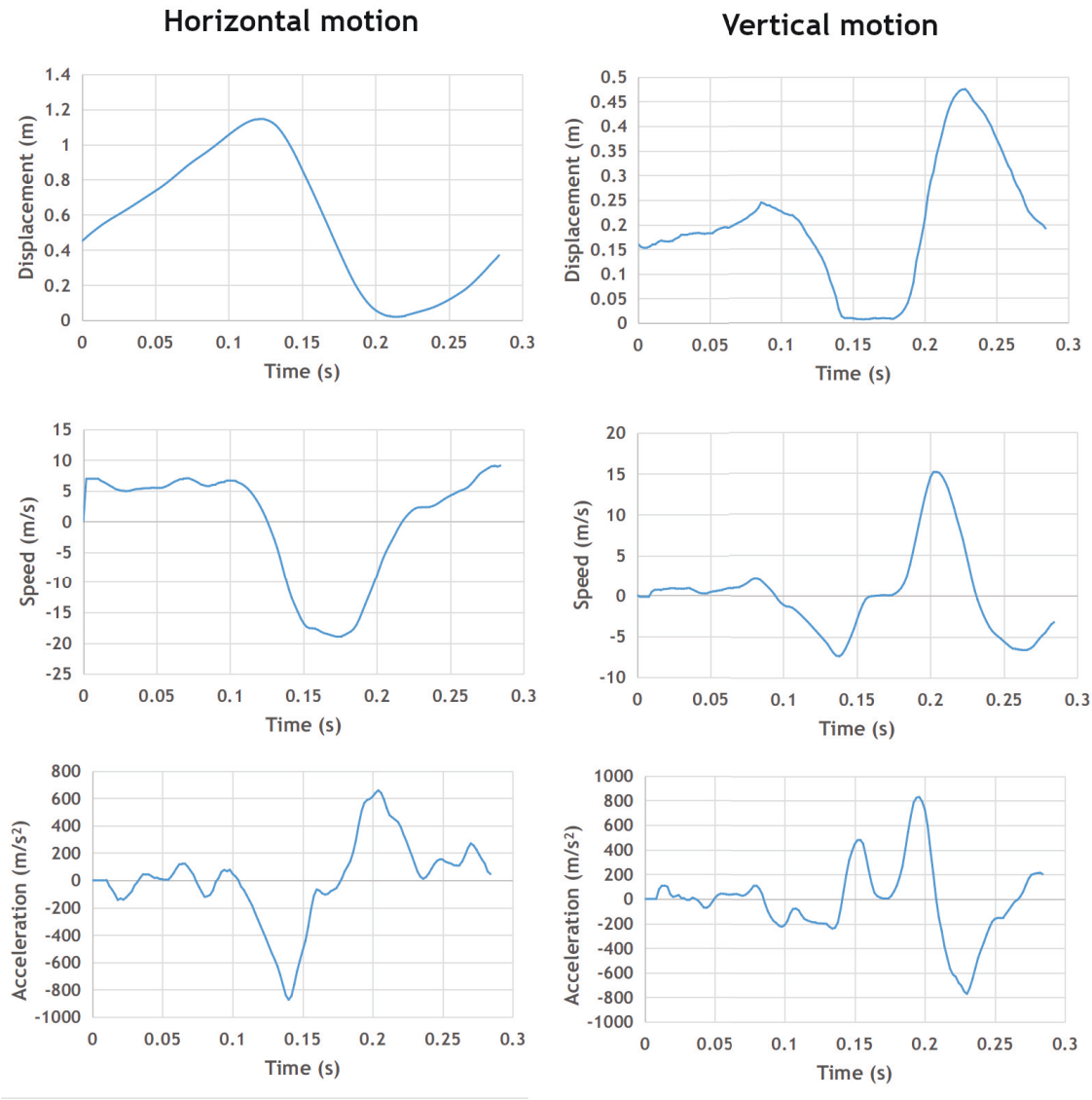

Figure 3.16: The motion of the hind left paw in a galloping stride with respect to a local frame.

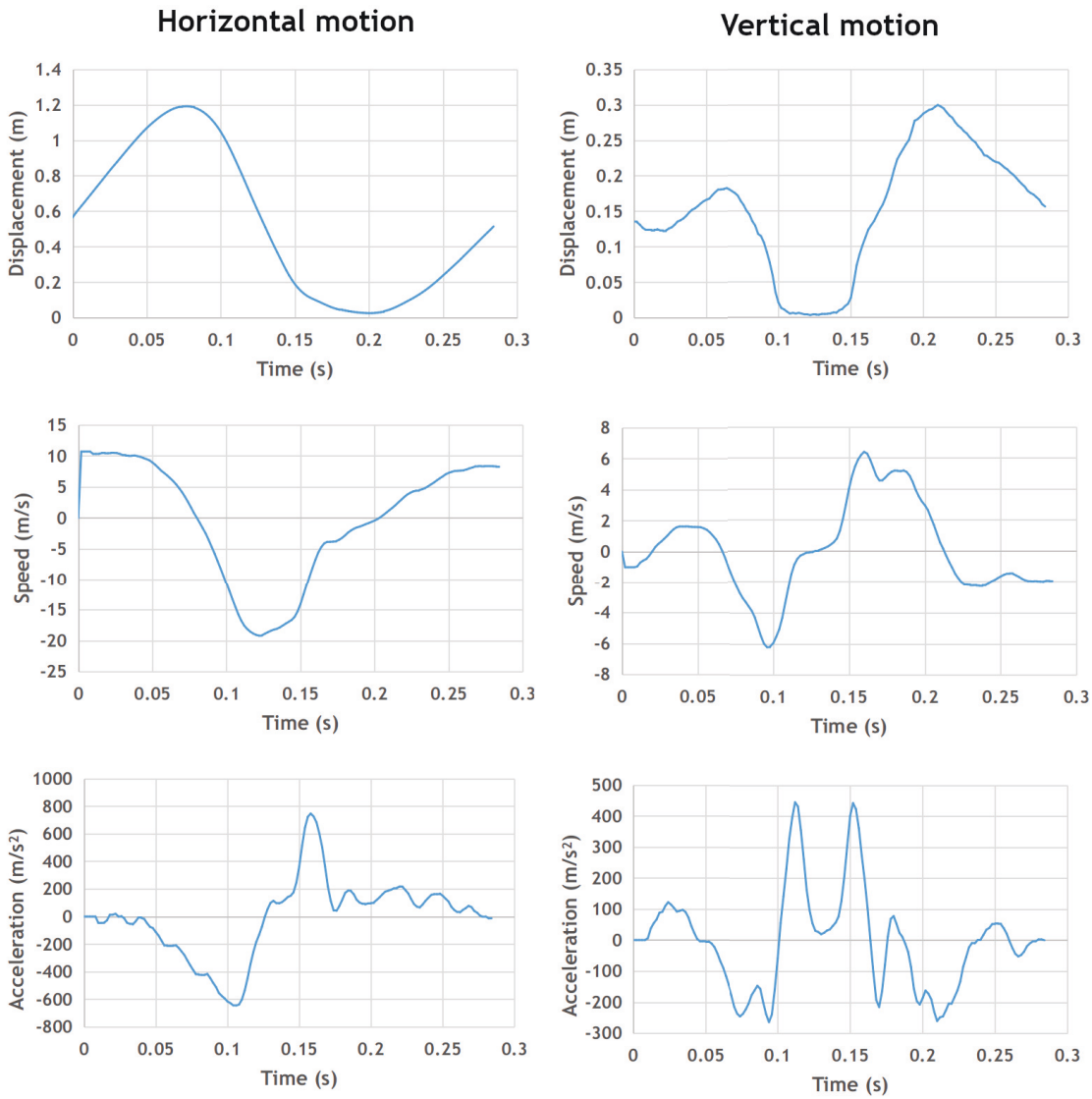

Figure 3.17: The motion of the hind right paw in a galloping stride with respect to a local frame.

Table 3.3: Greyhound galloping stride paw motion analysis.

	Left front paw	**Right front paw**	**Left hind paw**	**Right hind paw**
Maximum horizontal speed (m/s)	18.93	18.91	18.95	19.22
Maximum vertical speed (m/s)	10.94	9.55	15.14	6.39
Maximum horizontal acceleration (m/s^2)	633.10	870.14	873.14	746.84
Maximum vertical acceleration (m/s^2)	581.65	595.26	831.25	444.99

Quadruped galloping speed analysis from a paw's instantaneous speed while contacting the ground

Greyhound galloping speed was analysed by tracing the instantaneous velocity during a paw ground contact period. During galloping when a paw contacts the ground the instantaneous speed of the paw should match the galloping speed of a greyhound for the instance where both the ground's and paw's speed, relative to the greyhound's body is the galloping speed. Figure 3.18 shows a paw's ground contact tracing during a galloping stride to analyse the galloping speed from the paw velocity profile relative to a local greyhound frame of reference. Figure 3.19 depicts the velocity of the right hind paw of the greyhound during the galloping stride where the green region shows the time period the paw stayed in contact with the ground. As can be seen from the hind right paw velocity profile, after contacting the ground, the acceleration of the paw was significantly reduced where the maximum instantaneous speed of the paw was 18.5 m/s. Moreover, in Figure 3.19, the paw's instantaneous velocity tells us that the greyhound's galloping speed was varied between 15.4 and 18.5 m/s while the paw stayed in contact with the ground.

Figure 3.18: A greyhound's paw and ground contact tracing of the right hind paw as represented by the red circles during a galloping stride.

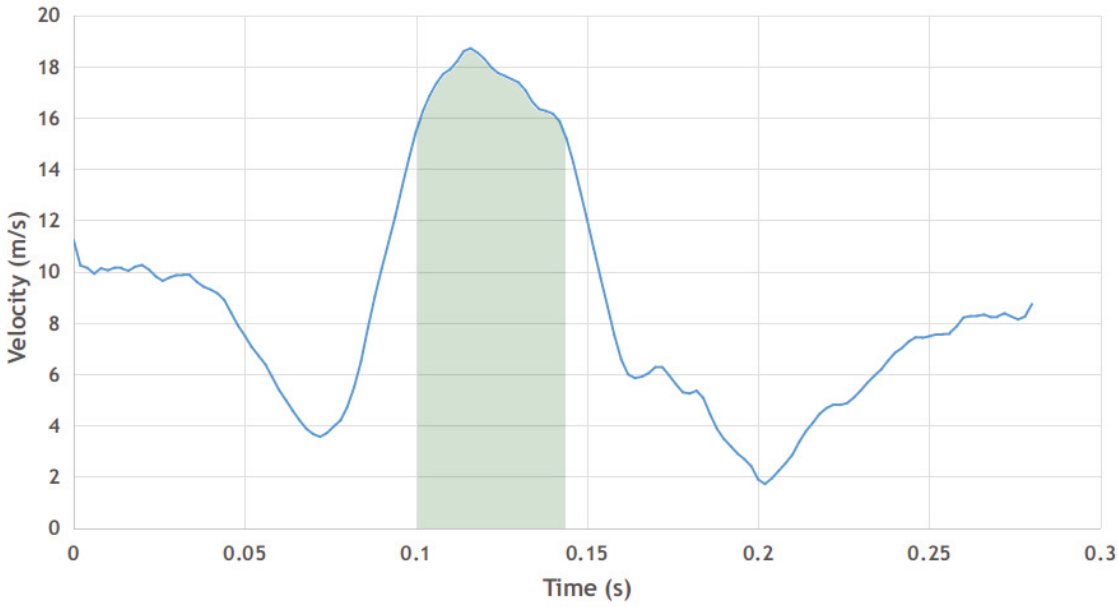

Figure 3.19: A greyhound's right hind paw velocity tracing during a galloping stride relative to the greyhound's local frame of reference.

Galloping greyhound leaning at a bend

During track visits, HFR videos were recorded to capture greyhounds leaning at the bends. The analysis of greyhounds leaning poses from the HFR video frames revealed greyhounds peak tilt at the bends. The following Figures show optimal greyhound tilts at a bend for a particular track as retrieved from several HFR video frames. Figures 3.20 and 3.21 depict tilting of single greyhounds in two different trail runs for the track which had a 51 m radius bend at the chainage line. Figure 3.22 shows that the leading greyhound has a much stepper tilting position when accelerating at the same bend.

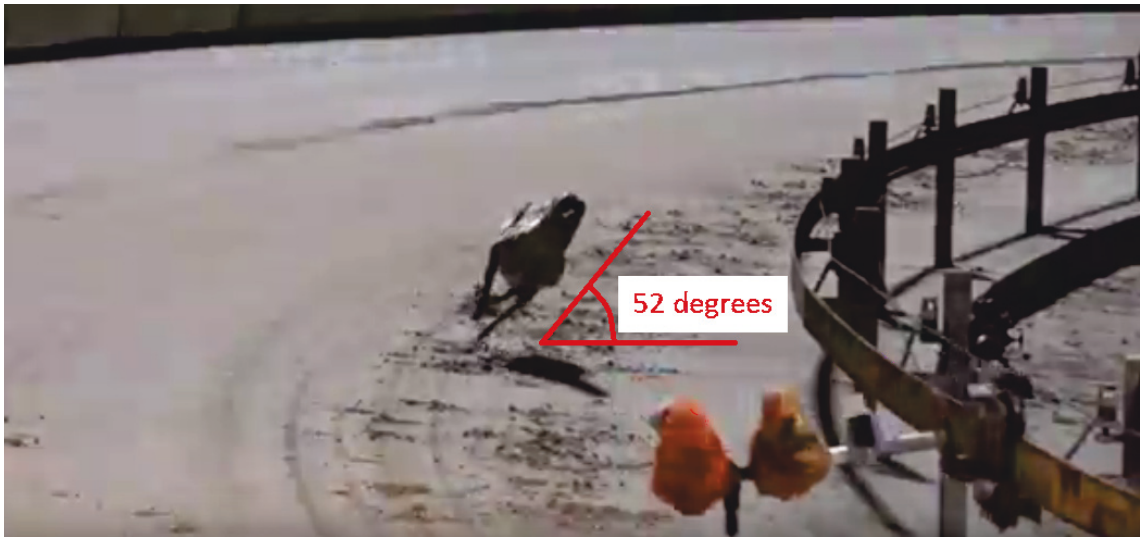

Figure 3.20: A high frame rate video still image showing a greyhound was in a moderate tilted position at a track bend to accommodate centrifugal force.

Figure 3.21: A high frame rate video still image showing a greyhound was in a moderate tilted position at a track bend to accommodate centrifugal force.

Figure 3.22: A high frame rate video still image showing a greyhound was in a step tilted position at a track bend to accommodate centrifugal force.

3.5.3 Inertial measurement unit data

The data from IMU devices shows proper accelerations of the racing greyhound, which are the apparent accelerations felt by a greyhound such that it is zero when there are no reactionary forces are acting on the greyhound. The IMU devices

used measured accelerations in three directions namely forward acceleration which measured acceleration in the direction of greyhound heading, lateral acceleration which measured acceleration perpendicular to greyhound heading and greyhound body length (traverse acceleration), and vertical acceleration which measured acceleration perpendicular to the track surface. These three accelerations indicated a greyhound's traction force to move forward, track surface shear force which provides the centripetal force, and normal force of the track surface which supports the greyhound weight. During a race, but after the initial acceleration phase, a greyhound's gait remains relatively stable and has cyclic patterns most of the time until the race ends. The cyclic gait movements were analysed from the IMU devices acceleration data. Figure 3.23 shows accelerations from one of the IMU devices data at a track bend for three seconds. As can be seen from the IMU accelerations data in Figure 3.23, there were cyclic patterns due to a greyhound's galloping gait mechanism in three different directions. Also, noticeable peak vertical acceleration was roughly double of both peak forward and lateral accelerations. Moreover, peak lateral acceleration was slightly higher than the peak forward acceleration. To extract the stride frequency components from this accelerations data a Band-pass filter and Discrete Fourier transform (DFT) algorithm were applied to the data, which removed the high-frequency noises and extracted the sinusoidal components in a stride. Figure 3.24 shows the stride's proper acceleration's cyclic components as distilled by the DFT algorithm by taking 300 acceleration data samples of a three-second period for the greyhound's forward acceleration. It was evident from the DFT analysis that too few or too many data samples would result in ambiguity in the stride components frequencies analysis. As found from the HFR videos, a greyhound's stride frequency is roughly between 3.2 and 3.6 Hz. Considering this DFT analysis, it showed that the greyhound's stride frequency to be roughly 3.3 Hz as indicated by the first peak and had an overall magnitude of 1.32 g for this forward

acceleration stride movement's cyclic component.

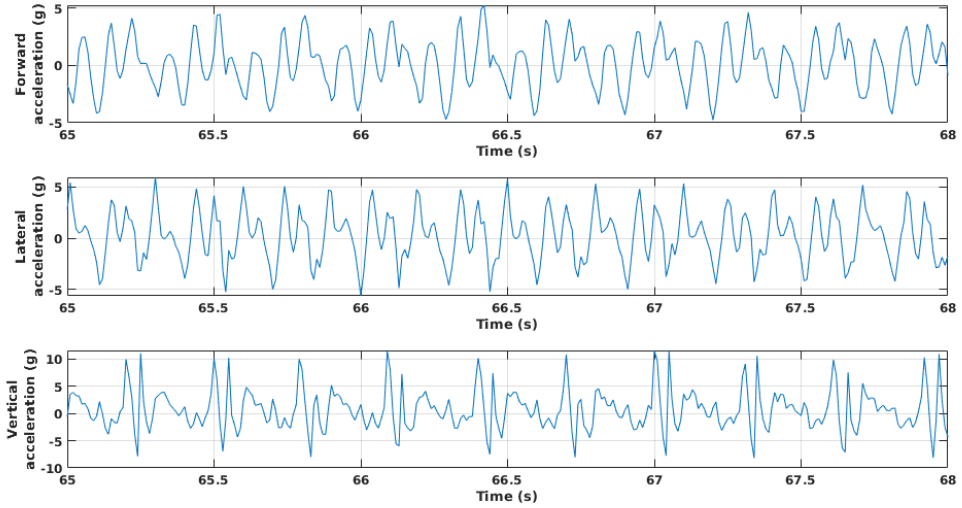

Figure 3.23: A greyhound's proper acceleration as acquired by an IMU device at the track bend with 51 m radius turn.

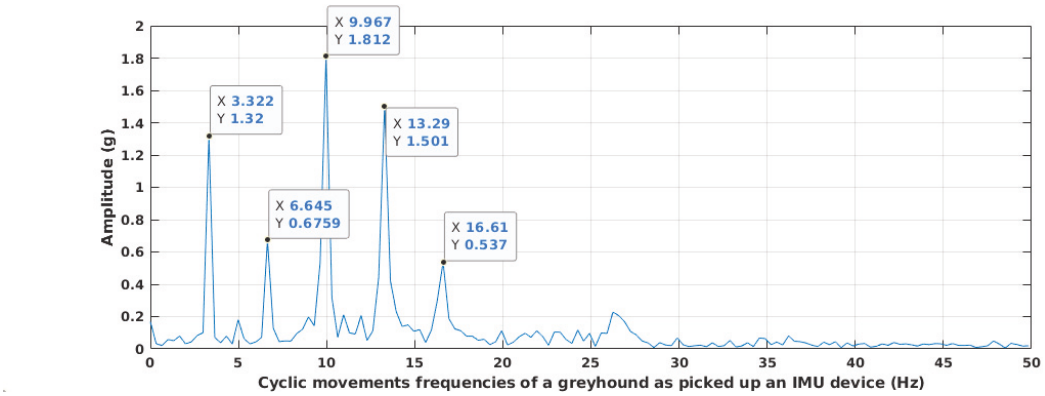

Figure 3.24: Proper acceleration's cyclic components analysis of a greyhound's stride over a three second period using a Discrete Fourier transform algorithm.

Instantaneous stride length and stride speed calculations

From the acceleration data, as retrieved from the IMU devices, the instantaneous stride speed and corresponding stride length were calculated to verify the proper

functioning of the IMU devices acceleration data collection. This calculation also proved that an IMU device could be used to retrieve instantaneous speed and stride length measurements effectively. Figure 3.25 shows one single stride's forward acceleration as retrieved from the 3-Space IMU device for a straight run at a track. The first large peak coincided with the greyhound's hind leg's push-off phase indicating a major forward acceleration action from the greyhound. We can calculate the total acceleration in this phase by looking at the data samples highlighted by the green box, as shown in Figure 3.25. Then, the instantaneous speed during this phase was calculated using Equation 3.3. In Equation 3.3, T denotes the period between the data samples while $v_I[k]$, $v_I[k-1]$, and $a_I[k]$ denote the instantaneous speeds and acceleration at the samples k and $k-1$ respectively. From the IMU data samples as shown in Figure 3.25, the instantaneous acceleration from this phase and corresponding instantaneous speed calculation using Equation 3.3 are shown in Table 3.4. Similarly, the instantaneous displacement during this phase was calculated by integrating the speed data samples, as shown in Table 3.4. By using integration by spline interpolation, the magnitude of the instantaneous displacement was calculated to be 4.3 m. The integration by spline interpolation was used as this method provides the best approximation among other numerical integration algorithms such as Trapezoidal and Lagrange approximations [49]. The calculated instantaneous displacement of 4.3 m provided a rough estimation of the greyhound's stride length. Finally, multiplying the stride frequency which was retrieved from the stride duration with the stride instantaneous displacement gave instantaneous stride speed of 14.5 m/s for the greyhound.

The instantaneous stride length and speed calculations from the IMU acceleration data approximated the actual stride length and the speed of the galloping greyhound. By considering lateral acceleration data of the IMU device along with forwarding acceleration data for the instantaneous stride length and speed calculations, a more

accurate approximation to the actual stride length and speed can be calculated. Finally, a map of instantaneous stride length and speed can be calculated for the entire IMU acceleration data containing a whole race by applying pattern recognition to the IMU acceleration data for recognising large acceleration peaks and calculating corresponding instantaneous stride lengths and speeds.

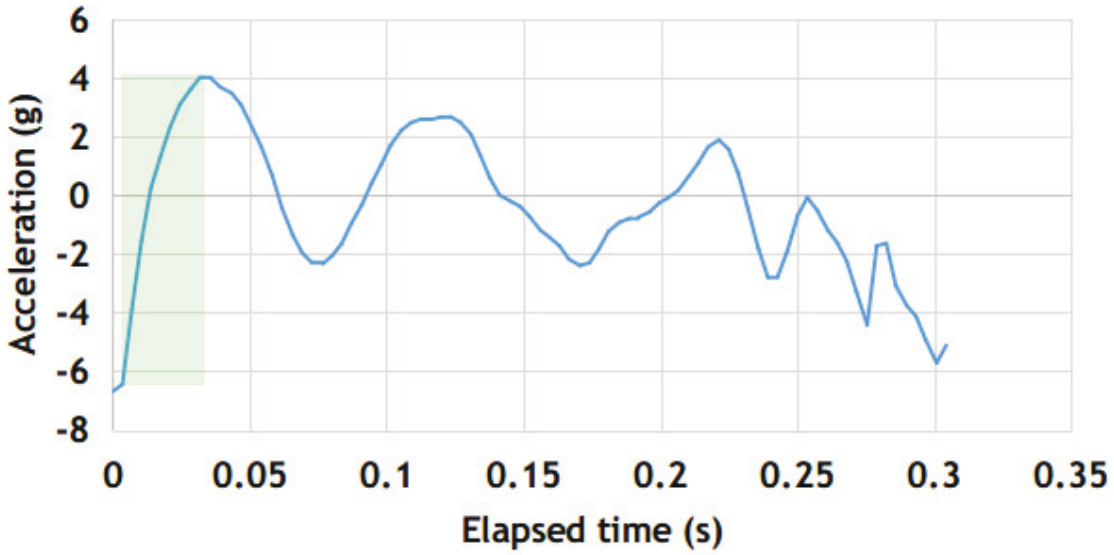

Figure 3.25: Forward acceleration vs elapsed time of a greyhound in the straight as measured by an IMU device's accelerometer for a single stride.

$$v_I[k] = v_I[k-1] + T \times a_I[k] \times 9.81 \tag{3.3}$$

Table 3.4: A greyhound's instantaneous speed calculation from the IMU acceleration data.

Elapsed time (s)	Acceleration (g)	Speed (m/s)
0	-6.69	-0.23
0.0035	-6.44	-0.45
0.0070	-3.88	-0.58
0.0105	-1.55	-0.64
0.0140	0.25	-0.63
0.0174	1.32	-0.58
0.0209	2.31	-0.50
0.0244	3.08	-0.40
0.0284	3.60	-0.26
0.0319	4.01	-0.12
0.0359	3.98	0.04

3.5.4 Real-time location tracking data

The real-time greyhound's location coordinate tracking data which was provided by GRV is a proprietary platform called IsoLynx. The platform captured real-time X and Y coordinates of moving greyhounds and lure during several races relative to a signal tower. The data from IsoLynx system had a sampling rate of 30 ± 3 and a location accuracy of ± 150 mm. However, due to the application of a particular technology for capturing the location data by the system, there were anomalies and noises in the RLT data for GR dynamics calculations. The RLT data of different races were saved in the CSV files, where each CSV file contained captured data samples for time, X and Y coordinates of racing greyhounds and lure for a race. To extract GR dynamics from the RLT data, a Python programming language module was developed during the research period, which processed and analysed the coordinate data. It was found that the RLT data dumped by IsoLynx platform was not

immediately useful for deriving an accurate model of GR dynamics for problems such as difficulty calculating higher derivative due to the presence of random noises in the data. Also, there were issues with the CSV files not following a particular data format for races, individual files not containing data for the entire race periods, and duplicated data samples for a race. The Python module resolved these issues to derive GR dynamics from the RLT data, as shown in Figure 3.26. The module calculated GR dynamics by re-sampling the RLT data to match a greyhound's stride cycle frequency as greyhound's dynamic state change is most observable with every stride. Also, to derive higher derivatives effectively such as velocity, acceleration, and yaw rate the RLT data was filtered as necessary using a custom-designed rolling average filter which removed lagging as usually found in a moving average filter Figure 3.27. Using this approach, the developed Python module generated greyhound's and lure's run distance, heading speed, heading acceleration, heading average speed, yaw rate, and trajectory path curvature from the RLT coordinates data.

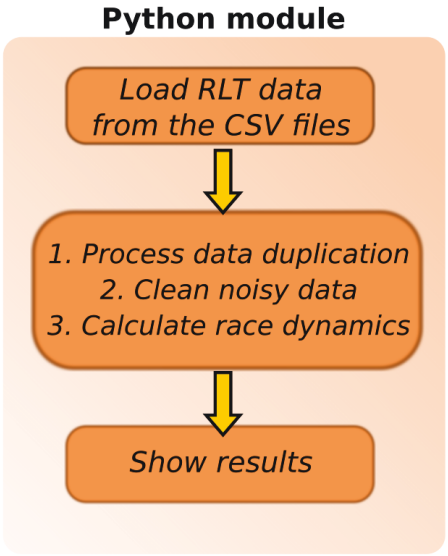

Figure 3.26: Python module functions for generating greyhound racing dynamics from the real-time location tracking data.

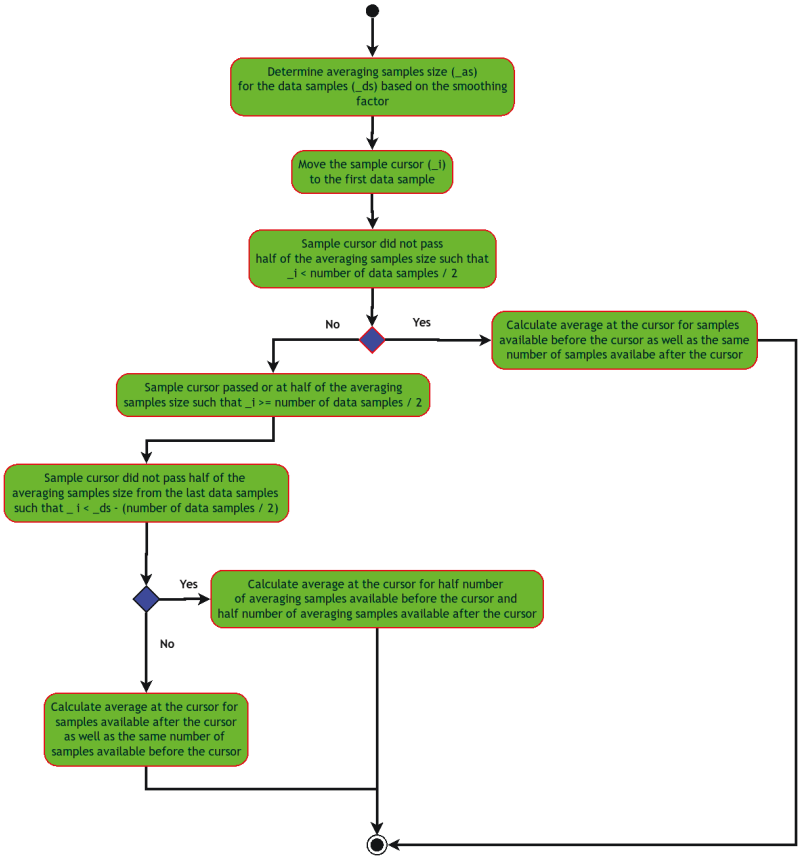

Figure 3.27: Unified Modeling Language activity diagram of a custom variant moving average filter which eliminates lagging or phase delay.

Figure 3.28 shows the diagram of a track for which the RLT data was studied. The track had three distances, a 525 m distance race which begins at the bend transition, a 600 m distance race which begins at the bend, and a 725 m distance which begins at the straight. These configurations for race distance starts are typically found at most oval-shaped GRNSW and GRV tracks. Furthermore, it was evident that by understanding the GR dynamics for these distances races, an abstract model of GR dynamics could be developed for all oval tracks. A total of 71 races RLT data was analysed in the Python module, where 531 racing greyhounds participated during the races. The 525 m distance start race was the most common of all distance races followed by 600 m distance race start. The following graphs illustrate GR dynamics

results as generated from the RLT data using the Python module. The graphs depict RLT data GR dynamics results for 412, 89, and 30 greyhounds for 525 m, 600 m, and 725 m distances races, respectively.

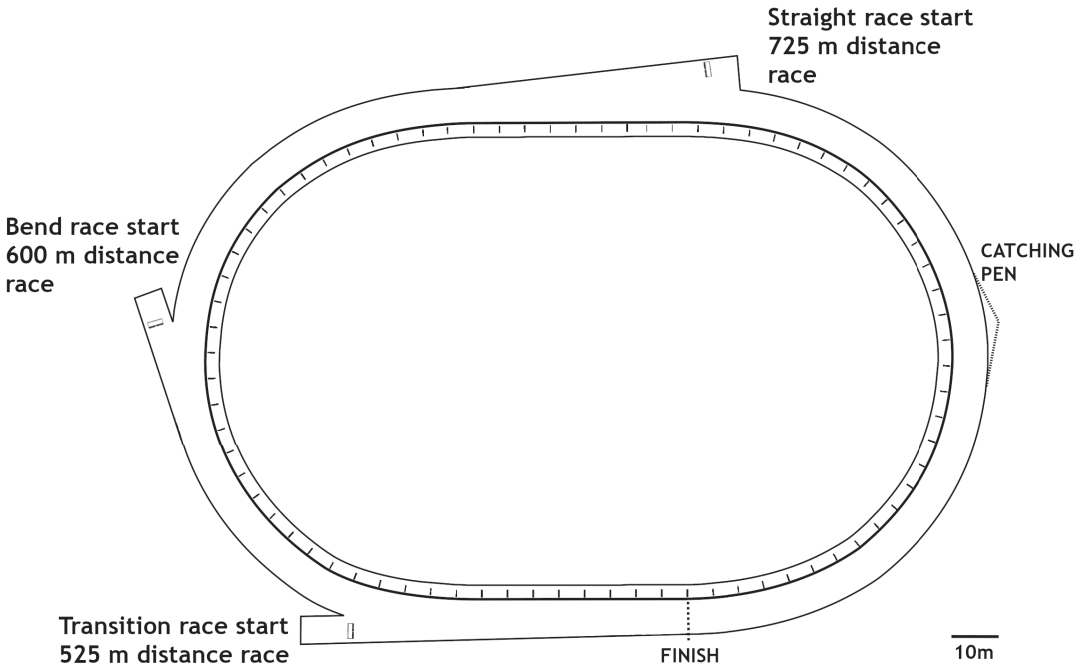

Figure 3.28: The greyhound racing track which conducted the real-time location tracking of racing subjects using IsoLynx platform.

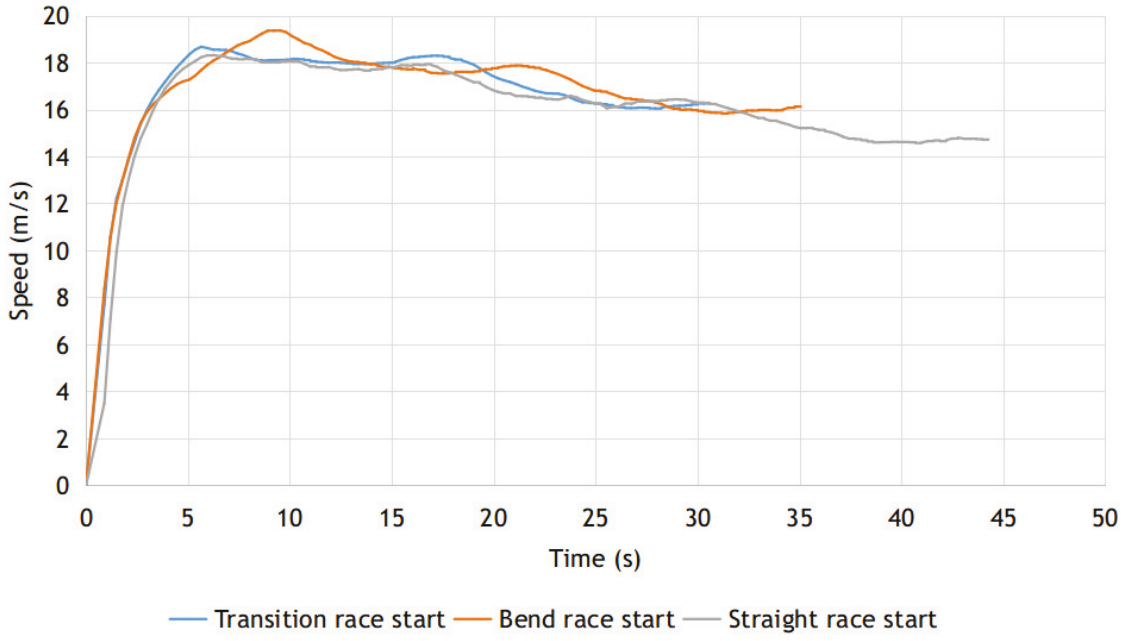

Figure 3.29: Average of greyhound instantaneous heading speed over time for 531 racing greyhounds as produced by the Python module from the real-time location tracking data.

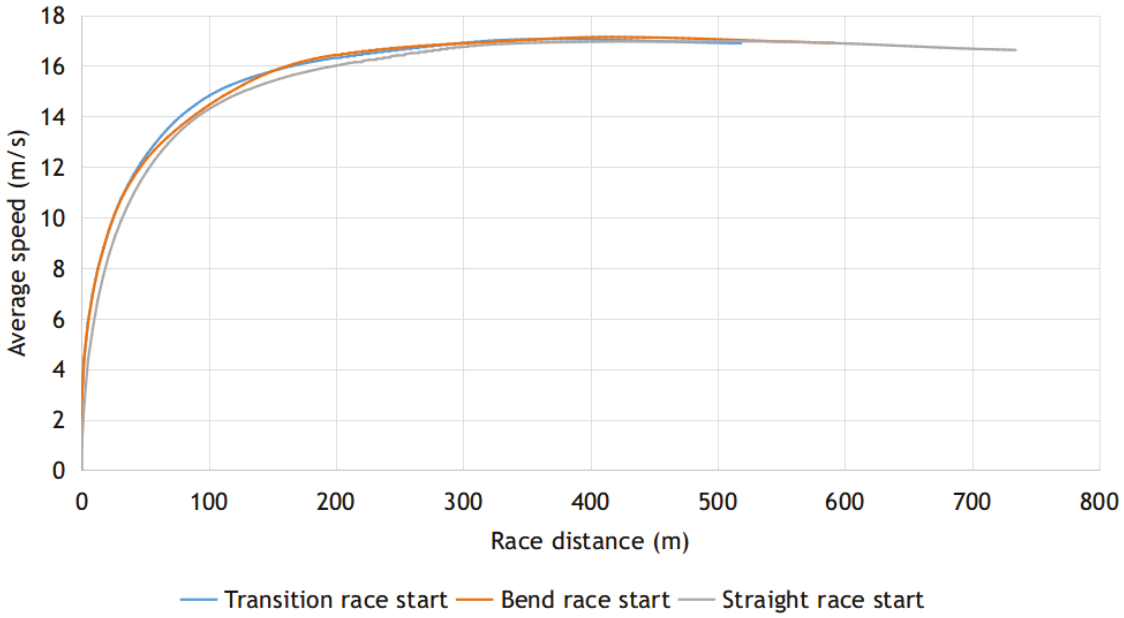

Figure 3.30: Average of greyhound heading's average speed over race distance for 531 racing greyhounds as produced by the Python module from the real-time location tracking data.

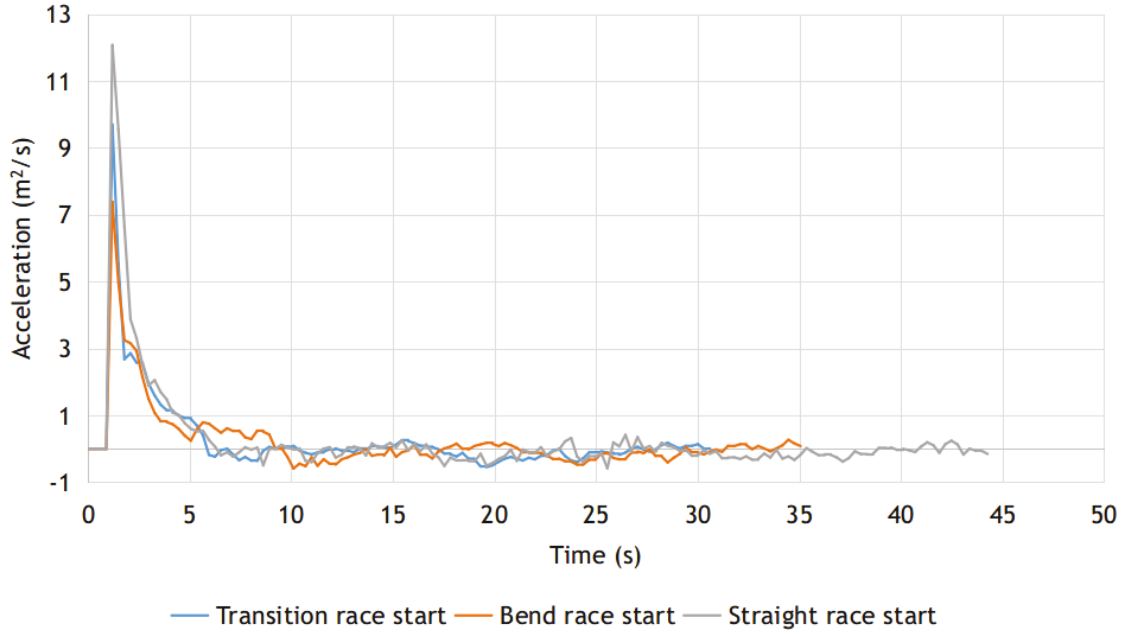

Figure 3.31: Average of greyhound instantaneous heading acceleration over time for 531 racing greyhounds as produced by the Python module from the real-time location tracking data.

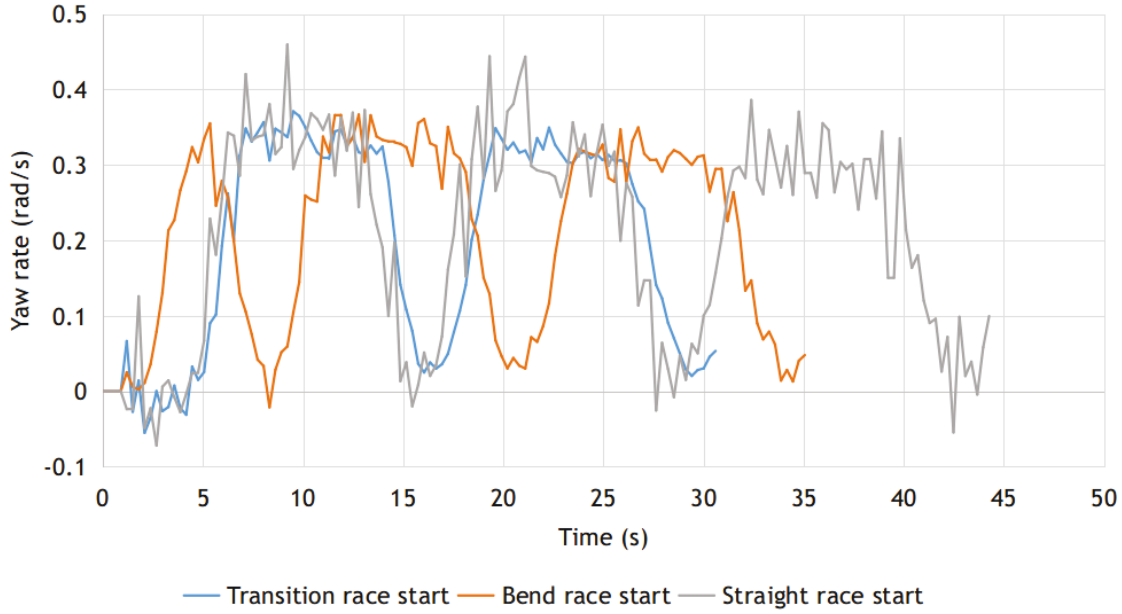

Figure 3.32: Average of greyhound instantaneous yaw rate over time for 531 racing greyhounds as produced by the Python module from the real-time location tracking data.

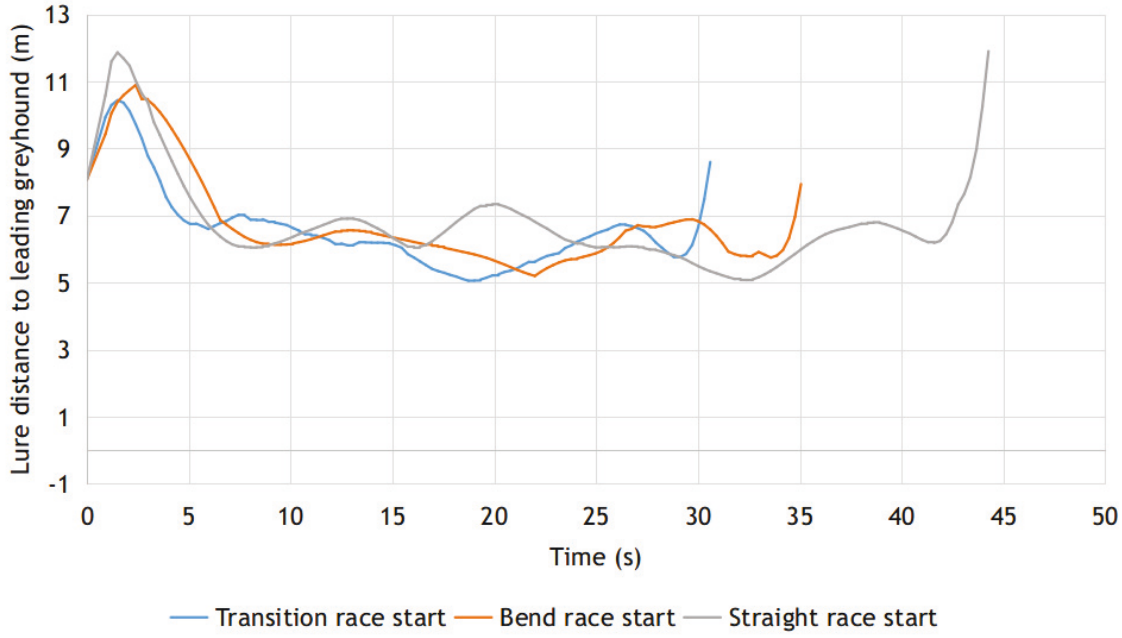

Figure 3.33: Average of a leading greyhound's instantaneous separation distance from the lure over time for 71 races as produced by the Python module from the real-time location tracking data.

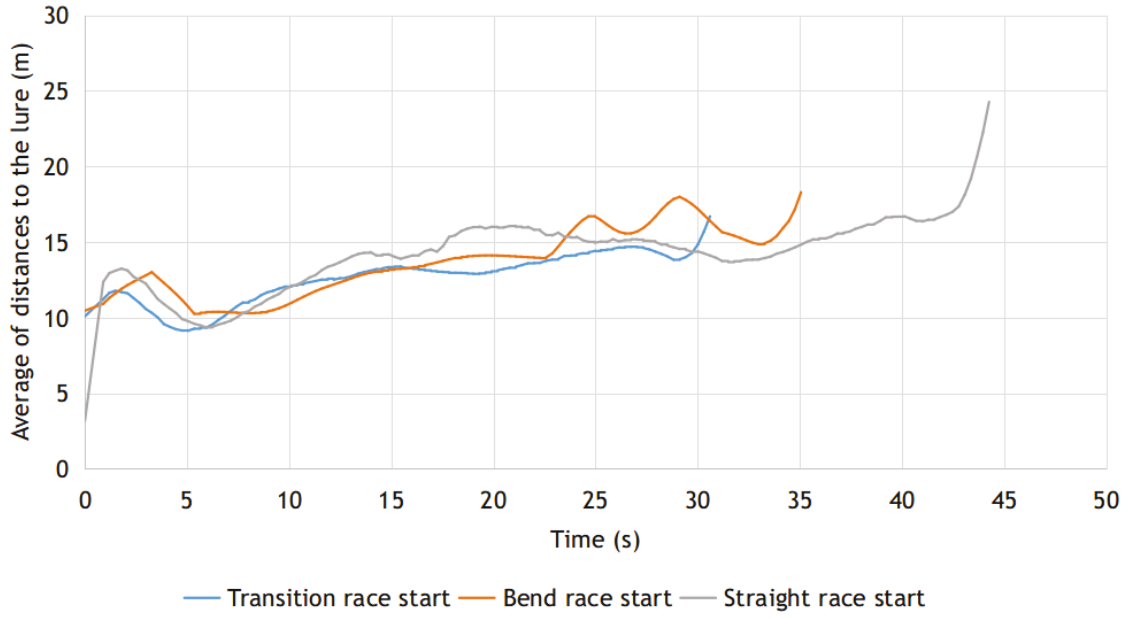

Figure 3.34: Average of greyhounds' instantaneous average distance from the lure over time for 71 races as produced by the Python module from the real-time location tracking data.

As can be seen from Figure 3.29 that greyhounds aggressively accelerated during the first 5 seconds of the races for all distances raced where their speed went above 64 km/h or 17.6 m/s. In terms of speed profile, both the transition and straight start distances raced were similar. However, the bend start distance races made greyhounds accelerate for a significantly longer period. Also, the maximum speed reached by the greyhounds for the bend start distance races was considerably higher with approximately 19.4 m/s compared to 18.7 m/s, and 18.3 m/s for transition and straight starts distances respectively. After the initial acceleration phase, the greyhound speed came down gradually for the remaining race periods and was proportional to the distances covered by the greyhounds. The lowest speed observed for the straight start 725 m race distance was 14.6 m/s whereas for the bend 600 m and the transition 525 m distances it were 15.8 m/s and 16.0 m/s respectively. The average speeds of the greyhounds are plotted in Figure 3.30 which showed that grey-

hounds acceleration was high within the 100 m run distance from the race starting points for all distances raced regardless of the starting point orientations such as straight, bend, or transitional starts. This implied that a greyhound would be accelerating at the bend if the track straight section is no longer than 100 m in length. Figure 3.31 depicts greyhounds' instantaneous heading acceleration which revealed that the initial acceleration was highest for the straight start distance raced while it was lowest for the bend start distance raced at roughly 12.0 m/s^2 and 7.4 m/s^2 respectively. After the initial jump out from the race start box acceleration phase, the peak heading acceleration during the races was similar for all start type race distances at approximately 0.54 m/s^2. The average greyhound yaw rates for races are presented in Figure 3.32, which measured how quickly greyhounds were turning during the races. Both the straight and the transitional start distance raced showed a similar pattern for the box to track transitional greyhounds' turning which can be seen between 0 and 5 seconds race periods where the greyhounds' directions fluctuated before entering the bend. The maximum boxes to the track path transitional turning occurred for straight start distance raced where it was around 0.13 rad/s, whereas the minimum seen for the bend start distance raced was about 0.03 rad/s. This showed that bend start races were more streamlined for greyhound racing lines. Figure 3.33 displays an average of the lure distances maintained from the leading dogs during races. It showed that lure distances were settled and fluctuated about 6 m from the leading dogs 5 seconds into the races. Moreover, it can be seen that the initial lure and greyhound separation distance was increased to more than 10 m for all distances raced, where it was rapidly reduced again within 3 seconds. Figure 3.34 illustrates the average of races for average greyhounds' distance from the lure where it showed the greyhounds distances from the lure increased gradually with the distance and was identical for the straight, bend, and transitional starts distances raced.

3.5.5 Paw prints survey data

The coordinate data of a greyhound's paw prints on the track surface was collected after a trail run as shown in Figure 3.35, which revealed stride length details at the various track sections of a track. From the coordinates of the paw prints, the average stride length for the track bend was found to be around 5.15 m whereas for the straight run it was about 5.5 m. This showed that the stride length varied depending on the nature of track path curvature although nothing can be said about the stride frequency from the same data analysis due to lack of time information for the paw prints. Finally, the paw prints coordinate data showed that the greyhound was making transitional trajectory into the bend rather than immediately merging with the bend when coming out from the straight which was found by measuring the perpendicular distances of the paw prints from the lure rail. For the straight run, the paw prints distances to the LRP fluctuated between 50 and 60 cm and from the start of the bend after the straight run the distances of the paw prints to the lure rail gradually increased to 120 cm which then again gradually dropped back to 50 cm at the bend. This indicated that the greyhound was trying to minimise the onset effect of centrifugal acceleration while travelling the track path.

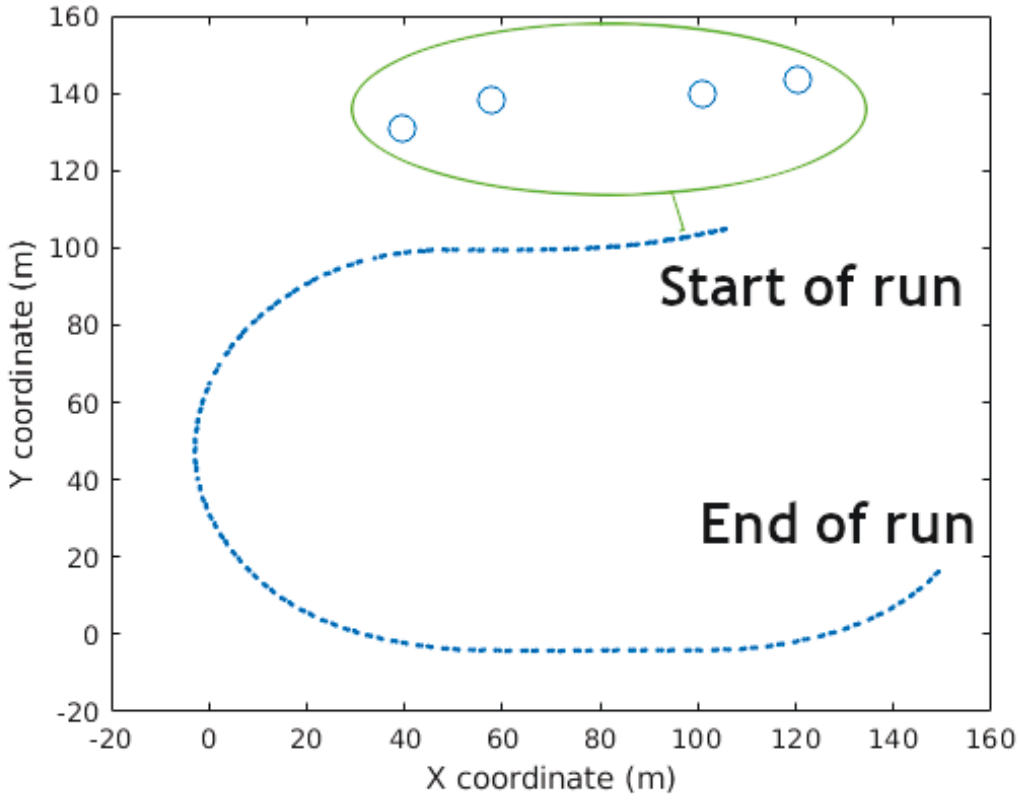

Figure 3.35: Paw prints on the track surface by a greyhound during a trail race at a track from the starting boxes to just before approaching the catching pen.

3.5.6 Radar gun speed data

A Stalker Radar Sport 2 was used to measure greyhounds' top speed at various track locations in two different tracks for several race trails. Figure 3.36 shows the aim and locations of the radar gun at the tracks while measuring the speeds of the greyhounds. The average value of speed measured by the gun to be 70.3 km/h. However, as the radar gun was not parallel to the heading of the greyhounds and the track path as can be seen from Figure 3.36, using trigonometry the corrected value for the average greyhounds' speed found to be 69.9 km/h or 19.4 m/s.

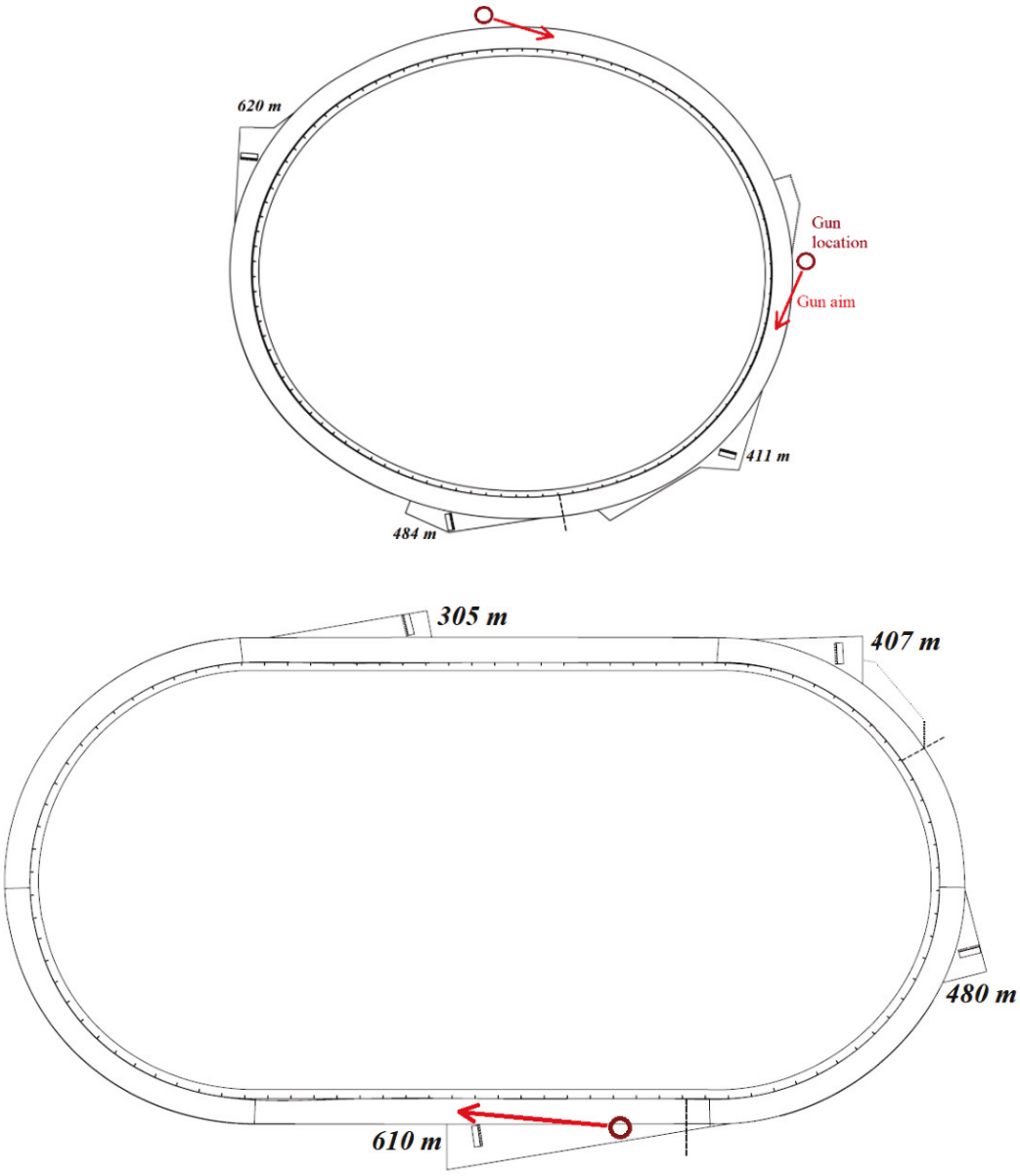

Figure 3.36: Placements and aims of a radar gun for greyhound speed measurement at two tracks.

3.6 Data modelling

3.6.1 Track path geometry modelling

The path of the GR tracks defines the apparent racing line for running dogs. It was essential to analyse the construction of the tracks' paths, to understand path

smoothing properties of a track layout's imposed racing line. The SD provided by GRNSW and GRV contained track paths as coordinate points and lacked details about track paths features such as horizontal transition type and extent. Two approaches were followed to model the actual track path between a straight and a bend from the SD. In the first approach, three points arc primitive tool was used in SolidWorks and AutoCAD CAD software to approximate a track's path where the points of the circular arc lied on the circumference. This gave the radius of curvature and the centre of curvature of the track path as determined from the points lying the circular arc. Then to create a track path transition, one or more point arcs were fitted into the track path coordinate points where the arcs were constrained by the tangent constraints. This approach gave a rough estimation of the nature of the horizontal transitions that exist at an SD track. Figure 3.37 shows a track path as modelled using the first approach which showed that the track transition was made up of a large constant radius bend as depicted between points A and B. In the second approach spline primitive tool was used in SolidWorks CAD software to find the precise curvature of the track path transition. The spline primitive used was a B-spline that can be used for modelling complex curves by manipulating several control points. A track path was modelled by placing the spline control points on the track path coordinate points and applying spline primitive internal curvature and tangent continuities and spline boundary tangent continuity. In this approach, the internal geometry of a track path transition was accurately modelled compared to the first approach. Both approaches used for modelling a track path transition revealed the degree of continuity of SD tracks paths. The modelling of the SD tracks paths showed that all tracks have either zero-order (position matches between the track segments) or first-order (tangent matches between the track segments) degree of continuity as shown in Figure 3.38. This pointed out that only the position and tangent matched between the track segments. Likewise, the modelling of SD tracks

showed that the maximum radius of curvature for tracks starts from a 1000 m radius. This implied that a straight segment of a track path consisted of several 1000 m radius arc segments.

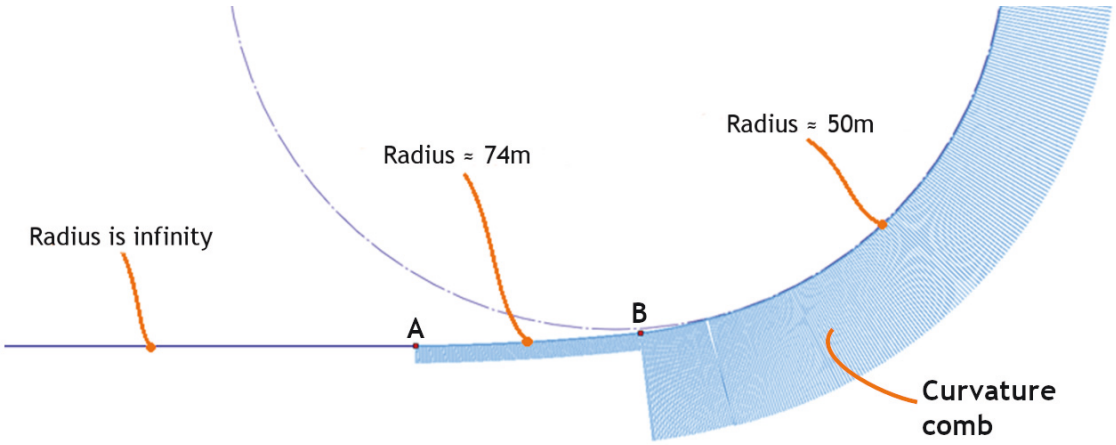

Figure 3.37: Modelling of a track path horizontal transition by three points arc tool, where the track path is depicted by a solid dark blue curve and the path curvature is depicted by the perpendicular lines comping out from the track path.

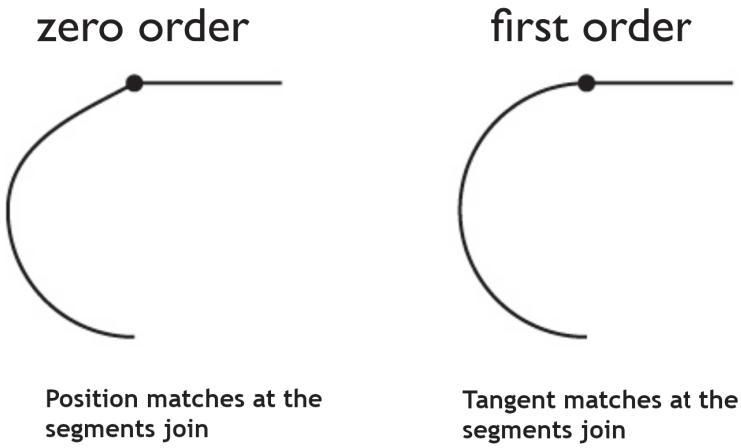

Figure 3.38: Track path geometry continuity kinds as found from modelling track path data coordinate points.

3.6.2 Centrifugal acceleration jerk calculation

Centrifugal acceleration is experienced by greyhounds when they navigate around oval tracks. Depending on the track radius of the bend there would be maximum centrifugal acceleration around the bend while no centrifugal acceleration in the straight. The bodies experience the change in centrifugal acceleration as centrifugal acceleration jerk [50]. Essentially, jerk can be thought of as an increasing or decreasing of the centrifugal force in the greyhounds. Furthermore, the jerk has applications in safety measurements in many disciplines, including civil designs such as road designs [50]. It was deemed to be paramount to analyse jerk outputs of quadruped greyhounds track designs to measure the safety soundness of the tracks.

The first step into jerk modelling for a track path was finding track radius of curvature at all points in the track path and relate that to the greyhound's path navigation instantaneous radius of curvatures. From the tracks SD the track path points were extracted. From that, the lure travel path was modelled by taking an offset of the LRP. The lure travel path which closely coincides with the chainage of a track path approximates the racing line of the leading greyhound which is not affected by other greyhounds. The leading greyhound racing line as defined by the lure travel path and track chainage can be thought of like the track path's exposure for the greyhounds which provides an estimation of track path conditions as exposed to the greyhounds. Likewise, it was found from the greyhound's gait analyses that the movements of a greyhound in the land can not be thought as continuous movement like in a car or in a train that stays on the ground all the time while it's moving. A greyhound applies forces to the ground whenever the paws contact the ground. From the gait analyses, it can be said that a greyhound changes its both heading speed and direction with every stride such that its dynamic state change occurs stride-wise as observed from the IMU and HFR data analyses. Figure 3.39 shows an example of greyhound turning while entering the bend, which is changing with

every stride. So, all location coordinates of a greyhound for every stride for the circumference of a track were calculated that gave the greyhound's approximate path navigation during a race, as shown in Figure 3.40. Then, in the second step, the instantaneous radius of curvatures of the greyhound running path was calculated from the greyhound's location coordinates using either the circumradius formula or the perpendicular bisectors method. The circumradius formula (3.4) was chosen between two methods as it provided more radius of curvature results for the location coordinates points Figure 3.41. The circumradius formula takes three location coordinates from the greyhound running path coordinates which are in sequence to calculate the radius of circumcircle which is the instantaneous radius of curvature during a stride. This way, all the instantaneous radius of curvatures of a greyhound running path for a track was calculated. In the last step, the centrifugal acceleration was calculated by plugging in greyhound's instantaneous speed as found from the data analyses into the acceleration Equation 3.5. Finally, the jerk was derived from the ROC in the centrifugal acceleration (3.6).

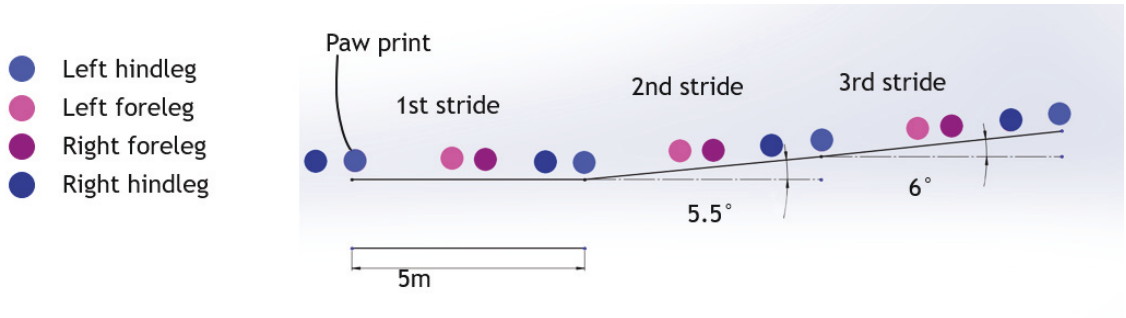

Figure 3.39: A greyhound's heading change angle while entering a bend from a straight.

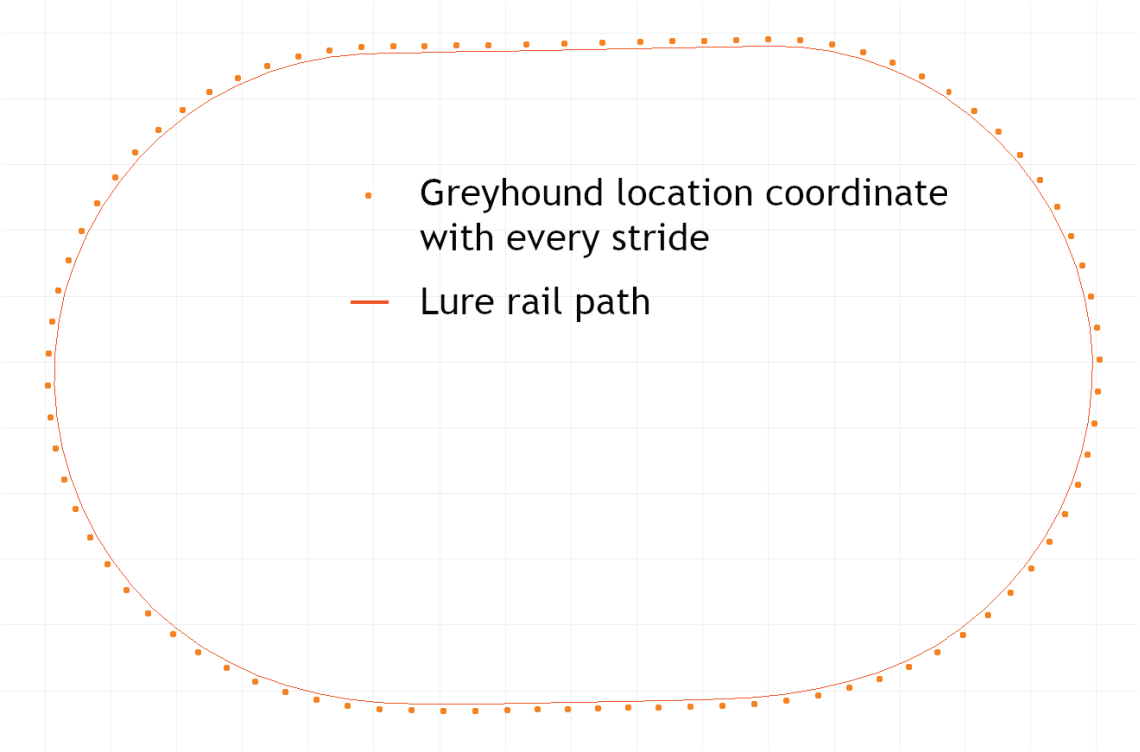

Figure 3.40: A greyhound's location coordinates(pink) at a track while following a lure.

$$\rho = \frac{abc}{4A} \tag{3.4}$$

Where a, b, and c denote the three sides of a triangle defined by the three adjacent greyhound location coordinate points and A is the area of the triangle.

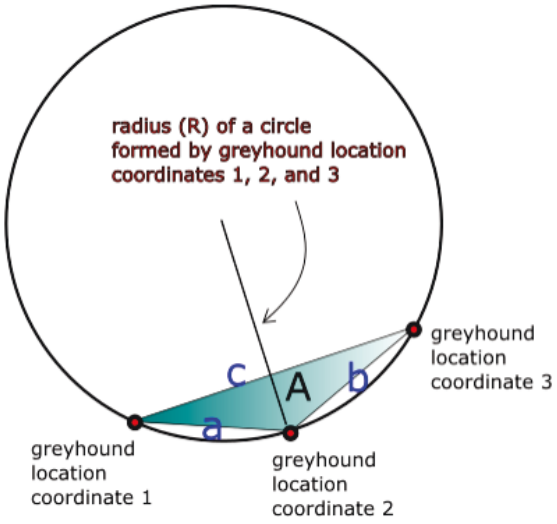

Figure 3.41: Circumcircle of a triangle formed from a greyhound's path navigation point coordinates lying in sequence.

$$a_c = \frac{v^2}{\rho} \tag{3.5}$$

$$j = \frac{\Delta a_c}{\Delta t} \tag{3.6}$$

Figure 3.42 depicts centrifugal acceleration (m/s^2) and corresponding centrifugal acceleration jerk (m/s^3) calculations for a GRV track race distance by taking RLT data greyhound average speed model and assuming 32 kg greyhound mass. Furthermore, for all the SD tracks analysed calculations showed maximum and minimum jerk values of 16.2 and 8 m/s^3 respectively for greyhounds when greyhound maximum instantaneous speed is 19.5 m/s, mass is 32 kg, and approximately followed track chainage line. This centrifugal acceleration jerk is deemed to be considerably higher than what is regarded acceptable in other areas such as railway and road designs. A maximum permissible jerk value of 0.3 m/s^3 is considered to be standard in moving railway vehicles [51] for maintaining passenger ride quality.

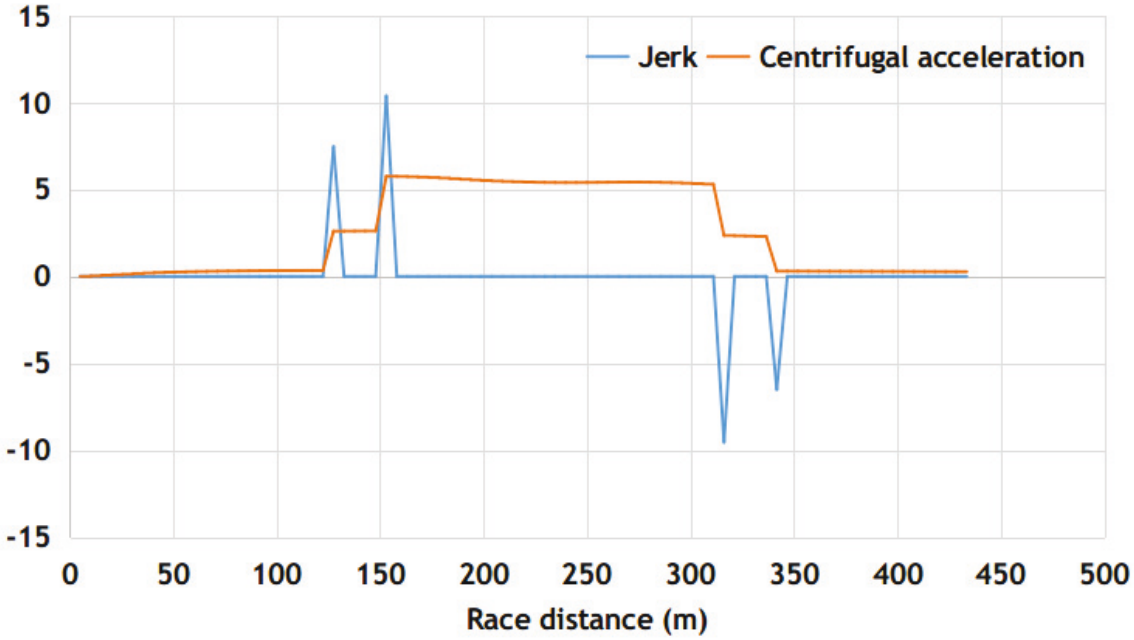

Figure 3.42: Theoretical calculation of centrifugal acceleration and centrifugal acceleration jerk for a greyhound race.

3.6.3 Maximum speed limits of a racing greyhound at a bend

Due to bends at the oval tracks, the centrifugal force would limit the maximum speed at which a greyhound could navigate around a bend without losing support from the ground. Furthermore, from Newton's second law (3.7), it can be said that the directional forces acting on a greyhound on the track are directly proportional to its motion. To find a greyhound's speed limit at the track bends a planer forces analysis was carried out to derive the equation of motion which would provide a theoretical speed limit hint when factors such as track bend radius, track bend cross fall, and surface static friction coefficient are known between a greyhound's paw and track ground. Figure 3.43 illustrates planer forces acting on a greyhound for an instance when the greyhound is about to slip as it is travelling a bend section of a track. The frictional force that is acting opposite to the centrifugal force would prevent the greyhound from sliding up the slope along the width of the track. The

parameters such as the greyhound's mass, lean angle, the track's cross fall angle, the coefficient of static friction between the greyhound's paw and track ground, and the track's radius of the bend would determine the maximum constant speed at which the greyhound can travel without paws slipping off the track. Now, for a greyhound moving along a curved path like track bend, all the acting forces can be grouped along three different axes namely t, b, and n like shown in Figure 3.43. The sum of tangential forces ΣF_t, acting along t axis (perpendicular to the figure) would accelerate the greyhound forward, whereas the sum of lateral forces ΣF_n, acting along the n axis would help the greyhound change its direction as required for navigating along the bend. And finally, the sum of vertical forces ΣF_b, acting along the b axis would keep the greyhound on the ground.

$$a = \frac{\Sigma F}{m} \tag{3.7}$$

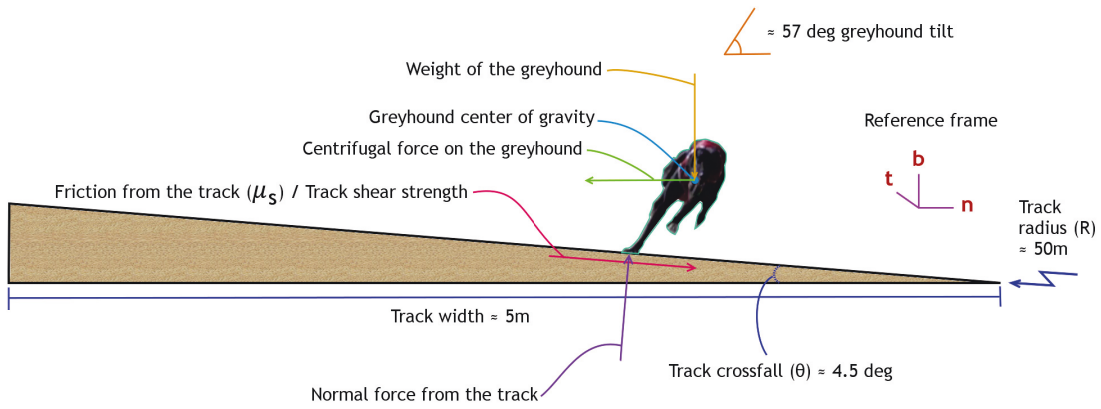

Figure 3.43: Planer forces on a greyhound at a track bend.

As can be seen from Figure 3.43, the main horizontal and vertical forces that are

acting on the greyhound along the b and n axes are:

1. The weight of the greyhound,

$$W_g = mg \tag{3.8}$$

   Where m is the mass of greyhound and g is the acceleration due to gravity.

2. The centrifugal force which is an inertial force,

$$F_c = \frac{mv^2}{R} \tag{3.9}$$

   Where v is greyhound speed and R is radius of curvature of the track bend at the instance.

3. The normal force N from the track ground which is a reaction force,

$$N = mgcos\theta \tag{3.10}$$

   Where θ is the track cross fall angle.

4. The frictional force from the track ground,

$$F_f = \mu_s N \tag{3.11}$$

   Where μ_s is the coefficient of static friction which depends on both the track ground and greyhound paw surface conditions.

Now, let us assume the greyhound in Figure 3.43 is travelling on a fixed navigation path where the curvature of the path closely follows track curvature and the vertical displacement of the greyhound is zero due to uniform track cross fall along the greyhound racing line. As a result, the sum of all the forces which are parallel to the reference frame axis b should be zero according to Newton's second law of motion like given below:

$$\Sigma F_b = ma_b \tag{3.12}$$

When $a_b = 0$ for no vertical displacement by the greyhound,

$$\Sigma F_b = 0 \tag{3.13}$$

Or,

$$(\uparrow +) N cos\theta - W_g - F_f sin\theta = 0 \tag{3.14}$$

Where $Ncos\theta$ and $F_f sin\theta$ are vertical force components of normal (N) and static frictional (F_f) forces respectively.

On the other hand, the lateral acceleration a_n acting on the n axis can be attributed to centrifugal acceleration $\frac{v^2}{R}$. Therefore, applying Newton's second law of motion for the forces parallel to n axis,

$$\Sigma F_n = m a_n \tag{3.15}$$

When $a_n = \frac{v^2}{R}$,

$$\Sigma F_n = m \frac{v^2}{R} \tag{3.16}$$

Or,

$$(\rightarrow +) N sin\theta + F_f cos\theta = m \frac{v^2}{R} \tag{3.17}$$

Now, from the Equations 3.14 and 3.17, the greyhound's speed is,

$$v = \sqrt{\frac{Rg(sin\theta + \mu_s cos\theta)}{cos\theta - \mu_s sin\theta}} \tag{3.18}$$

Here, v is the maximum speed of the greyhound achievable without sliding up the track slope. As can be seen from the Equation 3.18, the maximum tangential speed v_{max} of a greyhound is a function of a track's bend radius of curvature, a track's camber angle, and coefficient of static friction between a track's ground and a greyhound's paw. Now, let's assume the track ground and the greyhound's paw in Figure 3.43 have a coefficient of friction of about 0.5. This is based on the assumption that the coefficient of static friction for the majority of the organic and non-organic material interface surfaces contact falls below 0.6. Also, experiments show that with the increase of moisture in the contact interface the coefficient of friction stays under 0.5 for high to low friction coefficient materials [52]. Likewise, many greyhound tracks across Australia tend to have a minimum bend radius of 50 m and minimum cross fall angle of 4.5 deg for which the maximum achievable speed calculated using (3.18) for a greyhound is 17.2 m/s when the coefficient of friction is about 0.5. Table 3.5 shows calculations of achievable maximum dog speed when track cross fall is 4.5 deg and coefficient of static friction is 0.5 for different bend radii:

Table 3.5: Track bend radius and corresponding achievable maximum speed limit.

Bend radius (m)	**Limiting speed (m/s)**
50	17.2
55	18.0
60	18.8
65	19.6
70	20.3
75	21.1
80	21.7

As can be seen from Table 3.5, the tracks which have bend radius smaller than 65 m is not able to sustain maximum greyhound speed of 19.5 m/s as found from the various data sources when the track cross fall is 4.5 deg and track ground coefficient of static friction is 0.5.

3.6.4 Maximum leaning of a greyhound at a bend

The maximum greyhound leaning at a bend track section can be modelled by analysing the forces acting on a greyhound perpendicular to the direction of heading at the bend for an instance when a paw contacts the ground like shown in Figure 3.44. At the bend, when a paw contacts the ground it touches the ground at an angle that is approximately identical to the greyhound leaning angle. The normal force balances the force from the paw from the ground, which is a reaction force and has the same magnitude and angle as force delivered by the paw. To get the leaning of the greyhound, the angle of the normal force can be calculated. For this the inverse of the tangent function from the components of normal force such as force from the friction which balances the centrifugal force and weight support force which balances weight force of the greyhound can be taken. However, the forces from the friction and weight support force have the same magnitude as centrifugal force and greyhound weight, respectively. So, a greyhound's leaning angle at a bend can be calculated using Equation 3.19, which is the same angle for normal force from the ground.

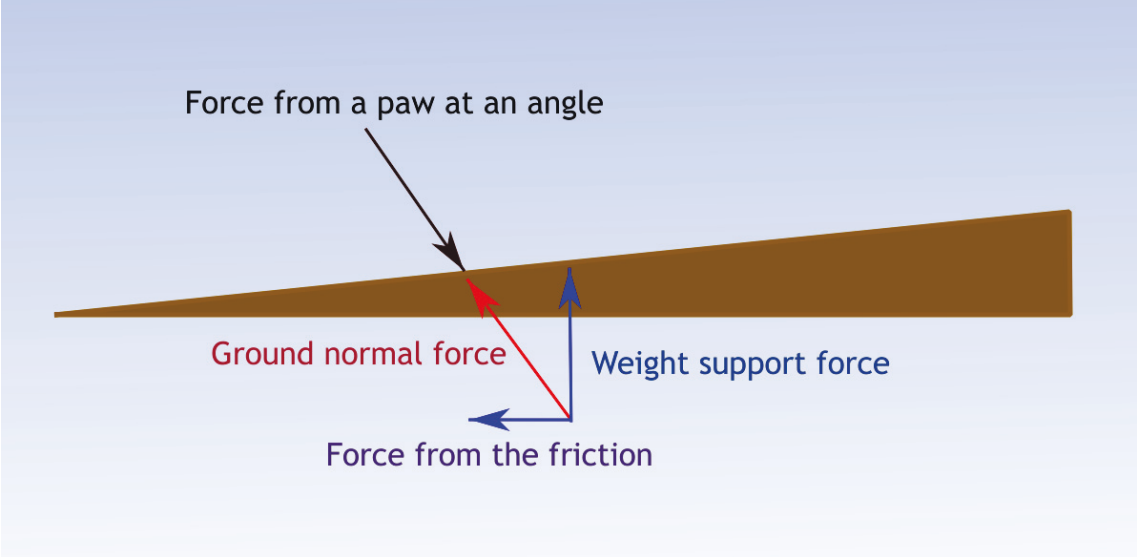

Figure 3.44: Greyhound ground normal force at the track bend.

$$\theta = tan^{-1}\left(\frac{gR}{v^2}\right) \tag{3.19}$$

Where v is the greyhound's instantaneous speed at the bend and R is radius of curvature of the track bend at the instance.

Equation 3.19 shows that the greyhound leaning amount at the bend does not depend on the mass of greyhound and only depends on the radius of the bend and its instantaneous speed. Now, by considering maximum greyhound speed of 19.5 m/s, the maximum and minimum leaning of a greyhound at the GRNSW and GRV tracks was calculated to be 60.3 and 47.6 deg respectively. However, this calculation assumed force from the friction to be exactly equal to the centrifugal force of corresponding tracks which may not be the situation for every track due to track cross fall preparation and track surface material differences between the tracks.

3.6.5 Paw ground impact penetration depth estimation

Depending on the race track surface nature and preparation, quadruped paws penetrate the upper layer of the ground which aids galloping gait. From the paws, vertical speed tracing HFR analyses data estimation of penetration depth due to paw and ground impact can be modelled using the principle of linear impulse and momentum and the principle of work and kinetic energy Equations 3.20 and 3.21. Now, dividing Equation 3.21 by (3.20) gives Equation 3.22 where Δx or h denotes the paw's ground upper layer penetration depth as shown in Figure 3.45. For example, using the Equation 3.22 the paw ground impact depth penetration calculation showed 66.5 mm and 57.0 mm ground penetration by hind left and right paws respectively for data showed in Figures 3.16 and 3.17. This is because the initial vertical velocity v_1 of the left hind paw was -7 m/s and the final velocity v_2 was 0 m/s as the paw displacement was zero after the ground penetration and the time duration for impact was 0.019 s. Likewise, the initial vertical velocity v_1 of the right hind paw was -6 m/s and the final velocity v_2 was 0 m/s and the time duration for impact was 0.019 s.

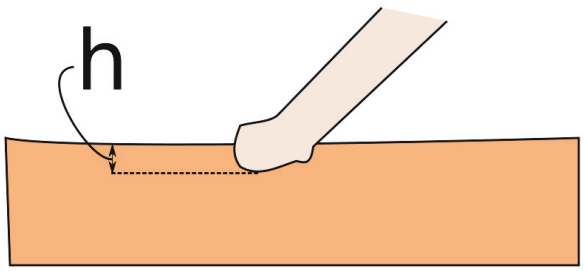

Figure 3.45: A quadruped paw's track surface penetration during galloping.

$$F\Delta t = m(v_2 - v_1) \tag{3.20}$$

$$W = F\Delta x = \frac{m}{2}(v_2^2 - v_1^2) \tag{3.21}$$

Where F is the average paw ground impact force, Δx is the ground impact penetration depth, Δt is the impact duration, and v_2 and v_1 are the final and initial speeds during the impact respectively.

$$h = \Delta x = \frac{\Delta t}{2}\frac{(v_2^2 - v_1^2)}{(v_2 - v_1)} \tag{3.22}$$

The paw ground surface penetration modelling Equation 3.22 would help design track surface for best greyhound dynamic outcome at the tracks and also benchmark various track surfaces. Furthermore, the equation can be used to identify and compare the performances of different galloping quadrupeds from the paw penetration depths data.

3.6.6 Paw ground impact force estimation

Calculation of forces experienced by the galloping quadruped paws is essential for learning anomalies in the gait and injury patterns. When a galloping quadruped paw hits the ground with a certain velocity, the impact force generated by the paw kinetic potential energy is represented by Equation 3.23. In Equation 3.23, m is the mass of impact which can be calculated by solving rigid-body dynamics for quadruped paw limb, limb joints, and quadruped body. Furthermore, the work carried out by a paw during an impact can be modelled by work done by a spring force, as shown in Equation 3.24. This is because the reaction force from the ground during the impact slows down the impacting paw as if an uncompressed spring would slow down an impacting object. The impact force magnitude of the paw is equal to the ground reaction force magnitude, as modelled by the spring force (3.25) with spring's stiffness constant k which is the stiffness of the ground upper penetration

layer. In Equation 3.25, F_{max} is the maximum force at the end of ground upper layer penetration due to maximum spring deformation like shown in Figure 3.46. Now, by plugging in $|kx|$ from Equation 3.25 into Equation 3.24 we arrive at Equation 3.26. Finally, as the kinetic energy of a paw is converted to work during the ground impact we can combine Equations 3.23 and 3.26 to derive paw impact force Equation 3.27.

$$E = \frac{1}{2}mv^2 \tag{3.23}$$

$$W = \frac{1}{2}kx^2 \tag{3.24}$$

$$F_{max} = |kx| \tag{3.25}$$

$$W = \frac{1}{2}F_{max}x \tag{3.26}$$

$$F_{max} = m\frac{v^2}{x} \tag{3.27}$$

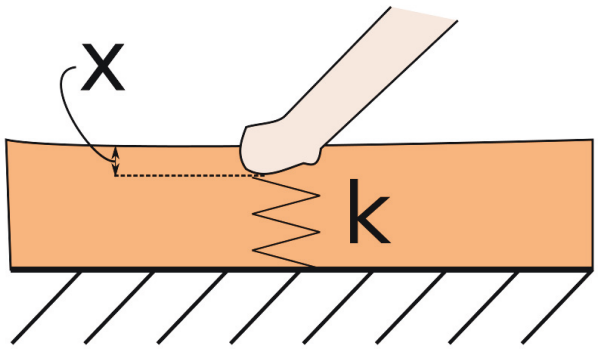

Figure 3.46: Track ground reactionary force as spring force for a quadruped paw during paw's ground upper layer penetration in a gallop.

From the previous section, it is calculated that for a straight greyhound galloping stride the hind left and right paws motion resulted in approximately 66.5 mm and 57.0 mm ground depth penetrations where the vertical speeds of the paws were -7 m/s and -6 m/s respectively. Now, by using Equation 3.27 and by assuming m is identical for both paws the paw impact forces for the hind left and right paws are 736.8m N and 631.6m N respectively.

3.7 Summary

The information gathering was a significant step for the research. A considerable amount of time and attention was required to understand and apply the diverse disciplined information for the research. The information gathered during the research period paved the way to learn all the fundamental aspects present in both the fast quadruped greyhound racing as well as existing race track designs and racing conditions. Major parameters were identified for the research, and accurate values of the parameters were observed through data processing, analyses, and modelling. Furthermore, a better understanding of simulation results and refinements to simulation models and procedures were possible due to information gathering and modelling. This also defined the goals for research for racing simulation and modelling techniques development.

Chapter 4

Formulating and implementing a quadruped racing simulation platform and modelling techniques for dynamically stable track designs

4.1 Introduction

With the advent of powerful computing in this age and time where the computer processors can crunch a large set of information quickly and efficiently computer simulation and modelling became a cornerstone in design and development. From an industry point of view computer modelling and simulation significantly reduces development time and cost while increasing task efficiency. One major area that has always been the focus of computer modelling and simulation is testing new designs and activities to collect evidence for production and deployments. For galloping quadruped racing at the tracks, a traditional approach for analysing race dynamics can be cumbersome and difficult to achieve. This is because traditional techniques such as graphical and analytical methods sometimes lack accuracy and the complexity can increase exponentially for a relatively simple practical problem [53]. An alternative solution is numerical analysis and methods through the fast processing of alphanumeric data, data formulation, and computational methods [53]. In the numerical approach, mathematical models are developed from the observation of physical and technical processes where derived equations are computed at discrete points in time [54]. Furthermore, the availability of corresponding physical or technical processes results would allow verification of numerical results or improvements to developed numerical model methods [54].

When this research began, there was little to no scientific evidence to support track design and race operational alternations and changes demands as required for GRNSW and other industrial jurisdictions. It was a necessary step forward to simulate race behaviours in the computer models to test and justify various decisions that were being taken by the industry. Also, it was an indispensable need for the data gathering process to simulate race dynamics to find provisions for the data gathering. As the effects of various track and racing elements on the race dynamics were not clear and race elements detail data was not available immediately, simulation and modelling of known and hypothetical factors paved the way for progressively bringing shifts and changes in the industry. This in result brought more varying and diverse data from the galloping quadruped racing events in the coming years.

Recently, the galloping quadruped racing sport has grown exponentially due to the accessibility of live wagering and various revenue sharing programs [55]. Consequently, it has become evident that better track designs are required to reduce the likelihood of quadrupeds getting injured at the tracks. Moreover, observations confirmed that in greyhound racing congestion occurs at the entrance of the first bend [56]. Likewise, it was shown that various track shapes have considerable effects on the greyhound injury rates indicating track curvature influences [57]. Also, when it comes to track shapes and smooth paths, transition curves are an essential part of path design in many areas such as road design and train track designs [58]. In the quadruped racing industry, the trajectory of a racing subject due to track path design is often overlooked for track designs and injury prevention measures despite its significance in dynamics outcome for the animal. As the trajectory of a racing quadruped defines its dynamic stability during races, this research proposed smooth trajectory path generation requirements for oval tracks for galloping quadrupeds track designs by using numerical methods. The methods discussed can also be used

for modelling existing tracks performances as well as for generating smooth running paths with G3 curvature continuity for quadrupeds and other racing subjects.

The central focus of the galloping quadruped modelling and simulation in this research was to find results for multi-variable factors involved during racing. The combined effect of multiple race-related factors was hard to analyse and not feasible using a traditional trial and error method while in simulation a variable's effect on the outcome can be isolated and confirmed. In the simulation, idealised conditions were created with maximum and minimum limit outputs for individual factor bearing variable to create race scenarios that could be easily debugged and analysed. Besides, dynamic constraints and limits as exposed by galloping quadruped physiological characteristics during different circumstances were found by emulating specific scenarios in the simulation virtual world.

4.2 Methodology

When a quadruped is racing, its motion can be defined and traced in terms of displacement, velocity, and acceleration in Euclidean space. While the nominal acceleration of greyhound can be directly related to forces acting on it, deriving the instantaneous displacement and velocity of a greyhound can be a complex task. This is because the instantaneous displacement and velocity of a greyhound in racing not only depends on the racing track design and racing operational running conditions but also relies on the adjacent greyhounds' dynamic profiles. This creates a greater unpredictability in a greyhound's instantaneous displacement and velocity during a race. Furthermore, observation has confirmed that a racing greyhound can bump into another adjacent greyhound as well as follow a path, which is not defined by its motion limiting force factors but are an inherent part of race dynamics. Consequently, the interactions between galloping quadrupeds in a race have a significant impact on the galloping quadruped race dynamics. A quadruped veering model

was developed for greyhound racing which outputs quadruped locations during a race from the start of the race till the end. The model predicts the path taken by an individual galloping quadruped during a race while having each quadruped its character in terms of velocities. The quadruped veering model calculates adjacent quadrupeds' location, track design and race operational influences and optimises potential locations of the greyhound during a race.

Figure 4.1 represents the fundamental working principle for the greyhound veering model for driving GR simulation. The model preserves its states from the previous dynamic events and takes into consideration current dynamic events during a race at a track to generate time-varying dynamic performance of a quadruped. Literature and quadruped biomechanics data modelling and synthesising (Chapters 2 and 3) provided several inputs for the dynamic quadruped model. The data from the inputs were fed into the model which generated outputs to tell the racing performance of the quadruped.

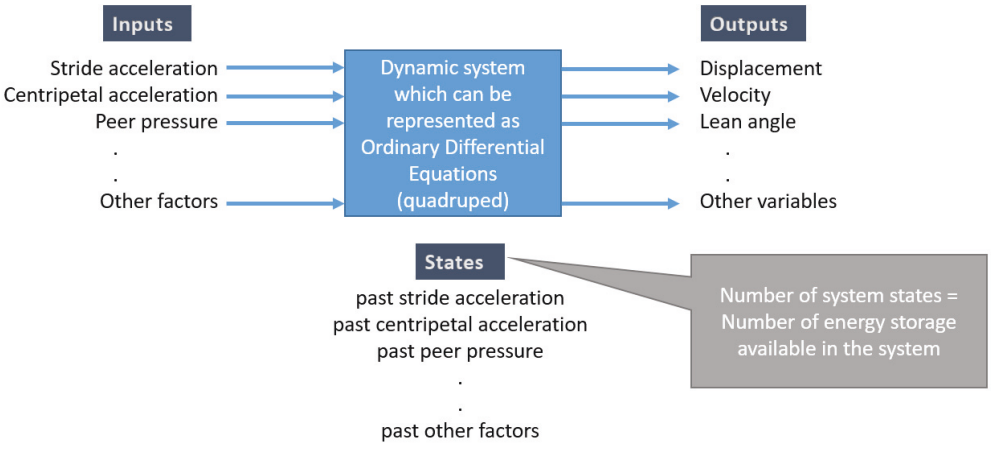

Figure 4.1: A quadruped in racing as a dynamic system where the states of the system changing with the time.

Two fundamental geometric aspects of a track design that define the dynamics for galloping quadrupeds are track path and track cross-falls. Ideally, a track path

would guide the moving subjects in a dynamically smooth manner while the track cross-falls would provide smooth ground supporting force and centripetal force in the curvilinear motion. However, the design requirements for a track's cross-falls depend on the design of the track path as the dynamics performance outcome of a moving subject is defined by its trajectory. Moreover, the dynamic stability of an object in motion depends predominantly on its trajectory where a smooth trajectory performance can solely manage the stability. In this research, a great amount of priority was given in solving smooth running trajectories for galloping quadrupeds and hence track path design as a step forward for developing design requirements of dynamically safe tracks.

One key parameter which determines the trajectory of a racing greyhound is the curvature of its running path. Curvature, $\kappa(s)$, is the change of heading relative to distance travelled [59]. Also, the curvature can be thought of as the inverse of the radius of curvature, which denotes the turning radius at any point in the path [60]. Furthermore, a related variable, sharpness α, is the change of curvature for distance travelled and also forms the basis for constructing continuous curvature path trajectories [59]. While designing a path, curvature change must remain smooth throughout the trajectory of a moving object as the centrifugal acceleration experienced is directly proportional to the path curvature [60]. As a result, in trajectory generation for motion planning the smoothness of a trajectory is directly related to the smoothness of its curvature profile [61]. Likewise, for a path to be feasible, it must conform to continuous position, heading, as well as curvature at all points [59]. Now, if the path of a trajectory is defined by a function $y = f(x)$, then the radius of curvature at any given point can be found from the following equation [62]:

$$\rho = \frac{[1 + (\frac{dy}{dx})^2]^{\frac{3}{2}}}{|\frac{d^2y}{dx^2}|} \tag{4.1}$$

Then, the curvature is,

$$\kappa = \frac{1}{\rho} \tag{4.2}$$

An ideal racing greyhound trajectory would involve optimising two major control factors, greyhound heading, which deals with curvature or sharpness of the running path and greyhound kinetics, which deals with the acceleration/deceleration of a greyhound. These factors can be calculated using Equation 4.2 and methods described in Section 3.6.2. During this research, numerical and parametric approaches were formulated for modelling and designing ideal path trajectories between straight and bend track path segments using a transition curve, as can be seen from Figure 4.2.

The continuity of a transition curve defines its performance under various conditions. When a transition curve has a G0 continuity or positional continuity, it only serves the purpose of having a common endpoint between two segments such a straight and a bend [63]. In this continuity, a greyhound's trajectory would have an abrupt and significant change in its heading. A G1 continuity between two segments provides a continuous path where the adjoining segments would have a common direction at the meeting points [63]. This type of continuity was observed in the GRNSW tracks SD where the heading of a greyhound would be continuous except the magnitude of the heading would be non-uniform. A G2 continuity of a transition curve ensures curvature continuity in the trajectory. For instance, a clothoid can join a line and an arc with G2 curvature continuity where both the tangent vector and curvature at the line-arc intersection are continuous [64]. Furthermore, G2 continuous paths allow comfortable driving while putting less mechanical stress on a vehicle [65]. However, it was found that the application of higher-order continuity is becoming more prevalent in various industries, including automotive, robot, and aerospace.

A higher-order continuity in a transition curve has direct physical implications on a moving a body, yet many studies still focusing on G2 continuity of a curve [66]. Such as transition curves design with G3 continuity now can be found in horizontal geometry designs and trajectories planning of mobile robots [66]. A G3 continuity in a transition curve is preferable when a steering system needs to maintain its dynamic constraints by limiting maximum curvature, maximum curvature rate, and maximum curvature acceleration [65]. Likewise, a G3 continuity ensures the same constant rate of change of the curvature in a transition curve.

Dynamic instability arises between straight and bend track path segments where there is a discontinuity in the trajectory curvature. Using numerical and parametric methods developed clothoid and algebraic curves transition segments were generated for racing quadrupeds using a sequential vector transformation method and ideal clothoid transition segments were approached, which would respect a quadruped's kinematic parameters and the boundary conditions of a track. Finally, the limitations of using a clothoid curve as transition between straight and bend track path segments for racing dogs track path design were analysed, and a smooth composite curve for track transition design was determined that roughly maintains G3 curvature continuity. The composite curve has smooth jerk to overcome limitations of a clothoid transition.

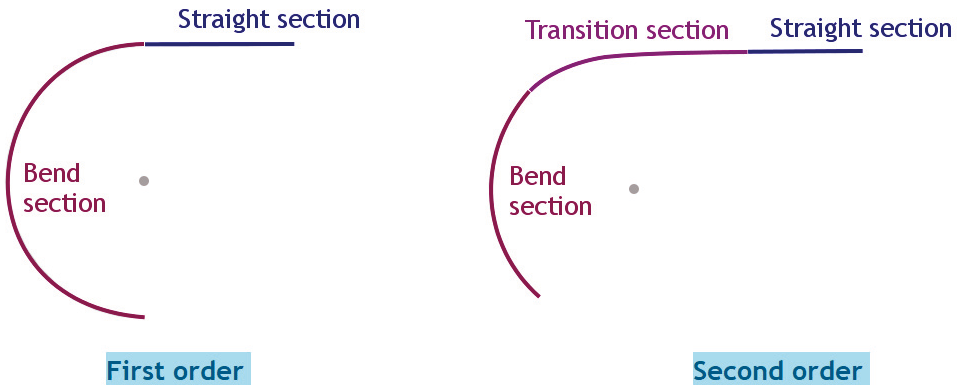

Figure 4.2: Oval track path design components two different options.

4.3 Requirements analysis for greyhound racing simulation models

To create a viable model for quadruped racing such as GR, numerous variables first need to be identified and addressed. These variables may come from within the racing track or from the greyhound or race operating conditions. By considering the race track and greyhound as different systems, their inherent system behaviour defining variables were identified. Furthermore, race operational configuration and running conditions define a system which by emulating created necessary inputs for a simulation model of GR.

There are several distinct elements that take part in GR. While some of these racing elements are dynamic, some elements are static and have a significant impact on a racing greyhound. The central dynamic bodies in racing are the lure during a race, adjacent racing greyhounds, and individual greyhound limbs which are required for greyhound locomotion. The fundamental static bodies relating to racing are race starting boxes locations and orientations relative to the track, track surface properties including surface traction, impact attenuation qualities, track camber,

and track racing line. During a race, lure, starting boxes, and track are regulated to certain degrees that their behaviours are controlled and follow a specific predefined pattern.

To develop a platform for race simulations that would allow generous flexibility in creating different racing scenarios, the following were identified as the foremost requirements for a GR simulation setup:

- To be able to have a different number of starts for a race distance
- To be able to have specific track geometry
- To be able to have different lure configurations and orientations at a track
- To be able to maintain a specific lure separation distance
- To be able to have specific initial lure acceleration after the start boxes gate opening
- To be able to configure starting boxes gate opening timing
- To be able to have variable speeds among quadrupeds during a race
- To be able to have a variable speed profile for individual quadruped
- To be able to manage accidents or major dynamic instabilities due to quadruped's dynamics in a race
- To be able to have a specific situation-aware race operating conditions

To be able to recreate various phenomenon's occurring during a race, different simulation strategies were utilised to achieve first-order approximation results from the simulations. For instance, deterministic simulation (DTS) was employed for

quadruped boxes to track transition, quadruped veering, cross-fall effect, centrifugal force effect, quadruped collision checking with track boundaries during a race. DTS strategy allowed consistent and converging results from the simulations for racing quadrupeds trajectories for a specific race scenario setup. Besides, simulation models' boundary conditions and limits were more effective using the DTS technique for the mentioned racing phenomenons. Continuous simulation (CS) was adopted for quadrupeds collisions detection and collision responses. This was achieved by using several collision detection check iterations for each simulation timestep. Moreover, CS was necessary as a quadruped can bump into any number of other quadrupeds during a race. Variability of stride performance, speed, and acceleration of a quadruped during a race were regarded as stochastic simulation (SCS). Variability of speed and initial acceleration profile among quadrupeds during a race simulation was also considered as SCS. Using different random number generators in PY and necessary maximum and minimum values limit a decent SCS performance was achieved which in result produced unique simulation races results even for an unchanging race scenario setup.

To tweak and debug a simulation model's performance, the simulation model needed to go through unit testing. Unit testing is a way to measure the reliability of a model under various input conditions. The following Figures 4.3 and 4.4 illustrate the quadruped veering model unit testing benchmarks, as utilised to tweak veering model performance to meet simulation requirements. In Figures 4.3 and 4.4, the pink bounding box represents a quadruped approaching the blue bounding box quadruped, while the green bounding box represents pink bounding box quadruped's possible heading direction in the simulation. As reflected in Figure 4.3, when the steering correction iteration for the veering model is constant, the model's performance converges for collision avoidance steering factor 0.5. Likewise, as shown in Figure 4.4 for constant collision avoidance steering factor the model converges for

steering correction iteration factor 25.

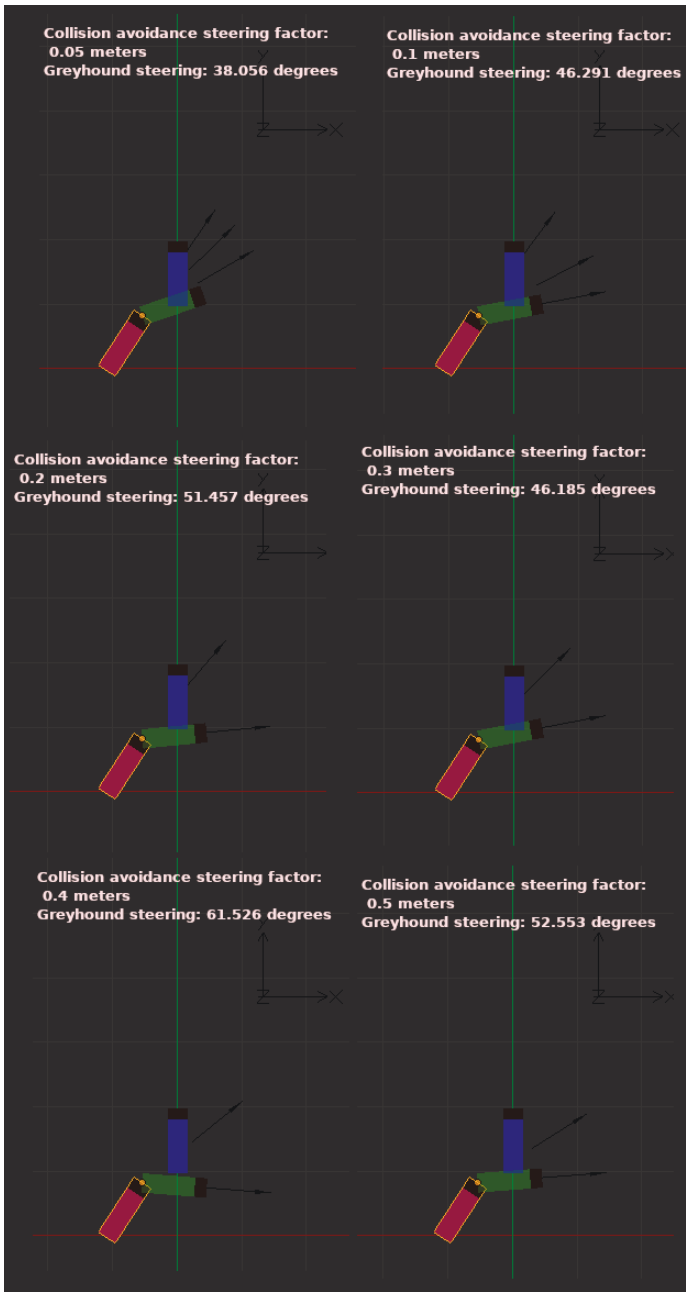

Figure 4.3: Quadruped veering model performance when the collision avoidance steering factor is variable and the steering correction iteration is constant about 15.

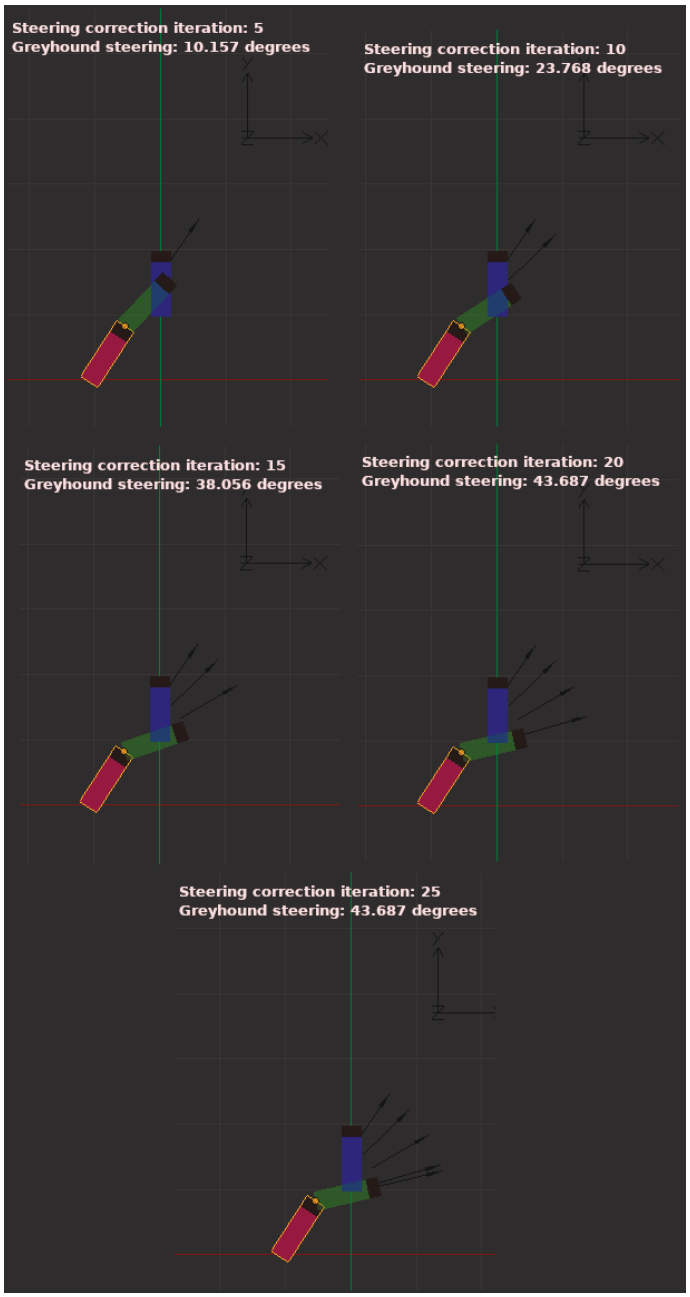

Figure 4.4: Quadruped veering model performance when the steering correction iteration is variable and the collision avoidance steering factor is constant about 0.5.

4.4 Greyhound racing simulation numerical models formulation

By considering a quadruped as a point object its overall motion in a race can be formulated by knowing the factors which induce the motion as well as the factors which alter the motion characteristics as a result of combined racing environmental and quadruped limits. The main driving factor for quadruped motion is quadruped stride, while the motion altering factors are quadruped natural steering limits, a collision in a race, track geometry and surface condition, lure velocity profile and track boundaries. These discrete factors were modelled using kinematics and vector equations where kinetic equations and input to output unit tests were used for finding initial and final values for the model equations. Superposition principle was applied to the model equations to solve for aggregated results of discrete race dynamic factors and calculate quadruped location during a race using EM. The summation of discreet factors can be expressed as Equation 4.3.

$$\begin{aligned} &V(f_1 + f_2 + v_3 + f_4 + f_5 + f_6 + f_7 + f_8 + f_9) \\ &= V(f_1) + V(f_2) + V(f_3) + V(f_4) + V(f_5) + V(f_6) + \\ &V(f_7) + V(f_8) + V(f_9) \end{aligned} \tag{4.3}$$

In which V is the final velocity vector function for $f_1 ... f_9$ discrete factors of race dynamics. The f_1 factor represents greyhound stride acceleration velocity due to the sum of all the forces exerted by a greyhound's stride which can be modelled using Newton's second law (4.4). This is also the forward acceleration of greyhound. It was assumed that a greyhound's exerted stride force remains constant for the entire race duration, although, in reality, data showed that greyhound acceleration is highly variable during the first three strides. However, as the fraction of time for the first three strides is relatively small compared to entire race duration, a lin-

ear acceleration model and an averaged value of greyhound maximum accelerations were appropriate for getting stable final velocity output. For constant acceleration, greyhound maximum forward acceleration was calculated using Equation 4.5 where greyhound final velocity (v) was 19.4 m/s, greyhound displacement (s) for reaching final velocity was 15 m and initial velocity (v_0) was 0 m/s. This maximum forward acceleration was plugged into Equation 4.6 to calculate the greyhound stride acceleration velocity factor f_1. In Equation 4.5, v_0 is greyhound velocity in previous time instant and dt is the time elapsed between v and v_0.

$$\Sigma F = ma_s \tag{4.4}$$

$$v^2 = v_0^2 + 2a_s s \tag{4.5}$$

$$v = v_0 + a_s dt \tag{4.6}$$

The purpose of the f_2 factor is to provide the greyhound with the motivation to race as well as steer greyhound heading as it moves in the track. Therefore, this factor is a function of a greyhound's line of sight to the lure, frictional force, and centrifugal force vectors. However, observation of greyhound race and race data has confirmed that line of sight to the lure is a significant guiding influence for greyhound path following around the track in the absence of other influences such as congestion due to adjacent racing greyhounds. As a result, the line of sight to the lure vector was also considered a function of frictional force, and centrifugal force vectors (4.7). The line of sight to the lure vector was constructed from lure and greyhound instantaneous locations in the track. The frictional force has two components where one is due to track camber (θ) and another one is the nominal friction due to greyhound instantaneous velocity as denoted by $m \times g \times sin\theta$ and

$C \times v$ respectively.

$$\begin{aligned} lure\ line\ of\ sight\ vector = lure\ line\ of\ sight\ vector \\ + centrifugal\ force\ vector \\ + paw\ and\ track\ surface\ frictional\ force\ vector \end{aligned} \tag{4.7}$$

$$centrifugal\ force = \frac{mv^2}{R} \tag{4.8}$$

$$\begin{aligned} &greyhound\ paw\ and\ track\ surface \\ &frictional\ force = (mgsin\theta) + (Cv) \end{aligned} \tag{4.9}$$

In Equation 4.8, R is instantaneous radius of curvature of greyhound path following and m is greyhound mass. In Equation 4.9, m is greyhound mass and C is a constant.

The f_3 factor is a tweaking vector to f_2 factor in getting precise greyhound heading movement without which results in unnatural greyhound heading movement behaviour. The reason for this is in real-world greyhound heading direction progress does not go through step change to meet the lure following path instead it goes through many mini-movements to catch up lure following path. This creates a lag between the greyhound spotting the lure location and the greyhound merging with the lure following path. Moreover, a greyhound has physical turning limits at an instant. All these phenomena were modelled using a steering vector which is a function of the greyhound current heading direction vector and lure line of sight vector.

$$\begin{aligned} steering\ vector = lure\ line\ of\ sight\ vector \\ - current\ heading\ direction\ vector \end{aligned} \tag{4.10}$$

The f_4 final velocity factor determines the outcome of the greyhound checking and bumping as well as the greyhound collision avoidance tendency to adjacent greyhound during a race, which results in the greyhound surrounding aware variable

velocities. These situations in a race were modelled by using a collision avoidance vector, which successively finds greyhounds in proximity and through many iterations constructs a clearance vector. The exact number of iterations was chosen based on simulation time stamps and convergence of the clearance vector. Furthermore, by assuming there is no collision between two greyhounds vertically, circle to circle collision detection was used for checking overlapping greyhounds.

$$\begin{aligned} collision\ avoidance\ vector = location\ vector \\ of\ greyhound\ in\ proximity \\ -\ location\ vector\ of\ greyhound \end{aligned} \tag{4.11}$$

$$\begin{aligned} clearance\ vector = current\ heading\ directionvector \\ -\ collision\ avoidance\ vector \end{aligned} \tag{4.12}$$

The f_5 factor finds the effect of track cross falls on greyhound veering. As the effect of cross fall can be proportional to track banking angle (θ) at spot location, a linear calibrated force was used along with the normal force vector for calculation. To find the banking angle at a given location in track, the track surface was discretised using small triangles where the vertices of each triangle were used for finding normal force vector (N) and corresponding bangle angle (θ).

$$N_x = U_y V_z - U_z V_y \tag{4.13}$$

$$N_y = U_z V_x - U_x V_z \tag{4.14}$$

$$N_z = U_x V_y - U_y V_x \tag{4.15}$$

$$\begin{gathered} normal\ force\ vector\ (N)\ magnitude = \\ (mgcos\theta) + (Cv) \end{gathered} \tag{4.16}$$

Where, $U = p_2 - p_1$ and $V = p_3 - p_1$ for $p_1, p_2, and\ p_3$ triangle vertices, and m is greyhound mass and C is a constant.

While a racing greyhound avoids colliding with track boundaries like the inside lure rail. The f_6 factor was used for applying a collision avoidance vector of track boundary to the final velocity vector. For this purpose, track boundaries were sampled with evenly spaced points, and by using the nearest points to a greyhound's location, a boundary collision avoidance vector was found.

$$\begin{gathered} boundary\ collision\ avoidance\ vector = \\ location\ vectors\ of\ adjacent\ points\ on\ track\ boundaries \\ -\ location\ vector\ of\ greyhound \end{gathered} \tag{4.17}$$

The f_7 factor models variable track surface conditions at different track locations as well as variable greyhound stride acceleration from greyhound to greyhound for the race period. Modelling of variable track surface conditions was essential as despite identical stride from a greyhound over the race period, non-uniform track surface conditions such as hardness, softness, and coefficient of friction determine greyhound stride acceleration. This factor is a function of stride duration, race time, and a random number generator.

The f_8 factor adds a specific greyhound behaviour to the final velocity vector, which occurs when a greyhound is significantly behind the lure as observed from various races. It was noticeable that a greyhound maintains an additional offset distance from a track inside-boundary to get a better sight of the lure depending on the distance between greyhound and lure. However, various races also indicated that this specific behaviour varies from greyhound to greyhound. This situation was

modelled by constructing a boundary offset vector which is a function of greyhound distance to lure, minimum offset from the boundary and a constant as given below:

$$\begin{gathered} boundary\ offset\ vector = \\ minimum\ offset\ from\ boundary \times \\ (\frac{distance\ to\ lure}{C}) \end{gathered} \tag{4.18}$$

Where minimum offset from boundary and C were calibrated to be 0.5 m and 5 m respectively.

The f_9 factor defines lure motion in terms of track path and leading greyhound location in the race. For this factor, a model function was created which takes into account track predefined lure travel path and lure and leading greyhound separation distance to provide lure instantaneous velocity which would maintain the lure driving for the duration of a race while maintaining a separation distance. The model function first calculates the heading direction of the lure by copying track curvature profile and then sets lure instantaneous speed, based on the lure and leading greyhound separation distance. The setting of lure instantaneous speed (S) was based on the following rules where the constants can be tweaked to meet the specific lure

driving performance:

$$\begin{gathered}((A > B \rightarrow (C > 30 \rightarrow X = 1.9489)) \wedge \\ (A > B \rightarrow (C > 20 \rightarrow X = 3.3378)) \wedge \\ (A > B \rightarrow (C > 15 \rightarrow X = 6.1156)) \wedge \\ (A > B \rightarrow (C > 10 \rightarrow X = 8.893)) \wedge \\ (A > B \rightarrow (C > 5 \rightarrow X = 16.9489)) \wedge \\ (A > B \rightarrow (C > 1 \rightarrow X = 17.504)) \wedge \\ (A > B \rightarrow (C > 0.2 \rightarrow X = 17.782))) \wedge \\ ((A < B \rightarrow (C > 14 \rightarrow X = 14)) \wedge \\ (A < B \rightarrow (C > 10 \rightarrow X = 18.62)) \wedge \\ (A < B \rightarrow (C > 5 \rightarrow X = 17.504)) \wedge \\ (A < B \rightarrow (C > 1 \rightarrow X = 16.9489)) \wedge \\ (A < B \rightarrow (C > 0.2 \rightarrow X = 20))\end{gathered} \tag{4.19}$$

In which A is the distance between leading greyhound and lure, B is maintaining separation distance, C is the difference between A and B, and finally, X is the lure instantaneous speed.

Lastly, in the greyhound motion model composition, the vertical acceleration velocity factor was neglected since instantaneous vertical velocity is negligible compared to other greyhound velocity influencing factors because of low track surface penetration by a greyhound's paw in a race.

4.5 Simulation of greyhound racing kinematics

Blender software package was used as the simulation platform for creating content for simulation visualisation as well as implementation, manipulation and data extraction of the simulation models using PY. First, the track 3D model was imported into Blender virtual Euclidean space from track survey data where it was

constructed and formatted to meet the needs of mathematical models. Then, 3D racing element models such as starting boxes, greyhounds, lure and shape defining objects such as track boundary curves were created in Blender virtual Euclidean space meeting mathematical model requirements. Finally, the Blender Python API was used for writing simulation code inside Blender software package. The primary components of simulation code were: greyhound object which defined a greyhound's dynamic model and states in a particular timestamp, a lure object which defined lure dynamic model and states in a particular timestamp, a method for calculating collision between greyhounds, and a method containing code for simulation numerical solver and updating 3D models in Blender virtual Euclidean space scene. For both lure and greyhounds' motions, the numerical solver calculated the time-varying behaviour of each dynamic system by solving model functions and numerical integration using the EM where the results from each model function were united using the SP. For example, the final location of each dynamic object was determined by integrating the velocity over time as follows:

$$S = \int x dt \tag{4.20}$$

$$S_{new} = S_{old} + v dt \tag{4.21}$$

Where S_{new} is the new location, S_{old} is the old location, v is instantaneous velocity and dt is the smallest unit of time in the simulation.

There were several global variables in the simulation setup which were lure initial speed, lure maintaining acceleration, lure starting acceleration, greyhound maximum average acceleration, maximum greyhound speed, minimum greyhound speed, lure greyhound separation distance, starting box locations and orientations, and lure offset from the starting boxes before racing. These variables were adjusted to match

various greyhound races scenarios.

Figure 4.5 illustrates the fundamental stages present in the simulation procession pipeline for deriving quadruped race kinematics at the tracks.

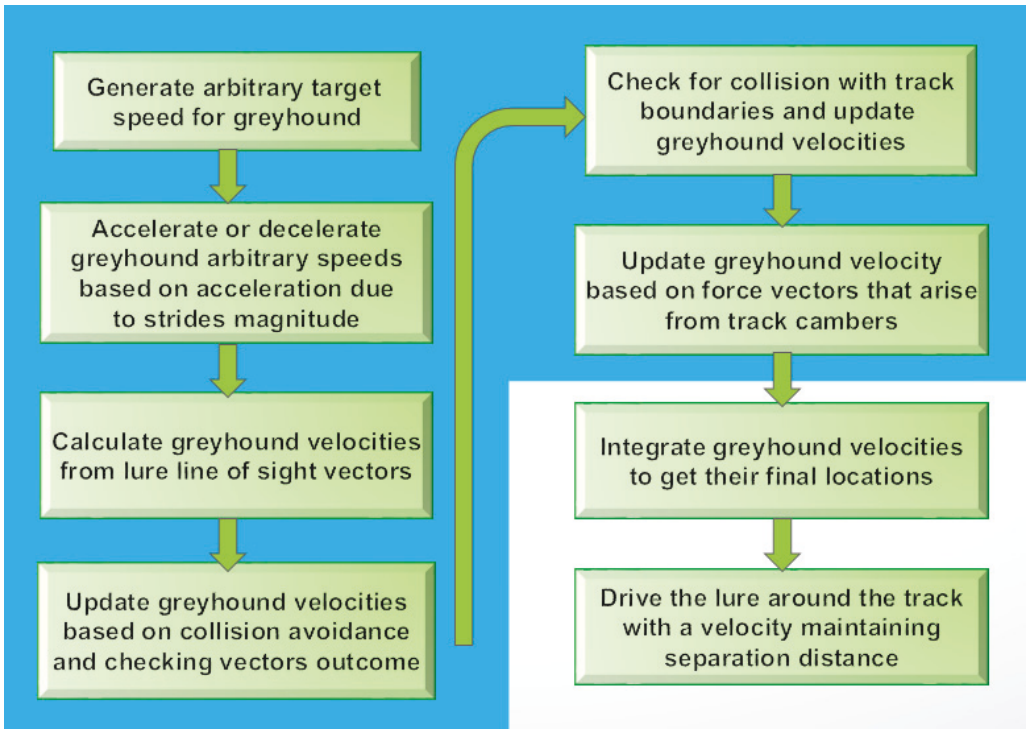

Figure 4.5: Major stages of the greyhound racing simulation processing pipeline.

4.6 Modelling of greyhound racing track path designs for galloping quadruped dynamics

Clothoid curves suitability as track path transition curve was analysed by modelling its jerk outcomes and ideal transition curves design requirements were modelled for galloping quadrupeds considering racing greyhounds.

4.6.1 Clothoid path segment for deriving natural greyhound racing trajectory

The clothoid segment is a curve known for its curvature proportional to its length [67]. This property of the clothoid is useful as it allows gradual development of centrifugal acceleration or can act as centrifugal acceleration easement, which significantly reduces the risk of accidents occurring [60]. Recent works from the researchers show that there are different types of curves already developed that can be used as centrifugal acceleration easement curves [60]. For example, Quintic polynomial and B-splines functions are computationally less expensive and also able to provide curvature continuity for curve design [61]. However, the drawbacks of these functions are complex curvature profiles which are hard to follow as they are not necessarily smooth [61]. This is where clothoid curves are useful as their curvature profile is a straight line making them easy to follow [61]. Furthermore, clothoid curves are characterised by a linear curvature, allowing minimal curvature variation where piece-wise clothoid curves exhibit excellent smoothness properties [68]. Due to these fundamental reasons, currently clothoid curves are extensively found in road design and robot path planning to achieve smooth transitions in the trajectories [68].

Furthermore, we found that clothoid curves are essential at the race track not only because of smooth path trajectories development but also for reducing the likelihood of certain types of race dynamics hazards. From the race videos, it was noted that a greyhound is more likely to change lane to higher radius upon entering the first bend. This could be due to the track bend lacking adequate transition to accommodate for greyhound natural instantaneous yaw rate change and leaning rate change limits. As a result, the prospects of the greyhound bumping into another nearby greyhound increases significantly. This specific race dynamic outcome can be reduced or nearly eliminated if the track path has clothoid segments that match greyhound natural heading turn rate change limits.

There are many methods available for computing the clothoid. Most methods involve approximations to the clothoid [64]. For example, it can be approximated by high degree polynomial curves [69], such as by an S-power series [70] as well as by an arc spline [64]. Also, continued fractions and rational functions are commonly used for approximations [64]. A more recent development in the spline primitives found in much computer-aided design software makes it easy to approximate a clothoid while respecting boundary conditions, such as curvature and tangent continuity. Also, spline primitives are known for good and fast controllability with positional and tangential constraints making them ideal for various applications [68]. Each of the methods available results in different degrees of accuracy and may not be suitable for efficient greyhound track path design purposes. This is mainly due to less controllability in generating a clothoid according to greyhound kinematics. Moreover, to accommodate the clothoid segment into the path design, a coordinate respecting system must be incorporated or derived from the existing clothoid methods that respects different design boundary conditions.

The most common method of computing a clothoid can be found in its definition in terms of Fresnel integrals [70] where it is computed using the Fresnel sine and cosine functions (4.22) and (4.23) and using some forms of Taylor series expansions on the functions which converge for independent variable [59]. Series expansion functions are extensively used because the clothoid defining formulas are transcendental functions [67]. The parametric plot of Fresnel sine and cosine functions provides coordinate values of the clothoid curve. However, this does not respect any form of unit scaling or boundary conditions and does not allow computing the clothoid for a specific rate of change of curvature, sharpness or smoothing applications. Similarly, Equations 4.24 and 4.25 are an approximation of Fresnel sine and cosine functions which converge for all independent variables. Another common method involves

utilising auxiliary functions (4.26) and (4.27) as shown below [59].

$$S(x) = \int_0^x sin\left(t^2\right)dt \tag{4.22}$$

$$C(x) = \int_0^x cos\left(t^2\right)dt \tag{4.23}$$

$$S(x) = \int_0^x sin\left(t^2\right)dt = \sum_{n=0}^{\infty}(-1)^n \frac{x^{4n+3}}{(2n+1)!(4n+3)} \tag{4.24}$$

$$C(x) = \int_0^x cos\left(t^2\right)dt = \sum_{n=0}^{\infty}(-1)^n \frac{x^{4n+1}}{(2n)!\,(4n+1)} \tag{4.25}$$

Equations 4.22 and 4.23 then can be written in the auxiliary function form as shown below [59]:

$$C\,(x) = \frac{1}{2} + f(x)sin(\frac{\pi}{2}x^2) - g(x)cos(\frac{\pi}{2}x^2) \tag{4.26}$$

$$S\,(x) = \frac{1}{2} - f(x)cos(\frac{\pi}{2}x^2) - g(x)sin(\frac{\pi}{2}x^2) \tag{4.27}$$

Where auxiliary functions f and g are defined as:

$$f\,(x) = \left(\frac{1}{2} - S(x)\right)cos(\frac{\pi}{2}x^2) - \left(\frac{1}{2} - C(x)\right)sin(\frac{\pi}{2}x^2) \tag{4.28}$$

$$g\,(x) = \left(\frac{1}{2} - C(x)\right)cos(\frac{\pi}{2}x^2) + \left(\frac{1}{2} - S(x)\right)sin(\frac{\pi}{2}x^2) \tag{4.29}$$

Likewise, for auxiliary function definition of the clothoid, a good rational approximation to compute the clothoid is using the following auxiliary functions [59].

$$f(x) = \frac{1 + 0.926x}{2 + 1.792x + 3.104x^2} \tag{4.30}$$

$$g(x) = \frac{1}{2 + 4.142x + 3.492x^2 + 6.670x^3} \tag{4.31}$$

Moreover, recently, researchers developed more efficient numerical methods where one such method is using arc length parameterisation [60]. It was found that analytical methods lack parameterisation for different application case scenarios, and researchers are becoming more reliant on developing numerical techniques for computing the clothoids.

4.6.2 A numerical approach for generating clothoid curve transitions for racing greyhounds and other galloping quadrupeds

It is evident that existing methods lack greyhound kinematic parameterisation for GR transition design purposes, as shown in the previous section. A numerical method is generally preferred as a first approach for incorporating different parametrisation into the clothoid curves. To develop a numerical technique for the clothoid that incorporates greyhound kinematics variables, we looked into the characteristics of the mathematical model of the clothoid curve. A clothoid curve transition accomplishes a gradual transition from the straight to the circular curve of the constant radius where the curvature changes from zero to a finite value. As a result, the tangent vector t_i, which lies on the clothoid curve also gradually rotates from zero to a finite angle Figure 4.6. Furthermore, let us assume a greyhound changes its heading with every stride as noted from the race data and galloping gait of a greyhound. With these two crucial pieces of information relating to the clothoid

curve tangent vector and the greyhound heading step-change length, we can apply vector transformation to generate a clothoid curve positional vector P_i Figure 4.6. Now, we define the clothoid tangent vector as a function of greyhound stride length constant as denoted by transition segment length and a variable denoted by transition deflection angle. The transition deflection angle a_i defines the local rotation of the clothoid curve tangent vector at a specific transition segment location i relative to the horizontal axis. Moreover, as a clothoid curve transition would gradually increase its curvature with constant curvature acceleration, the transition deflection angle a_i is a function of the transition deflection angle acceleration constant. The transition deflection angle acceleration d defines the rate change of curvature per transition segment length of the clothoid curve, which essentially tells us how quickly the clothoid tangent vector rotation is accelerating. Finally, once the transition deflection angle is calculated for the local ith transition segment the clothoid curve positional vector can be calculated as shown in Figure 4.6 and Equation 4.33. To generate the entire clothoid curve for the specified number of transition segments by the constant n the process of translating and then rotating the clothoid tangent vector is iterated to get the clothoid positional vectors for all the transition segments. For instance, Figure 4.7 shows a clothoid curve generated using this method when transition segment length s equals 1 m, the number of transition segments n equals 250 segments and transition deflection angle acceleration d is 0.02 deg.

$$d = transition\ deflection\ angle\ acceleration$$

$$a_i = transition\ deflection\ angle\ relative\ to\ horizontal\ axis$$

$$s = transition\ segment\ length$$

$$n = number\ of\ transition\ segments$$

$$t_i = transition\ tangent\ vector$$

$$i = transition\ segment\ number$$

$$t_i = f(s, a_i) = \begin{bmatrix} cos(a_i) \times s \\ sin(a_i) \times s \end{bmatrix} \tag{4.32}$$

$$P_i = f(t_i, P_{i-1}) = P_{i-1} + t_i \tag{4.33}$$

Where,

$$a_i = \sum_{k=1}^{i} d \times i = 1 \times d + 2 \times d + 3 \times d + ... + i \times d$$

And,

$$d \times i \propto \kappa$$

Where, κ denotes curvature of the clothoid curve.

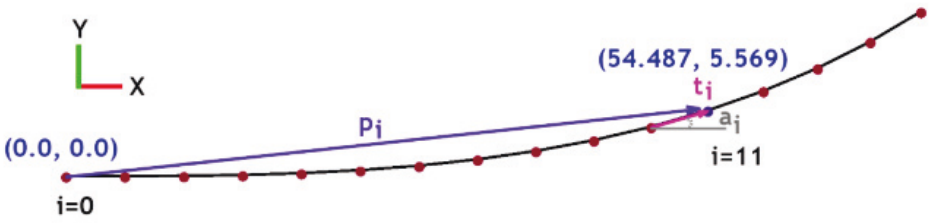

Figure 4.6: Racing quadruped clothoid path generation using numerical method parameterisation.

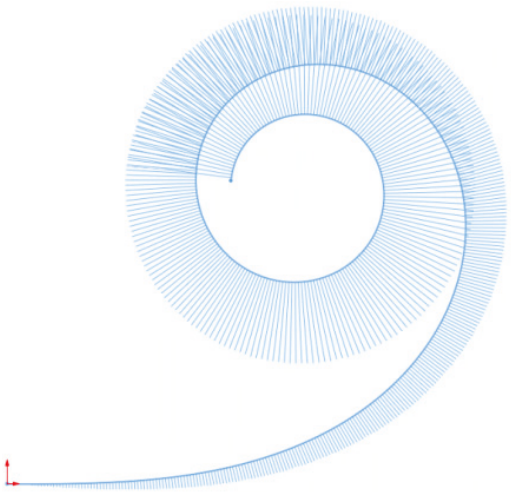

Figure 4.7: A clothoid curve with curvature combs containing 250 single meter segments and with a turning acceleration of 0.02 deg per segment.

Now, as an illustration, using the numerical method explained above to generate a clothoid curve transition for racing greyhounds with a transition exit radius of approximately 52 m and a total transition length of 45 m, we would have to consider the d constant to be 0.69 deg per transition segment, the s constant to be 5 m (assuming average stride length of a greyhound is roughly 5 m) and the n constant to be 9. The curvature and jerk results of this clothoid transition curve for racing greyhounds are shown in Figure 4.8. The numerical calculation of a_i and P_i is shown in Table 4.1.

Table 4.1: Numerically calculated values of a_i and P_i variables for a clothoid curve.

i	$\mathbf{a}_i$ **(deg/segment)**	$\mathbf{P}_i$ **X coordinate (m)**	$\mathbf{P}_i$ **Y coordinate (m)**
1	0.69	5.00	0.00
2	2.07	10.00	0.06
3	4.14	15.00	0.24
4	6.9	19.98	0.60
5	10.35	24.95	1.20
6	14.49	29.87	2.10
7	19.32	34.71	3.35
8	24.84	39.43	5.01
9	31.05	43.96	7.11

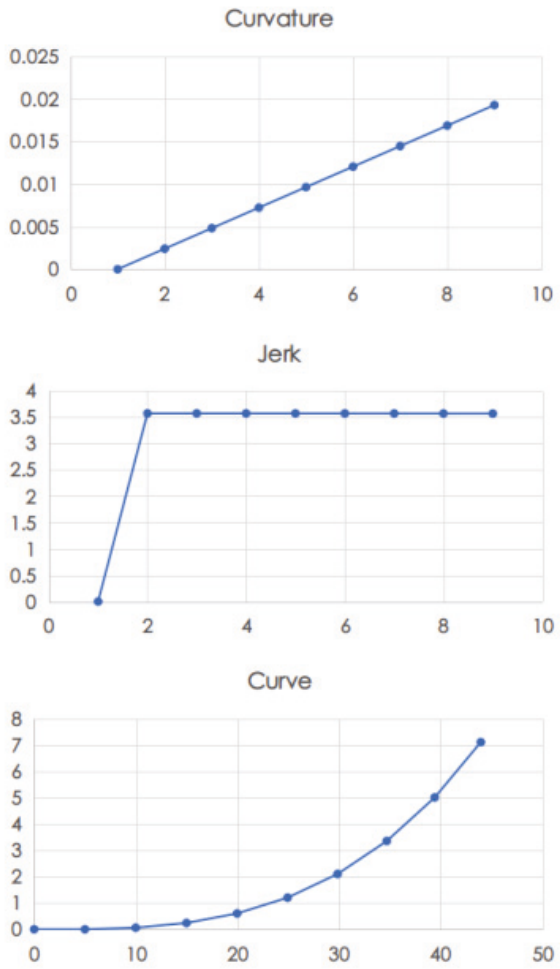

Figure 4.8: A clothoid curve transition's performance for racing greyhounds with a total 45 m transition length having an approximately 52 m turning radius at the end of the transition.

Using this numerical method approach an optimised clothoid curve transition can be determined numerically by tweaking curve generating factors. The controlling of initial values as set by d, s, and n allows generating of any combination of clothoid curves as required for different kinematic path design goals.

4.6.3 Designing and modelling ideal clothoid segments for racing greyhounds and other galloping quadrupeds

When designing clothoid segments, it is essential that greyhound heading is not changing at the maximum performance rate since such a heading would put a greyhound into a limit state turning while maintaining a high speed. An ideal clothoid segment would have continuous curvature to allow a greyhound to navigate the path with a minimal amount of veering. In the next section, we derive a helper equation that can be used for specifying ideal clothoid transitions as well as modelling of dynamics for racing greyhounds at the tracks.

Equation 4.39 produced a relationship between greyhound kinematics such as heading turn angle acceleration and turning radius at the end of a natural clothoid transition. First, let's assume for a clothoid transition a racing greyhound would pass ns number of strides with a constant s meter stride length. Now, if the total clothoid transition length is T meters, then the number of greyhound strides ns in a transition is given by Equation 4.34. Again, since the length of the greyhound's strides remains unchanged in the clothoid transition, the greyhound's turning angle a in the last stride of the transition can be defined by Equation 4.34 if the greyhound heading turning angle is accelerating with d deg per stride. Now, using Equation 3.4, to calculate a greyhound's heading radius of turn R near the end of the clothoid transition, we use Heron's formula (4.38) to calculate the area of the triangle A (from Equation 4.39) formed by last two greyhound strides s_1 and s_2. Furthermore, using the cosine rule we calculate the unknown side s of the triangle formed by the last two greyhound strides s_1 and s_2. Finally, by plugging in values for R and simplifying the equation, we reach a final form of Equation 4.39 which defines a racing greyhound turning radius R at the end of the clothoid transition in terms of transition length T greyhound heading turning acceleration a and greyhound constant stride length s. Consequently, as Equation 4.39 relates greyhound heading turning parameters to

clothoid transition parameters it is useful for modelling and designing ideal clothoid transitions for racing greyhounds.

$$d \;=\; transition\; deflection\; angle\; acceleration\; (per\; stride)$$

$$a \;=\; deflection\; angle\; of\; greyhound\; heading\; for\; last\; greyhound\; stride$$

$$ns \;=\; total\; number\; of\; greyhound\; strides\; in\; the\; transition$$

$$s \;=\; length\; of\; a\; single\; stride$$

$$R \;=\; transition\; last\; stride\; turn\; radius$$

$$T \;=\; transition\; length$$

$$ns \;=\; \frac{T}{s} \tag{4.34}$$

$$a \;=\; d \times (ns - 1) \tag{4.35}$$

$$s = \sqrt{s_1^2 + s_2^2 - 2s_1 s_2 cos(a - 180)} \tag{4.36}$$

Where s_1 and s_2 are racing greyhound's last two strides in the transition.

$$p \;=\; \frac{s_1 + s_2 + s}{2} \tag{4.37}$$

Where p is semi-perimeter of the inscribed triangle in the circle formed by racing greyhound's last two strides s_1 and s_2.

$$A \;=\; \sqrt{p(p - s_1)(p - s_2)(p - s)} \tag{4.38}$$

$$R = \frac{\sqrt{2}s^2\sqrt{2s^2 cos\left(\frac{\pi d\left(\frac{T}{s}-1\right)}{180}\right)+2s^2}}{2\sqrt{-s^4\left(cos\left(\frac{\pi d\left(\frac{T}{s}-1\right)}{90}\right)-1\right)}} \tag{4.39}$$

4.6.4 An approach to designing ideal transitions for racing greyhounds and other galloping quadrupeds

As can be seen from Figure 4.8, it was found that clothoid transition curves have a significant flaw. Although the development of the curvature is gradual as can be seen from the curvature plot of Figure 4.8, the jerk profile is not smooth and almost jumps instantaneously from zero to a higher value. This is important, as such a dramatic change of jerk would impose a high energy release in a short time resulting in considerably unstable conditions for greyhounds navigating in and out of the transitions. Furthermore, the clothoid curve generation for racing greyhounds using the numerical method above showed that regardless of transition curve length jerk goes through a step change within one transition segment or one racing greyhound stride. Consequently, clothoid curve transition was deemed not to be an ideal fit for racing greyhound track path designs.

The clothoid transition curve does not maintain a smooth jerk initiation for a racing greyhound. Hence the curve can only be considered G2 continuous with matching curvature at the entrance and exit of the transition curve. This imposes several disadvantages in greyhound race dynamics at the tracks. For example, we can break down the disadvantages into two main categories, namely clustering related problems and path smoothing, where each is entangled with the other. The clustering of racing greyhounds is a common issue during races. This happens mainly due to single lure convergence as a result of the number of following galloping greyhounds. A tight convergence of the greyhound pack is noticeable at race tracks in the locations

where track path curvature change is sudden and abrupt. As clustering is a precursor to various dynamics unstable conditions such as bumping of one greyhound by another, maintaining a smooth path profile as such G3 curvature continuity where the clustering occurs becomes vital. As greyhounds follow the lure, they occupy different lanes such that they have different path radii and tend to cut corners forming various individual transitions into the bend which are all unique. A G2 curvature continuity as found in the clothoid transitions where the rate of change of the jerk is not smooth would induce all the racing greyhounds following the lure to follow one unique transition into the bend to keep instantaneous jerk to the minimum. This is not feasible.

To overcome the limitations of clothoid transitions, we applied the numerical method of generating clothoid curves discussed in the previous section to develop moderate G3 curvature continuity transition curves for racing greyhounds. Also, two different transition curve configurations were selected for generating the curves as these configurations best match the many current tracks found in Australia in terms of real estate requirements. The configurations are a 45 m transition with transition end radius of 52 m and a 75 m transition with transition end radius of 70 m.

First, we assume $a_i = X$ and plot for different X expressions to derive different curves where the curvature results for the curves are shown in Figure 4.9. The X expression defines the nature of curvature function as the curve length increases from the origin. As seen from the plots in Figures 4.9 and 4.10, when the X expression is linear it is a clothoid transition where the jerk is initiated immediately within one transition segment for both 45 m and 75 m transition configurations. To get G3 curvature continuity curves we tried $X^{0.6}$, $X^{1.5}$, X^2, and $((1.2)^x - 1)$ expressions. As can be seen from the plots, all the curves except the clothoid curve X and $X^{0.6}$ curve maintain a moderate G3 curvature continuity with a smooth jerk profile. However, as X expressions are in power and logarithmic function form for $X^{0.6}$, $X^{1.5}$, X^2, and

$((1.2)^x - 1)$ these curves result in higher jerk in the second half of the transition. This suggested that $X^{1.5}$, X^2, and $((1.2)^x - 1)$ curves could be used to develop a G3 curvature continuity transition curve for racing greyhound if the jerk could be maintained in the second half of the transition. So, we decided to use these curves as auxiliary curves which would provide smooth jerk initiation for the transition. However, compared to other curves, the overall jerk and smoothness performance of the $X^{1.5}$ is optimum.

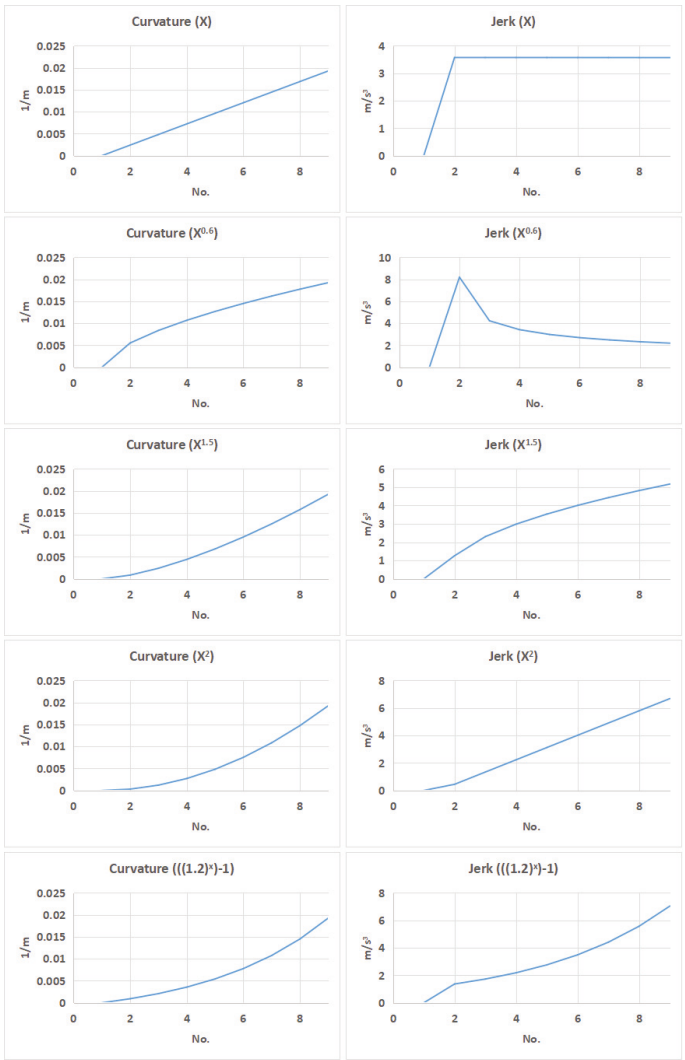

Figure 4.9: Different smooth curves curvature and jerk results as 45 m transition curves for greyhound racing.

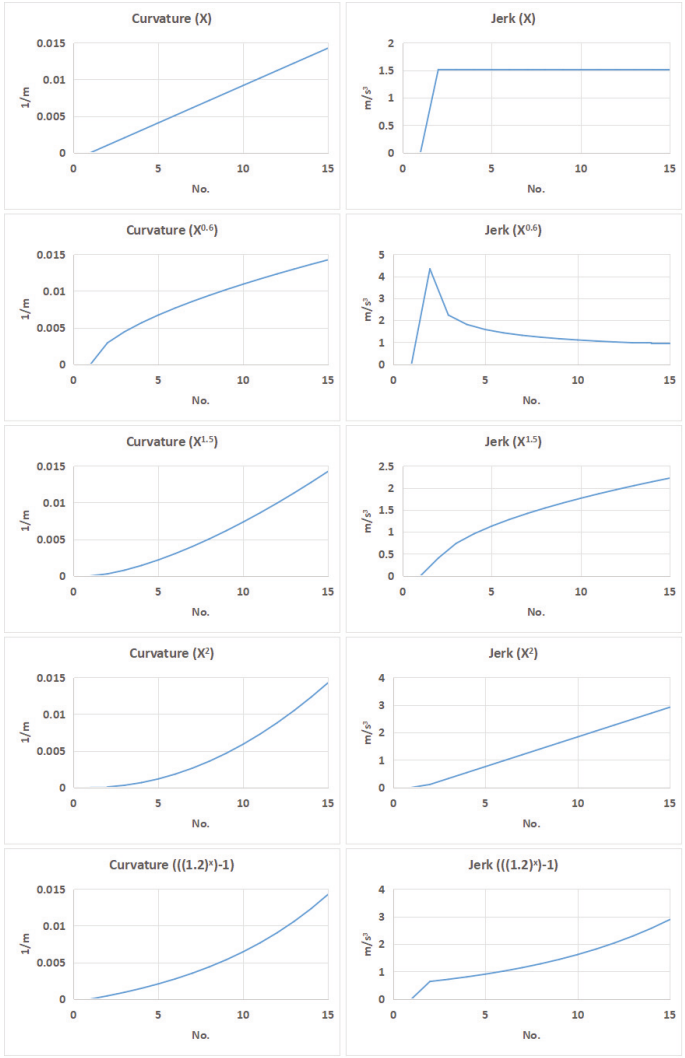

Figure 4.10: Different smooth curves curvature and jerk results as 75 m transition curves for greyhound racing.

Here, we generate composite transition curves with various degrees of G3 curvature continuity for racing greyhound ideal path design. Each composite transition curve generated combines the $X^{1.5}$ curve as an auxiliary curve and a clothoid curve as the main curve. So, the overall transition curve generating function can be considered as a piecewise function shown in Equation 4.40 where the auxiliary curve function

g is applicable until q transition segment is reached.

$$f(x) = \begin{cases} g(x)\ if\ x < q \\ z(x)\ otherwise \end{cases} \tag{4.40}$$

Where,

$$x = y(d, i) \tag{4.41}$$

4.7 Summary

The simulation and modelling of galloping quadrupeds racing primarily aimed to investigate various factors affecting greyhound racing dynamic performance. By analysing various synthesised data, the models were tweaked and refined over time and reached a certain level of maturity where the outputs from the models giving comparable results to actual race data. The numerical techniques presented are robust and can be algorithmically controlled to achieve defined goals compared to existing approaches for designing racing quadrupeds transitions. Moreover, models and numerical methods presented can be extended to meet new design criteria as well as used for the optimisation of quadrupeds dynamic stability in racing conditions. The successful application of introduced models and techniques would provide evidence to support tracks injury data. Finally, the methods presented here can also be used in designing and modelling trajectories for other moving bodies, including but not limited to horses, vehicles, and trains.

Chapter 5

Simulation and modelling results

5.1 Introduction

This chapter introduces and presents the findings and studies from race simulation and modelling of greyhound galloping path dynamics. The results show what can be achieved with regard to improving the stability of racing quadruped dynamics and factors that require optimisation.

5.2 Interpreting results

The results presented from simulation and modelling do not include psychological impacts in the outcome. Rather considerations from quadruped dynamics, race track condition and racing related subject matter are considered. The numerical results from both simulation and modelling techniques presented in Chapter 4, were highly convergent and sensitive to the variation of model inputs. This allowed the production of identifiable outcomes with a high degree of reliability in the generation of results. Various scenarios created resemble existing setups in the industry and setups from potential deployment options. From these results, it was possible to identify and analyse variables which define individual quadruped dynamics in racing, while ruling out racing conditions that have insignificant impacts in quadruped performance.

5.2.1 Greyhound heading

During a race greyhounds primarily chase a lure that stays ahead of them for the entire race period. Observations of single greyhounds from race trails indicated that the line of sight to the lure influences their motion at the track. Figure 5.1 shows lines of sight to a lure for greyhounds at the track. It was hypothesised at the beginning of this research that the line of sight to a lure determines the path taken by a greyhound while coming out of a starting box. This assumption was based on observation from several trail races like the following race trail videos, which were recorded during a track visit. Video 1 and 2 show box to track transition a greyhound's veering behaviour. In the videos, greyhounds followed a path defined by the line of sight to the lure instead of going straight towards a bend. However, since a race occurs in a pack where multiple greyhounds participate for a race distance, other influences such as congestion and peer pressure from nearby quadrupeds are also relevant.

Video 1: `http://bit.ly/379TttO`

Video 2: `http://bit.ly/363gBsY`

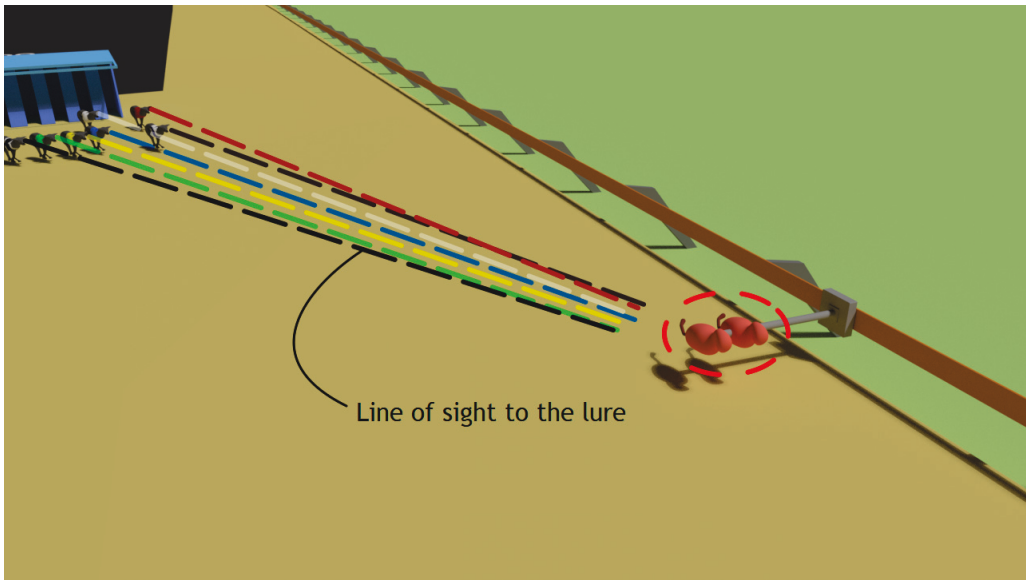

Figure 5.1: Lure visual contact of greyhounds after starting boxes gate opening.

In the simulation, a greyhound's heading was defined in terms of line of sight to the lure, peer pressure from nearby animals and other factors. However, the line of sight to a lure vector took precedence over any other factors and was a major guiding force for greyhounds. Furthermore, single greyhound paw print data from a track were compared to similar simulation setup results. This verified that the simulation results were comparable to the actual on-track behaviour. Consequently, it was found that the line of sight to a lure vector and the instantaneous speed defined the trajectory, hence the heading of the greyhound as shown in Figure 5.2. However, more analysis from the RLT data showed that a quadruped's heading is also dependent on the combined factors of starting box orientation at a track and the presence of surrounding quadrupeds. Figures 5.3 and 5.4 show the trajectory trace of greyhounds from the RLT data for boxes at different locations. It shows quadrupeds maintained a straight heading from the start for boxes located with offsets to the track whereas the heading was defined by the line of sight to a lure for starting boxes located at the track transition.

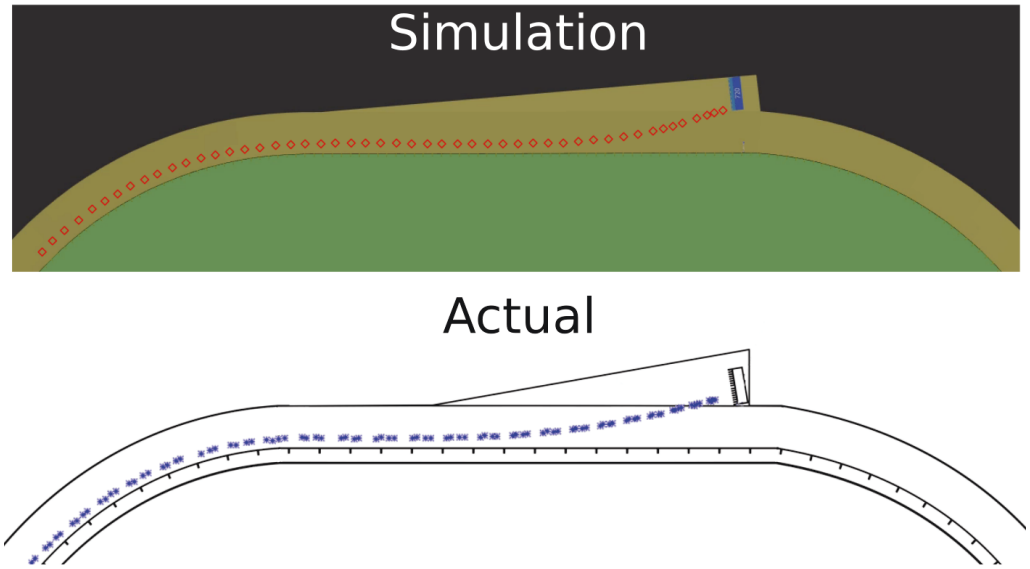

Figure 5.2: Path tracing of a greyhound from a race trail and a simulation.

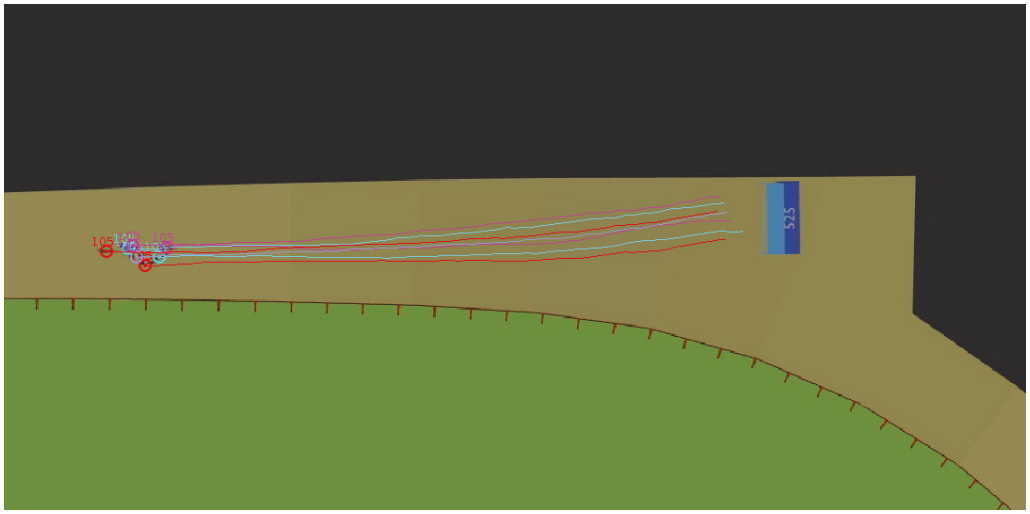

Figure 5.3: Path tracing of racing greyhounds for starting boxes located near a track's transition as derived from real-time location tracking data.

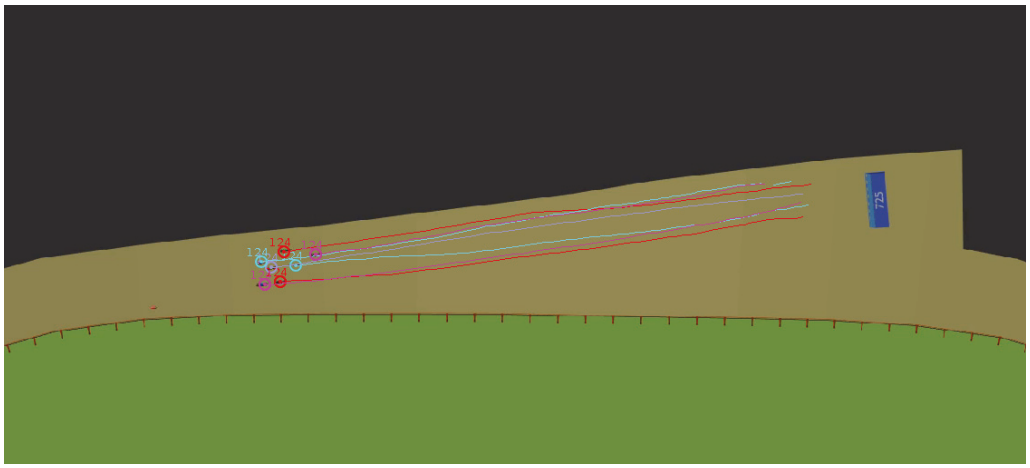

Figure 5.4: Path tracing of racing greyhounds for starting boxes located offset from a track's straight as derived from real-time location tracking data.

The line of sight to a lure following greyhounds tend to converge due to greyhounds heading toward a single point. This introduces congestion at various points at the tracks, as shown in Figure 5.5.

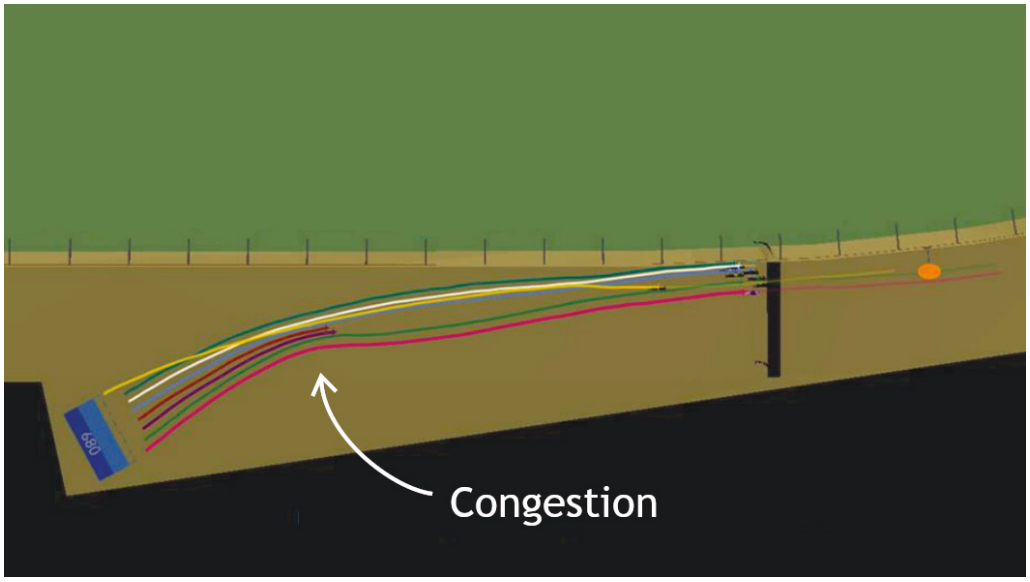

Figure 5.5: Greyhounds' trajectories converging due to single line of sight to a lure vector path following.

5.2.2 Greyhounds pack bend entry dynamics

In racing, there are various circumstances responsible for the dynamics at a bend. The bend imposes several challenges for fast-moving subjects. Notably, the approach into a bend requires precise and specific trajectory planning to maintain a smooth transition and dynamics stability to ensure a safe and effective outcome. Likewise, the dynamics states, such as leaning of a quadruped just after entering a bend have a determining factor in coping with the bend, as shown in Figure 5.6. Figure 5.6 shows that if the leaning of a greyhound is not adequate after entering the bend, the moment from the centrifugal force is going to rotate the greyhound anticlockwise. The following variables were deemed to be major contributing factors for bend entry dynamics.

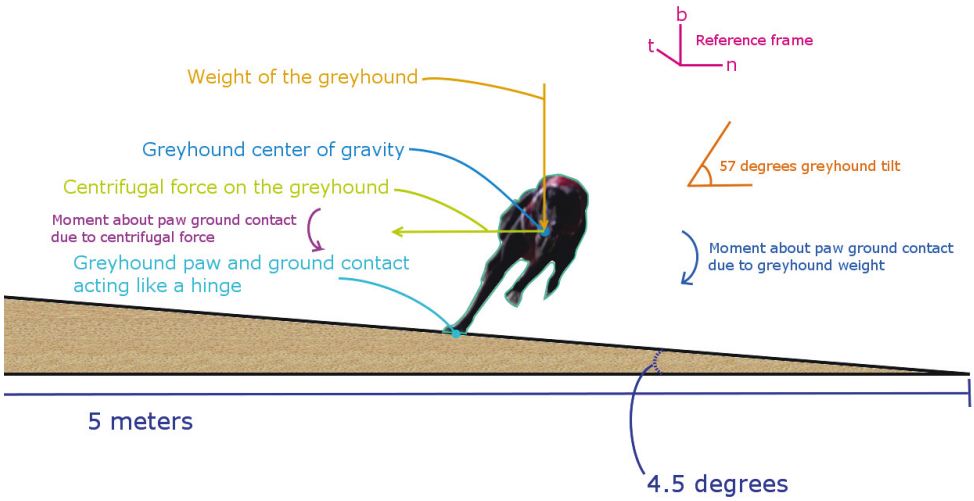

Figure 5.6: Key moments which act on a greyhound's centre of gravity at a bend.

Yaw rate

The yaw rate of a quadruped is the instantaneous variation of heading. It measures how quickly a greyhound is required to turn or change heading during a race. So, it

represents the angular velocity of a greyhound's body around the vertical axis [57]. In a straight path, the yaw rate is minimal while it would be highest in the curved or transition paths. Once the yaw rate is known, the corresponding heading turning radius can be calculated from Equation 5.1. Since the yaw rate is also a function of a greyhound's velocity and turning radius, a higher yaw rate involves higher acting lateral force on a greyhound.

$$R = \frac{Instantaneous\ speed}{Yaw\ rate} \tag{5.1}$$

Peer pressure

When several quadrupeds participate for part of the race distance, there are inconstant dynamic race outcomes due to distinct actions from the quadrupeds and corresponding situations arising at different instances in time. The vicinity of other quadrupeds in a group creates peer pressure or lack of clearance hindering sideways movements as well as going quicker or slower as the animals compete directly. Peer pressure is an important constituent in racing as most races occur in assemblies. One way to look at the peer pressure and its intensity and influence on an individual quadruped is to identify the amount of surrounding free space available for a quadruped. Various quadruped formations that occur during a race create different levels of peer pressure. Also, since greyhounds come out from the starting boxes with different velocities and accelerations, different orders in the pack are observed from the beginning of the race. The race simulations show the following major formation patterns commonly occur throughout the race, as shown in Figures 5.7 to 5.15. In simulations, the pack formations usually went through various transformations during a race, where the transformation patterns were unique for each race. For instance, during a race, the pack formation may take a large leading pack form to an evenly spread and then from an evenly spread to a twin cluster and finally a

twin cluster to a single leading greyhound at the finish line. These transformations in the pack formation were triggered at different points on the track, notably at various transitions, such as straight to bend and bend to straight. Each formation creates different intensities of peer pressure for competing quadrupeds. For example, a tightly packed formation, as presented in Figure 5.14, would create the highest peer pressure, whereas greyhounds line formation, as depicted in Figure 5.13, would create the least amount of peer pressure for different runners.

Figure 5.7: Single greyhound leading during a race simulation

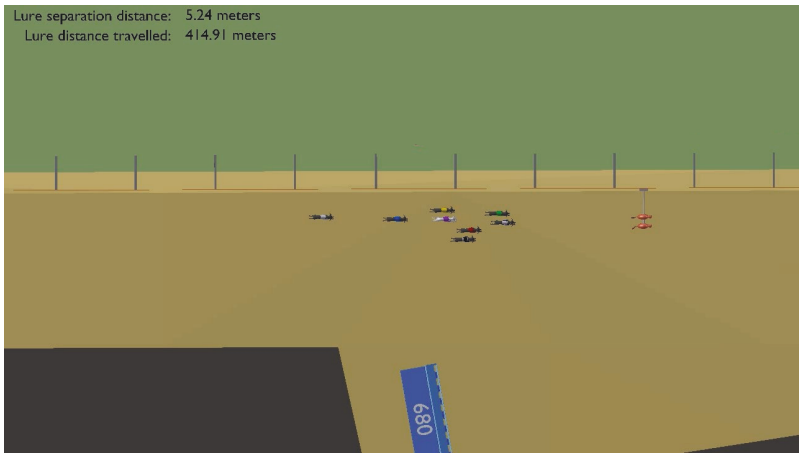

Figure 5.8: Single greyhound lagging behind during a race simulation.

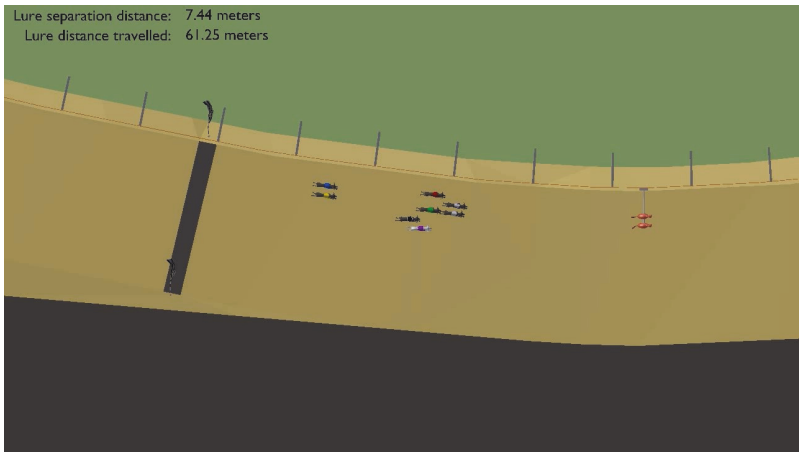

Figure 5.9: A number of greyhounds leading together during a race simulation.

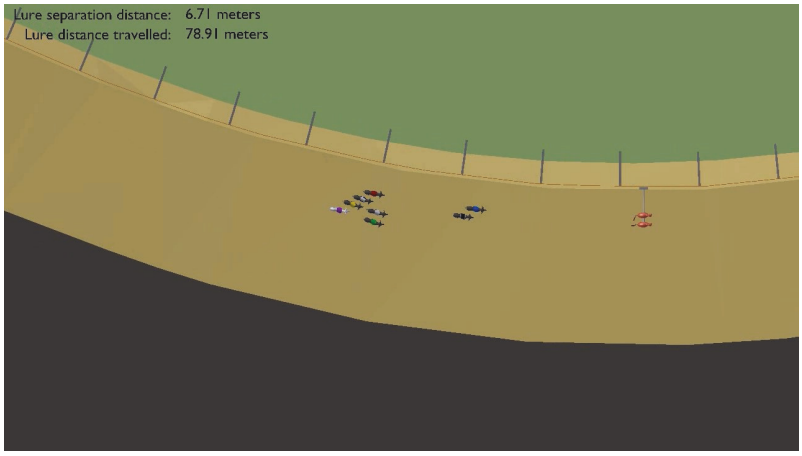

Figure 5.10: A number of greyhounds lagging behind together during a race simulation.

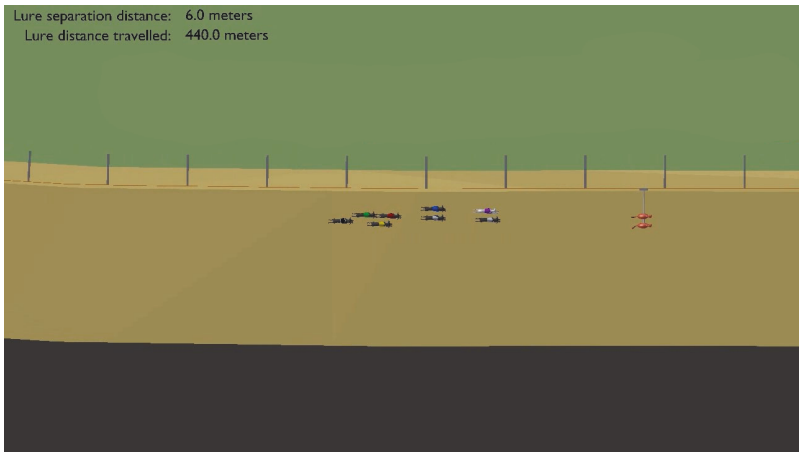

Figure 5.11: Evenly spread greyhounds maintaining chainage line during a race simulation.

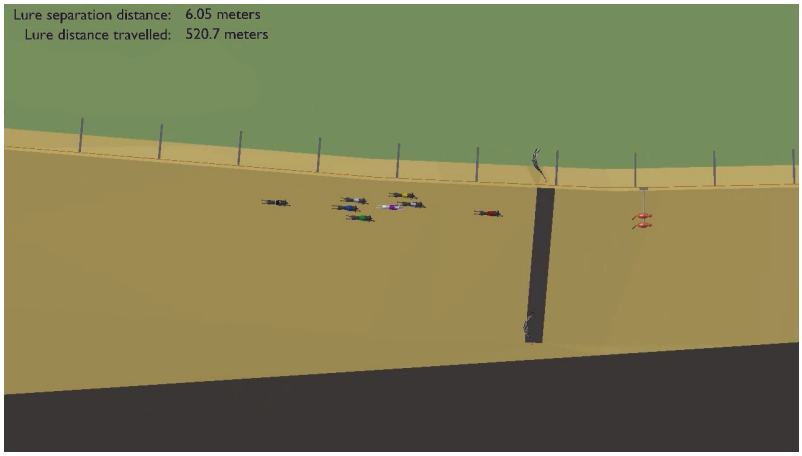

Figure 5.12: A cluster of greyhounds between leading and lagging greyhounds during a race simulation.

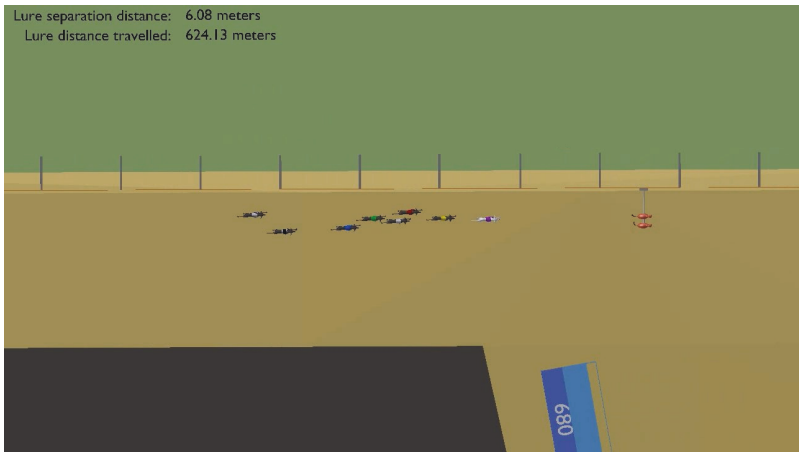

Figure 5.13: Greyhounds almost forming a line during a race simulation.

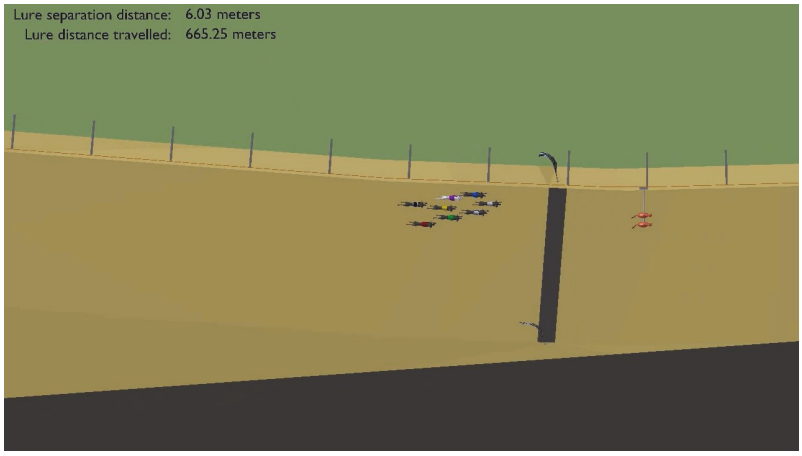

Figure 5.14: Tightly packed greyhounds during a race simulation.

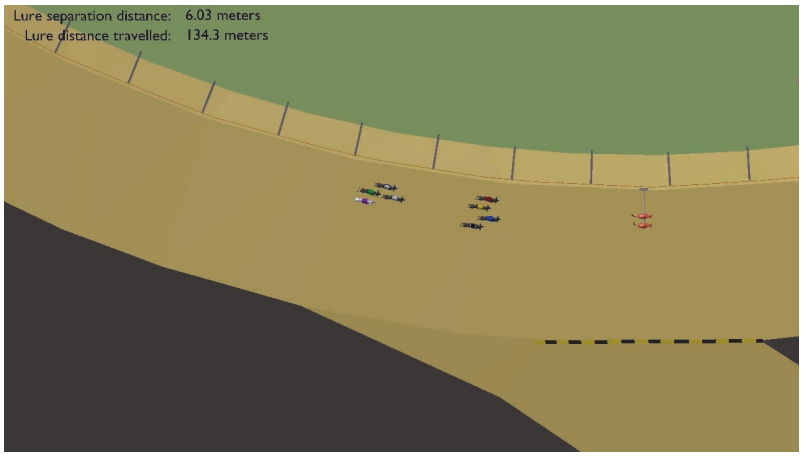

Figure 5.15: Greyhounds forming two clusters during a race simulation.

Two methods were utilised for analysing peer pressure from the race simulations. For the first method, the location of the greyhound pack centroid and then distances of individual runners from the centroid were averaged where the average distance gave a rough indication of peer pressure intensity influencing individual quadrupeds. Figure 5.16 illustrates the centroid location for a pack's formation for a race simulation instant. The second method was more elaborate in determining peer pressure intensity. It involved algorithmically finding the number of quadruped clusters present in a pack formation based on cluster radius, then calculating the average distances between one or more quadrupeds present in a cluster for all clusters in the pack formation. Figure 5.17 shows the identification of clusters during a race simulation instant for peer pressure interpretation using the second method. Both methods provide evidence of peer pressure, where the first method was more precise in recognising the overall pack congestion while the second method more accurately recognised the distances between a quadruped and its cluster.

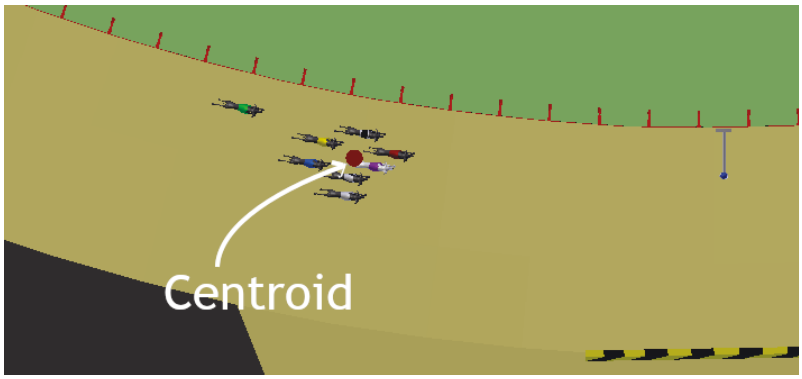

Figure 5.16: Greyhounds pack's centroid location during a race simulation.

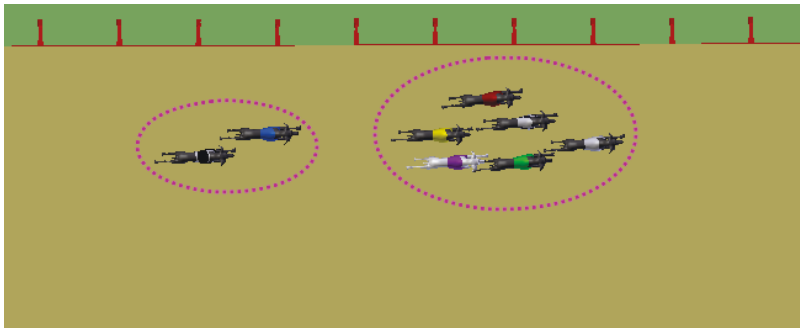

Figure 5.17: Greyhounds pack's clusters' locations identification during a race simulation.

Racing line

The racing line is an essential consideration for getting into and out of a bend smoothly in the shortest amount of time. It is the optimal path to move around any corner in a dynamically efficient manner. Depending on the severity of the corner, an optimum fit racing line can vary. Figure 6.9 shows an ideal racing line for a sharp turn racecourse where the moving subject would maintain outside edge before entering the corner and gradually would move towards the apex of the corner, and again gradually it would move towards the outside edge while leaving the apex. In GR, the bend entry lateral dynamics of multiple and single racing quadrupeds

is highly dependent on the close following of an optimum fit racing line. Thus, by comparing all quadrupeds' bend corner entry and exit trajectories to an ideal fit racing line, the dynamic balance of the quadrupeds can be known. Ideally, racing subjects should maintain a strong following of an optimum fit racing line by maintaining appropriate speed and steering during transitions into and out of a corner apex. Figure 5.18 gives the speed vs. distance relationship of a moving subject, which would closely follow a racing line. Furthermore, the diagram in Figure 5.19 illustrates a race line configuration for a greyhound track chainage. It shows preemptive turning significantly before the bend is required for quadrupeds to follow the racing line.

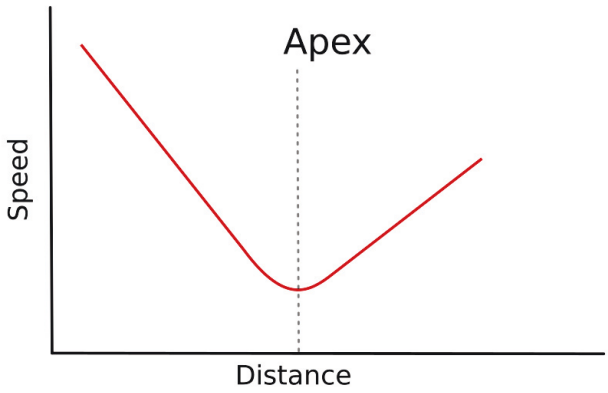

Figure 5.18: An optimum fit racing line's speed profile for a given apex of a corner [1].

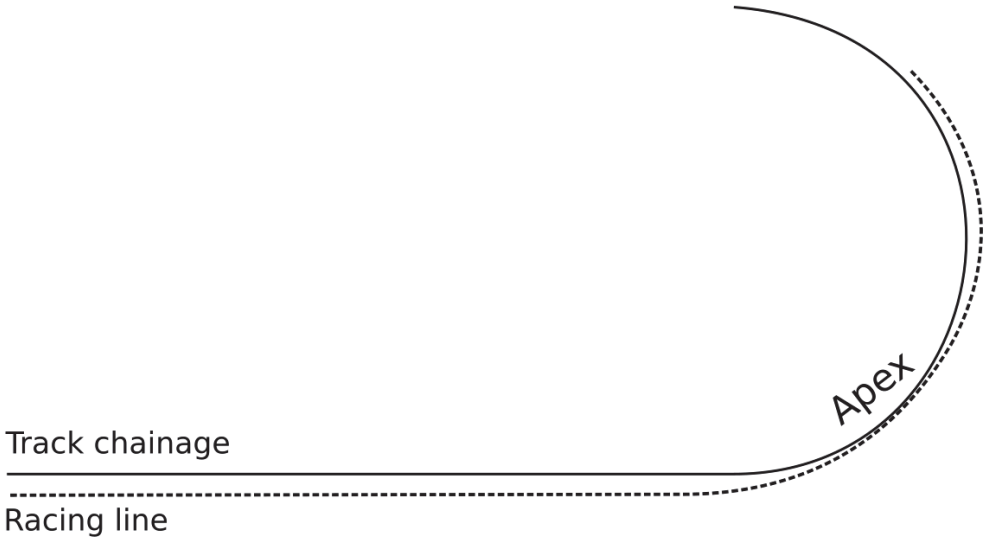

Figure 5.19: An optimum fit racing line for a given oval track's chainage path.

Simulation of greyhounds trajectories for bend entry

The simulation of GR revealed differences in the outcome of the dynamics of greyhound packs entering a bend. It showed that the misalignment of several factors is the leading cause of compromised dynamic stability after entering a bend. Figures 5.20 to 5.22 present the trajectories of greyhound packs as traced from simulations for three different race dynamics outcome scenarios during an approach to the first bend. First, the misalignment of yaw-rate and heading of greyhounds at the bend entrance from the ideal racing line and track bend tangent causes greyhounds to move into the bend in a straight path. This requires the production of a surge in the centrifugal force acting on the animal as the turning radius tightens due to the delay in initiating the turn, as can be seen from Figure 5.20. In Figure 5.20, the trajectories of pink, black, and yellow greyhounds deviated from the track path curvature after entering the bend and greyhound turning is delayed, tightening the turn radius afterwards because of yaw rate and heading misalignment at the bend entrance. This was due to a particular greyhound pack formation before the bend

entrance, which produced peer pressure that caused the misalignment of yaw rate and heading at the bend entrance in Figure 5.20. The peer pressure effects cascaded through the greyhounds, which, as a result, diverged the pink, black, and yellow greyhounds heading and yaw rate, resulting in significant dynamics instability for the greyhounds. On the other hand, in Figure 5.21 all greyhounds headings and yaw rates except green were in alignment with the track bend at the bend entrance, which resulted in smooth entry to the bend. Figure 5.22 reveals a similar situation to the scenario in Figure 5.20 where the green was deviated due to heading and yaw rate misalignment to the bend.

Simulation for Figure 5.20: `http://bit.ly/2uhyreg`

Simulation for Figure 5.21: `http://bit.ly/2NGQMZO`

Simulation for Figure 5.22: `http://bit.ly/36aTn47`

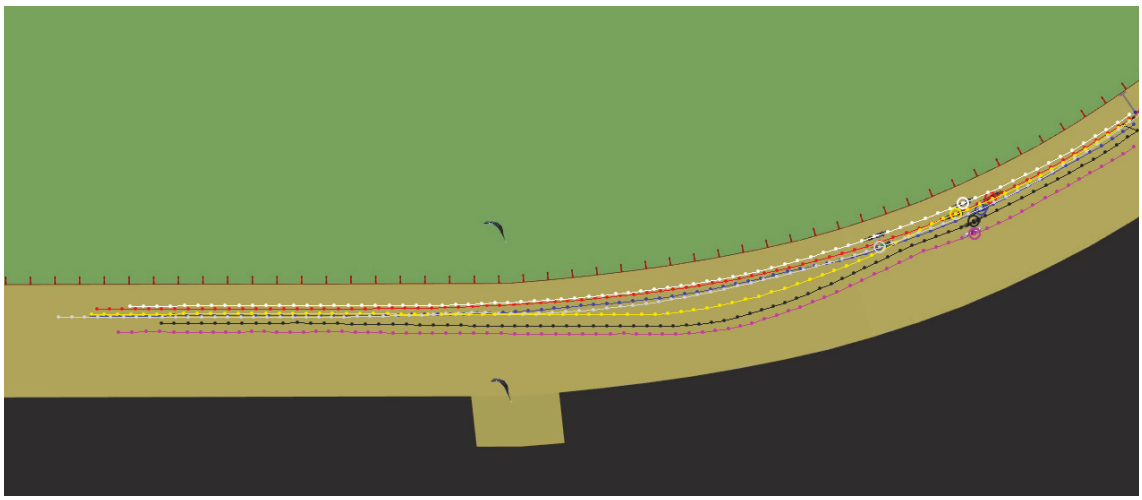

Figure 5.20: Trajectories of greyhounds entering the first bend during a race where the heading of some runners was deviated extremely towards outside edge after entering the bend.

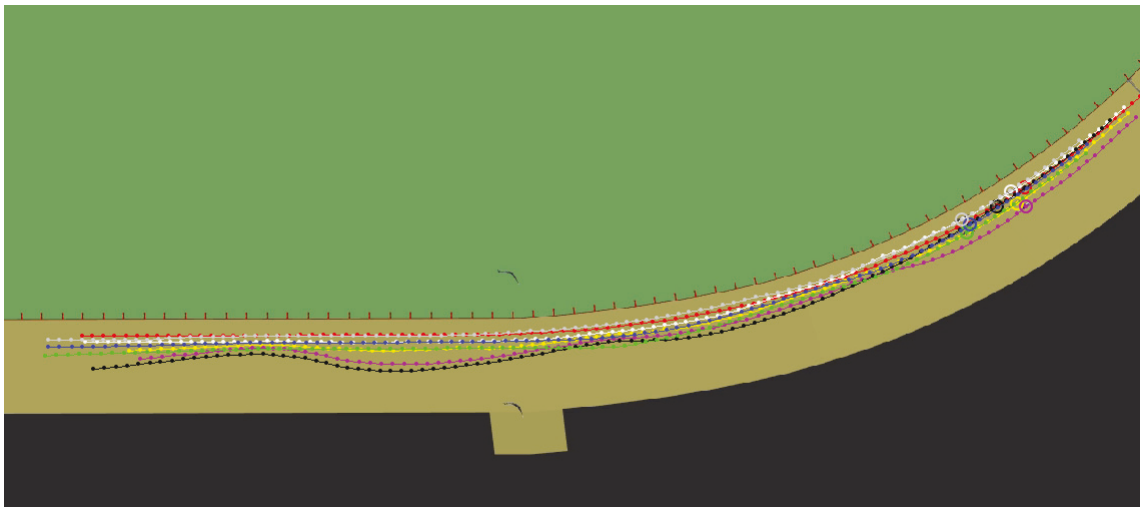

Figure 5.21: Trajectories of greyhounds entering the first bend during a race where the heading of all runners was aligned with the bend tangent at the bend entrance.

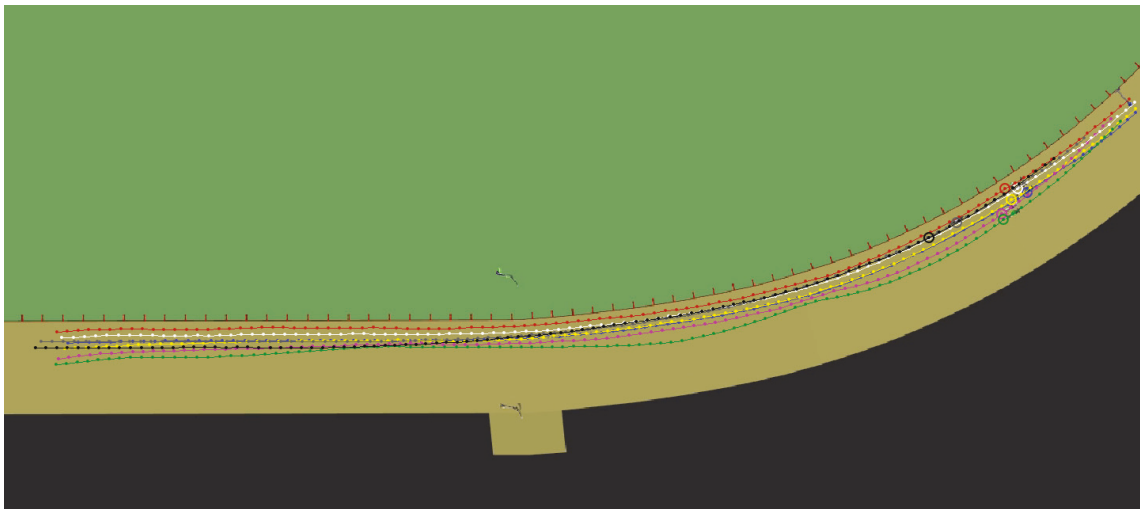

Figure 5.22: Trajectories of greyhounds entering the first bend during a race where the heading of all runners except one was aligned with the bend tangent at the bend entrance.

The evaluation of simulation results, as described above, shows the heading and yaw rate at the bend entrance is one of the principal determining factors for the dynamic stability of quadrupeds after entering the bend. Moreover, the heading and yaw rate

outcome at the bend can be defined by peer pressure and possible the line of sight to a lure in certain circumstances only. The specifics of peer pressure at the bend entrance come from the nature of pack formation before the bend entrance. The final trajectories of greyhounds due to bend entrance dynamics show the alignment of greyhound trajectories to the optimum fit racing line. The Equation 5.2 shows the main influencing variables for bend entry trajectory of a quadruped.

$$\begin{aligned} &Peer\ pressure + \ the\ line\ of\ sight\ to\ a\ lure\ influence = \\ &yaw\ rate + \ instantaneous\ speed + \ heading \\ &= \ trajectory\ immediately\ after\ entering\ bend \end{aligned} \tag{5.2}$$

5.2.3 Congestion in a race

Various race incident reports indicated that congestion in the race is an important matter that contributes to quadruped injuries. Congestion primarily occurs when there are interfering headings from multiple quadrupeds. Furthermore, as a consequence of high peer pressure within a pack and path selection decisions made by different competing quadrupeds, congestion introduces imbalances in the animal dynamics. In GR simulations, congestion was investigated in terms of peer pressure and lateral dynamics. Additionally, the possibility of high-risk congestion also has to do with the speed profile of racing quadrupeds. When heading acceleration among the racing quadrupeds is substantial, dynamic stability is significantly compromised even for moderate to low congestion due to significant forces required in the quadruped running gait. Accordingly, from the race simulations, high heading speed or acceleration change was derived from the average speed of a racing quadruped. The average speed provides a good indicator of the overall speed profile of a quadruped during a race regardless of momentary disturbances. Figure 5.23 represents simulations that obtained an average speed of a racing quadruped that

conforms with almost all oval tracks analysed. The average speed profile, as can be seen in Figure 5.23, shows that within an 80 m race distance, heading acceleration was considerably high, meaning congestion outcome within this distance would cause highly unstable dynamic states. Figure 5.24 portrays an oval track where the high heading acceleration is mapped as obtained from the quadruped average speed profile. Like shown in Figure 5.24 almost all GR oval tracks analysed for this research showed that quadrupeds enter the bend with a high heading acceleration due to 80 m distance placements of the starting boxes from bends.

In simulations, congestion-related dynamics were benchmarked by three key parameters, namely: yaw rate, vertical acceleration and pack density. The yaw rate determined the turning tendency of a quadruped during a race. Similarly, the vertical acceleration showed the movement along the width of a track. Through the pack density, the proximity between quadrupeds was examined. When there is congestion, a higher yaw rate or rate of rotation of heading shows up compared to the yaw rate for track path curvature following, collision avoidance, bumping, and checking. This considerably higher yaw rate is shown in Figure 5.25, where it shows that the average of instantaneous yaw rate of quadrupeds across 100 simulation races skyrocketed at three distinct locations at a track, as marked by three circles in the graph. The first two locations where yaw rate of quadrupeds abruptly increased were three seconds after the quadrupeds jumped out from the boxes. Likewise, the third sudden change in the yaw rate, as indicated by the circle in Figure 5.25 happened five seconds into the race following the entrance to the track bend. When this yaw rate result was compared to the average vertical acceleration of quadrupeds for the same simulated races, it showed the similar occurrences in the quadrupeds' vertical acceleration. As can be seen from Figure 5.26, the vertical acceleration of quadrupeds was highest within the first three seconds of races considering boxes to track navigation needed greyhounds to move closer to the lure running rail track

inside edge by moving across the track width which was inclined due to the track cross falls. Likewise, the immediate spikes in the vertical acceleration after five seconds into the races following the bend entrance indicated movements of greyhounds across the width of the track. Further, the sudden spike in vertical acceleration after five seconds into the race was due to the aftermath of high congestion and resulting deviations of greyhounds paths from the track path curvature.

A related finding from the pack density study of the same simulated races revealed that the inverse of pack density reached a minimum after five seconds into the race, following the track bend entrance and then went up again to the original value. This pack density result is shown in Figure 5.27, where it shows the inverse of pack density as calculated by taking the inverse of the average value of the quadrupeds' distances to pack centroid. A lower and higher value in the inverse pack density indicated higher congestion and lower congestion, respectively. Additionally, for pack density calculations, the inverse value of the average of the quadrupeds' distances to pack centroid was preferred because it classified the predominant pack density occurring from the race data.

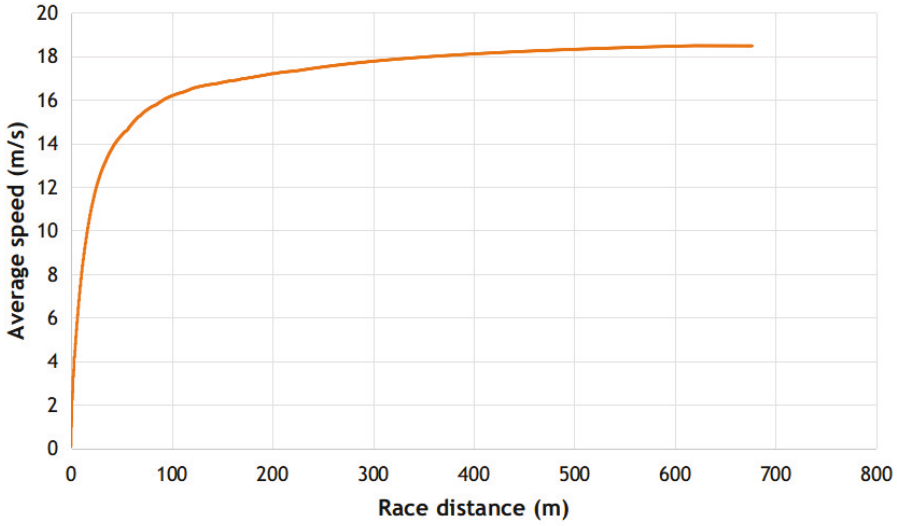

Figure 5.23: Average speed of a quadruped during a race as calculated from simulation races average.

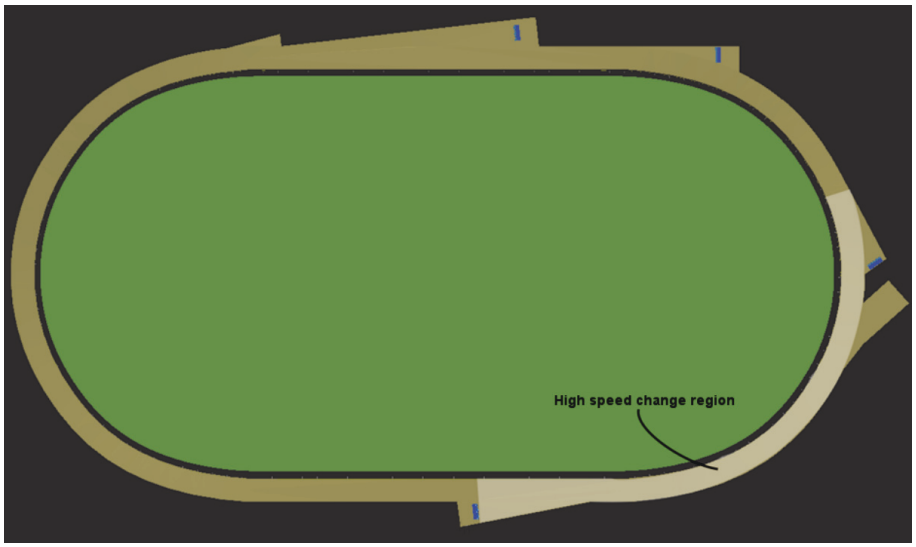

Figure 5.24: High speed change region at a track as indicated in simulated races.

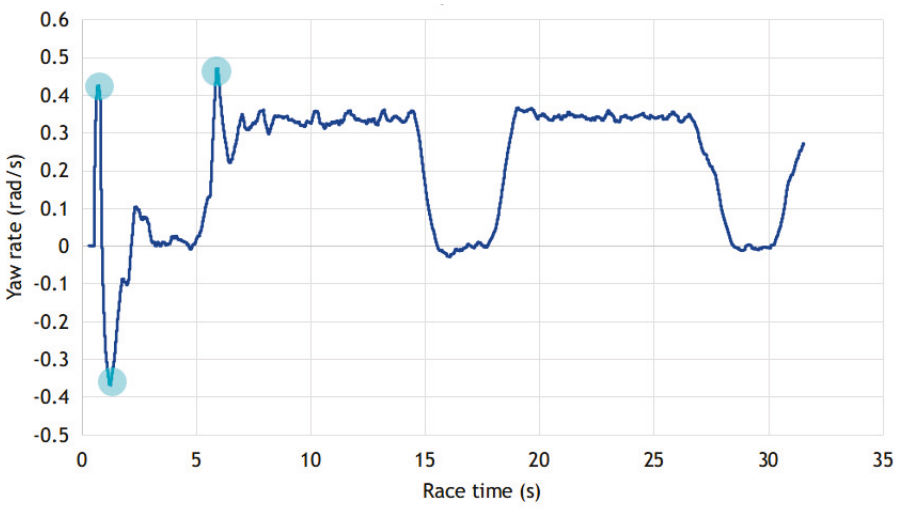

Figure 5.25: Yaw rate of greyhounds' average for 100 simulation races for a track.

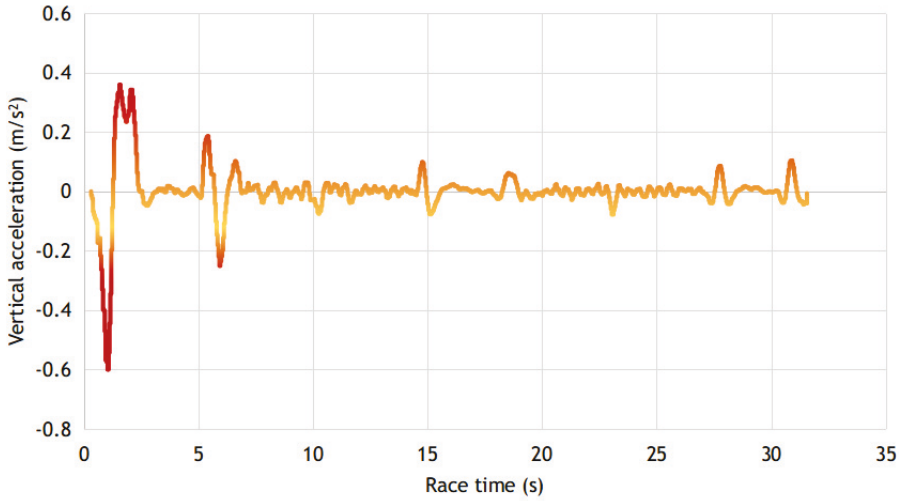

Figure 5.26: Vertical acceleration of greyhounds' average for 100 simulation races for a track.

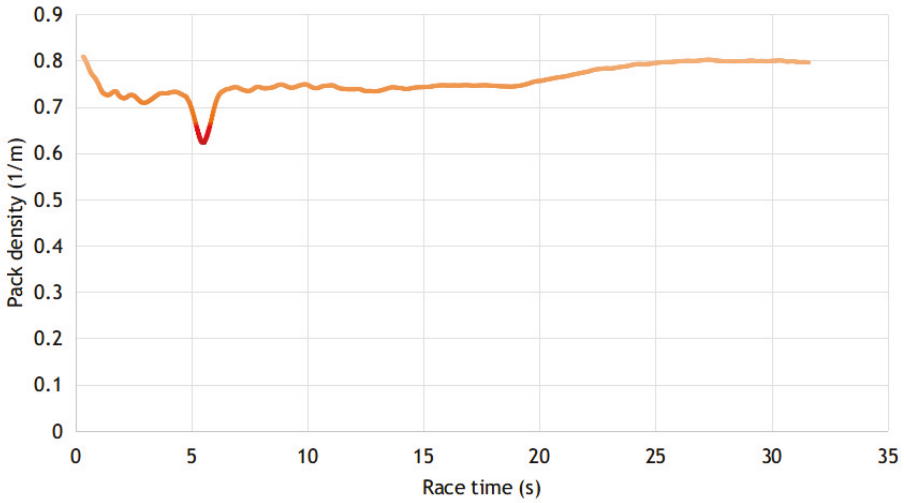

Figure 5.27: Greyhounds' peer pressure result as indicated by the inverse of pack spacing value for 100 simulation races for a track.

5.2.4 Driving conditions of a lure

The following lure setups and corresponding race dynamics performances were investigated.

Starting boxes opening and a lure's location

In GR, greyhounds are ordered in their respective starting boxes before a race begins. In race simulations, lure location and instantaneous speed after the opening of starting boxes affected the quadrupeds' transitions from boxes to track trajectories. Additionally, it was recognised from actual races that the apparent location and motion of the lure motivated the quadrupeds to run faster or slower. Likewise, it was verified from actual race videos that sharp heading deviations and convergence of the quadrupeds running path from starting boxes play a role in congestion occurring as those shown in the following videos:

Race Video 1: `http://bit.ly/2FSk4jp`

Race Video 2: `http://bit.ly/36Y4TB3`

In race simulations, this sharp deviation of a quadruped beginning from a starting box was alleviated by locating a lure further ahead of the starting boxes, as shown in Figure 5.28. Figure 5.28 shows the lure placement and its distance along the lure rail at the time of the boxes opening to ease the sharp deviations of the quadrupeds.

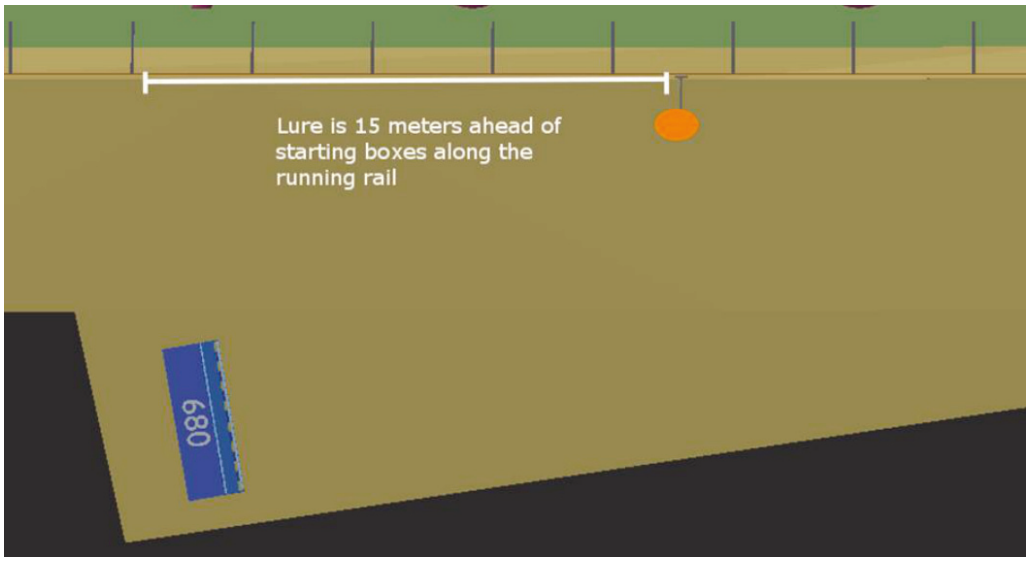

Figure 5.28: The track inside edge lure location the moment a race starts.

In race simulations, the effect of the lure location at the time of the starting boxes opening was analysed. This is shown in Simulation analysis 1-5 below. The optimal lure race starting time location varied slightly for different location placements of starting boxes. However, starting boxes which are located outside of a track within the straight path boundary is most exposed to the effect of lure race starting time location. For this reason, lure location criteria at the time of a starting box opening was established for this location on a track. Now, when the lure is nearest to the greyhounds at the time of the boxes opening the dogs had to change their direction rapidly towards the lure running rail, as can be seen from Simulation analysis 1. For a lure that was placed further away from the greyhounds during the boxes opening, greyhounds turned more gradually as shown in Simulation analysis 5.

Simulation analysis 1: `http://bit.ly/35YFtSy`

Simulation analysis 2: `http://bit.ly/30mwWro`

Simulation analysis 3: `http://bit.ly/2tZoouv`

Simulation analysis 4: `http://bit.ly/2uO5pmN`

Simulation analysis 5: `http://bit.ly/2tZ0wXL`

Figure 5.29 depicts the running path outcomes for Simulation analyses 1 - 5. As depicted in Figure 5.29, for scenario one, the lure location was nearest to the greyhounds' pack at the time of the boxes opening. Whereas, in scenario five, the lure location was most distant. Two parameters were identified for a lure location to yield optimum dynamics for the quadrupeds pack trying to merge with the track chainage line from the boxes. Namely the smoothness of individual greyhound path and the convergence of quadrupeds. Each scenario outcome in terms of these two parameters is given in Table 5.1.

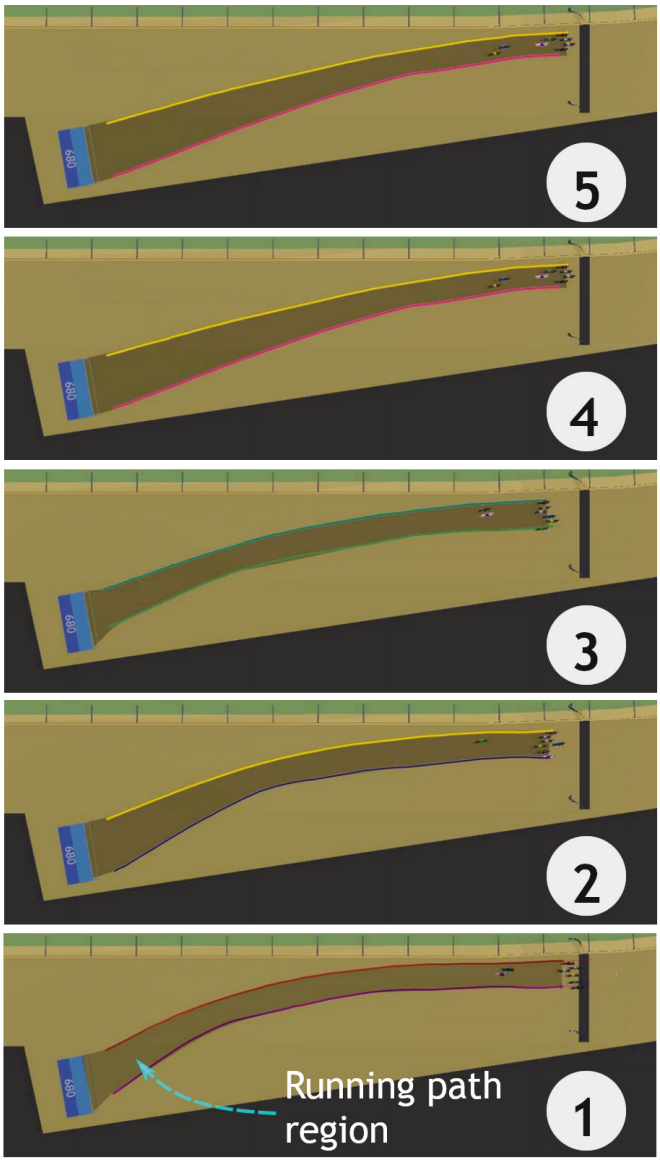

Figure 5.29: Different lure location configurations at the time of boxes opening resulted in different running paths for a greyhounds pack.

Table 5.1: Scenarios analysis for different lure location configurations at the time of boxes opening.

Scenario	Outcome
1	The trajectories of greyhounds leaving the boxes were similar to their trajectories for going around a bend yet the convergence of greyhounds was relatively decent.
2	As the lure was somewhat distant during the boxes opening which resulted in high initial dogs concentration, so there were high step deviations in the greyhounds' path.
3	The lure distance was raised a little further which made the greyhounds choose of path progressive and less abrupt while maintaining decent convergence.
4 and 5	High convergence as well as low path smoothing for the greyhounds due to lack of lure influence in boxes to track transition development which resulted in a sudden change in heading near the end of the transition.

The alignment of a lure inside a track

At the GRNSW and GRV tracks the lure was supported by a track inside edge rail as shown in Figure 5.30. Simulation of races showed a lure's alignment with respect to the track defines some aspects of race dynamics regardless of the lure supporting infrastructure. As a lure travels around a track, it creates a pursue path for greyhounds that depends on the lateral location of the lure inside the track as depicted by Horizontal location in Figure 5.30. The pursue path of a lure sets greyhound heading yaw rate, where the optimum yaw rate is a function of starting box alignment with respect to the track and lure traverse location inside the track.

Simulation data recorded that within a first few hundred milliseconds into a race greyhounds would reach their first maximum yaw rate. Also, the lateral location of a lure defines the line of sight to a lure vector more strongly than the vertical location of the lure since the vertical distance between the lure and a greyhound is minimal. Consequently, in race simulations, the effect of a lure's lateral location inside the track and the corresponding yaw rate was examined.

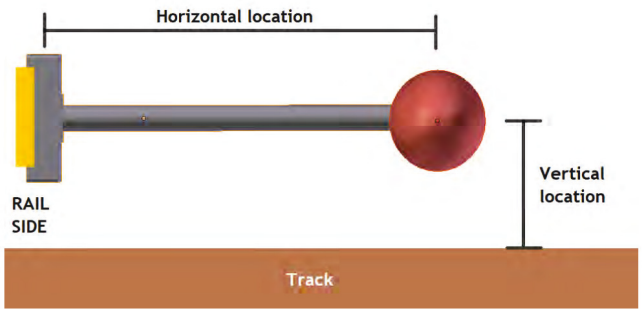

Figure 5.30: Lure alignment inside a track.

Simulation of a single greyhound running at different tracks showed that placing a lure closer to the starting boxes increases greyhounds yaw rate. A lower and gradually varying yaw rate is beneficial as it would imply a smooth heading of a quadruped and regular lateral force acting. Figure 5.31 illustrates yaw rates of a greyhound from race simulations for different lateral lure locations relative to the track inside lure rail for a starting distance. As shown in Figure 5.31, the 0.5 m lateral location of the lure created a maximum yaw rate while an abrupt change was occurring at around 1.92 s. No abrupt change in the yaw rate was noticeable for the 1.2 m, 1.5 m and 2.0 m lateral lure locations. The sudden change in the yaw rate for the lateral lure locations 0.5 m and 1.0 m was consistent with the path correction needed by a quadruped due to speed profile incompatibilities. Also, the lateral location of 2.0 m was required for a minimum race opening yaw rate. This analysis of the yaw rate showed that a lure and quadrupeds speed profiles, as well

as the lateral location of the lure, all need to be compatible with one another for optimum path smoothing for the quadrupeds.

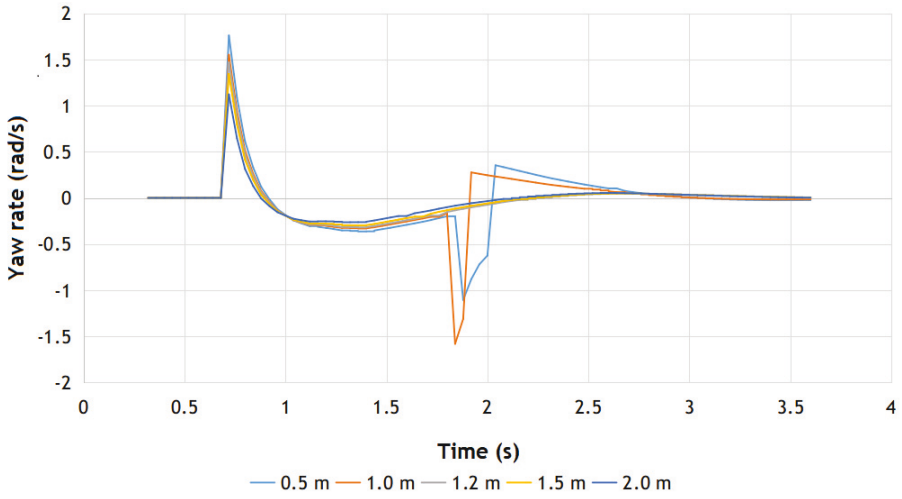

Figure 5.31: Yaw rate variations for different lure lateral locations inside a track.

Following are the simulation videos for Figure 5.31 results:

Simulation for 0.5 m: `http://bit.ly/35XG9aK`

Simulation for 1.0 m: `http://bit.ly/2tplSxo`

Simulation for 1.2 m: `http://bit.ly/2Nv4pe6`

Simulation for 1.5 m: `http://bit.ly/2TrEBTH`

Simulation for 2.0 m: `http://bit.ly/2QV54Ye`

Lure separation from greyhounds

A number of race simulations of identical setups were conducted where the only factor that was variable among the races was lure separation distance from the greyhounds pack. The objective of these setups was to see if there is a direct relationship between the distance of lure to a leading greyhound and race dynamics outcome. This sensitivity analysis of maintaining different lure and greyhound separation distance was accomplished by examining two separate greyhounds pack

spacing parameters. The intent of this analysis of pack spacing parameters was to understand quadrupeds pack formation variability to different lure separation distances. Three different overall lure separation distances of 5 m, 6m, and 7 m were selected for the study. Figures 5.32 and 5.33 portray the pack spacing results of race simulations for a track. Figure 5.32 presents a pack spacing parameter results as derived by calculating an average of quadrupeds' distances from the pack centroid. This parameter gave an indication of pack formation type and corresponding peer pressure.

As shown in Figure 5.32, pack spacing outcome was comparable for the 6 and 7 m lure separation distances meaning that the average distance of greyhounds from the pack centroid followed the same pattern for the conditions of these two lure driving races. Also, when the lure separation was maintained at 5 m greyhounds congested for a more extended period compared to 6 and 7 m lure driving conditions as indicated by a lower pack spacing value. For the 5 m lure separation distance, the dispersing of greyhounds happened to occur at least 100 m later into the races. Figure 5.33, illustrates results from another pack spacing parameter as derived by calculating an average of distances between a greyhound and its neighbouring greyhounds present in a greyhounds cluster for all greyhounds. As can be seen from Figure 5.33, the distance between the greyhounds fluctuated at different points at the track for all lure separation distances. Compared to 5 and 7 m separations, the 6 m separation resulted in improved congestion in the first bend, which can be between 100 and 200 m distance, where the quadruped's distance from each other was higher for 6 m lure separation. The 7 m separation lure driving resulted in the lowest clearance between the greyhounds for the first 100 m distance into the race compared to the 5 and 6 m lure separations. These analyses of pack spacing parameters showed that the 6 m separation distance to lure improved congestion of racing greyhounds compared to the 5 and 7 m lure driving conditions.

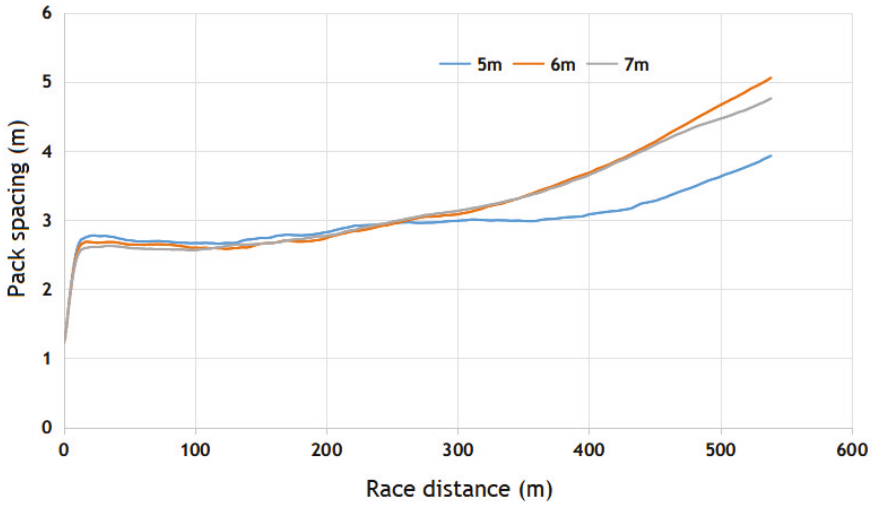

Figure 5.32: Pack spacing calculation using pack centroid to quadrupeds distances for 525 m distance race simulations.

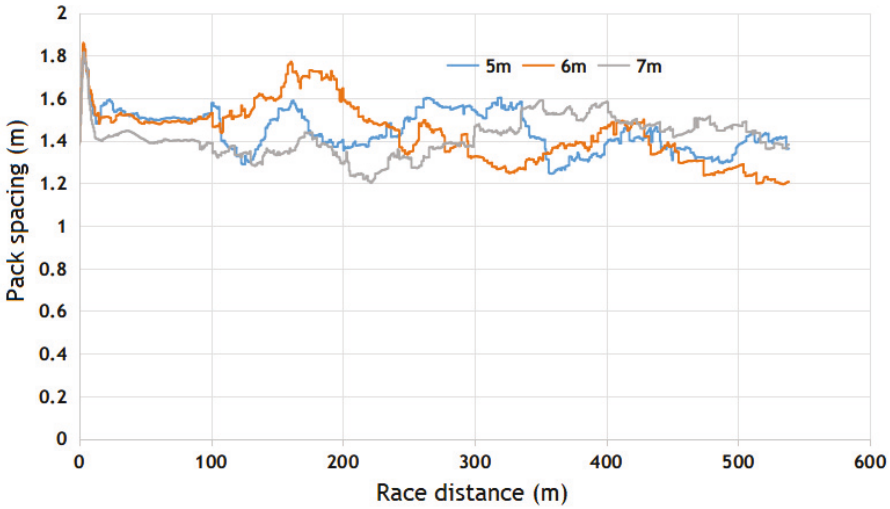

Figure 5.33: Pack spacing calculation using quadruped distance to other quadrupeds present in different clusters during a race for 525 m distance race simulations.

Motion of a lure

The lure driving scenario during a race can be another factor that affects race dynamics. Three different lure driving scenarios, as denoted by Configuration A, B,

and C, were designed in the race simulations to observe race dynamics sensitivity to lure motion. In the first scenario, lure separation distance to greyhound was kept nearly constant for the entire race duration as can be seen from Figure 5.35. In the second scenario, the lure separation was fluctuated for the first 17.5 s into the races and then maintained relatively constantly afterwards. In the third scenario, the lure distance to the greyhounds was reduced gradually until 14.8 s into the race and then kept constant afterwards.

The inverse of the average greyhounds' distances to the pack centroid, as presented in Figure 5.35 shows substantial congestion locations occurred at different points on the track for the alternative lure driving configurations. Further, an increase in the inverse value indicates an increase in congestion. For all three scenarios, the first bend of the track produced substantial congestion. As can be observed from Figure 5.35 between 5 and 6 s, the inverse of pack density reached a low, indicating a sudden change in clearances for greyhounds during that period. The inverse pack density decreased gradually for the first scenario, indicating a gradual decrease in congestion for this type of lure running condition. Likewise, the third scenario where the lure separation distance gradually lowered, resulted in a persistent congestion pattern over the race distance period. Lastly, for the second scenario where the lure running configuration resulted in overall lure separation distance under 8 m and the separation distance varied according to the track path curvature for the first half of the races produced an increase in greyhounds congestion over the race distance period as shown in Figure 5.35.

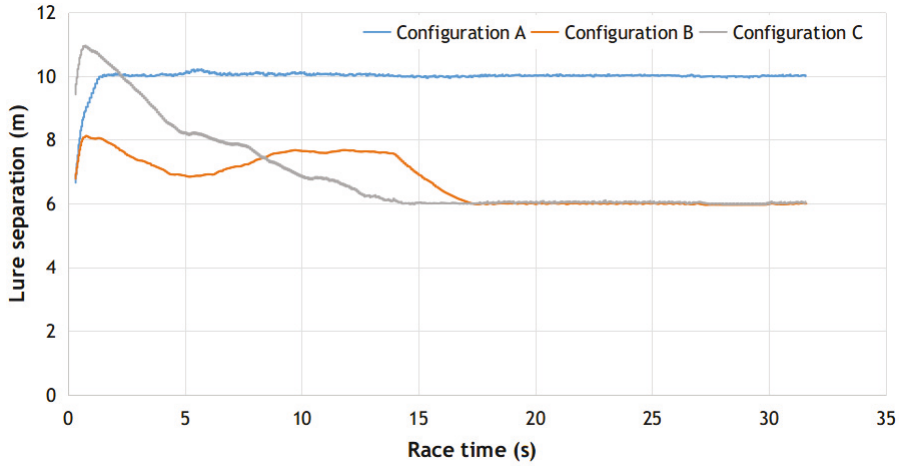

Figure 5.34: Lure separation distance performance for three different lure driving configurations.

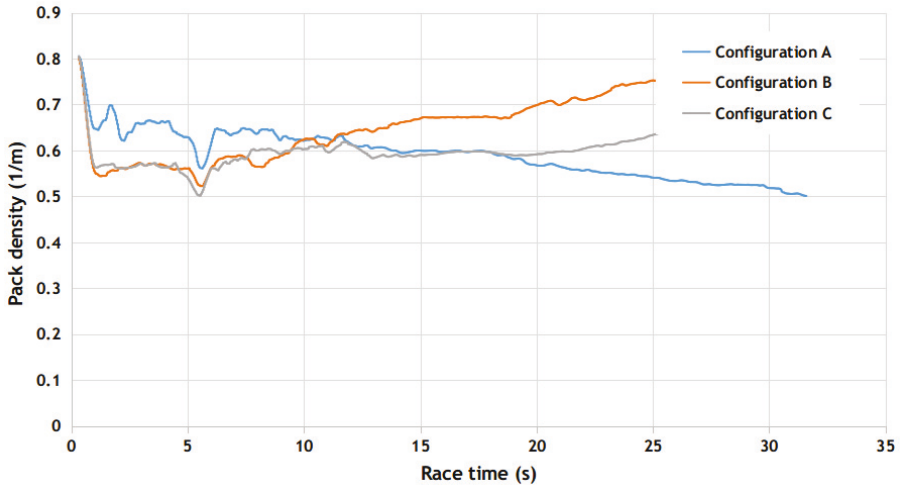

Figure 5.35: Greyhounds' peer pressure result, as indicated by the inverse of pack spacing value for three different lure driving configurations.

Similarly, overall yaw rate was highest for the first lure driving scenario, which is shown in Figure 5.36. The overall yaw rate was slightly higher for the second lure running scenario in comparison to the third scenario, which indicated a close following of track path curvature by the quadrupeds even though the track path was

not optimum.

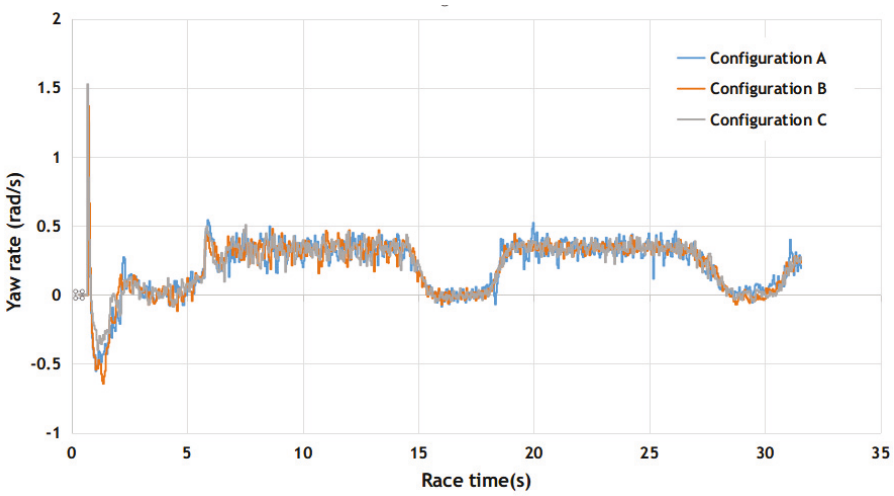

Figure 5.36: Average yaw rate of greyhounds for three different lure driving configurations.

When it comes to vertical acceleration of quadrupeds the third lure driving scenario as designed by Configuration C created unstable vertical motion among the greyhounds compared to the lure running scenarios Configuration A and B. This motion related to the climb up and down the track cross falls at a higher rate for the distance up to the first bend, as can be seen between zero and 6 s in Figure 5.37. The overall vertical acceleration was highest for the lure running Configuration A and lowest for Configuration B.

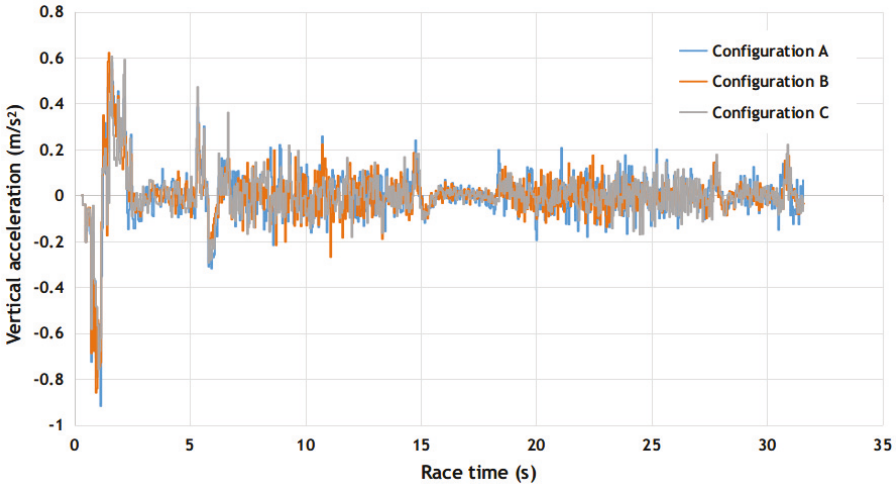

Figure 5.37: Average vertical acceleration of greyhounds for three different lure driving configurations.

This particular study of lure motion configuration established that lure driving is a visible determining factor in race dynamics outcomes where a track path situation adaptive approach to lure driving would improve efficient dispersing of the quadruped pack.

5.2.5 Arrangements of starting boxes

Starting boxes are containers for quadrupeds from where they begin a race. In Australia, it is typical to find eight greyhounds competing for a race distance where all the greyhounds jump off from a single unified starting box with individual stalls for each greyhound, as shown in Figure 5.38. The most common thing to notice with starting boxes is the path interference of greyhounds shortly after leaving the box. This can be seen in Figure 5.39. This interference is due to the arbitrary headings of greyhounds while coming out from the boxes. The path interference increases the possibility of greyhounds bumping into one another from all sides. Another common phenomenon is starting box alignment with a track causing greyhounds to make swift changes in their headings and yaw rates, as can be seen in

Figure 5.40. This happens when the boxes are laid out without considering the natural trajectories of greyhounds. Here the trajectories are not within the bounds of a track, requiring greyhounds to undertake sudden heading alterations. Similarly, starting box locations at a track can also influence the box-to-track transition of greyhounds trajectory, as shown in Figure 5.41. In Figure 5.41 trajectories of greyhounds coming out from the boxes are an optimal fit with the track chainage line. The following sections summarise simulation results pertaining to starting box setups and corresponding race dynamics performance outcomes.

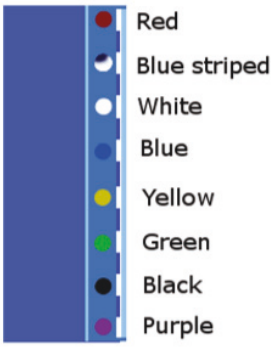

Figure 5.38: Starting boxes arrangement inside a container for 8 greyhounds.

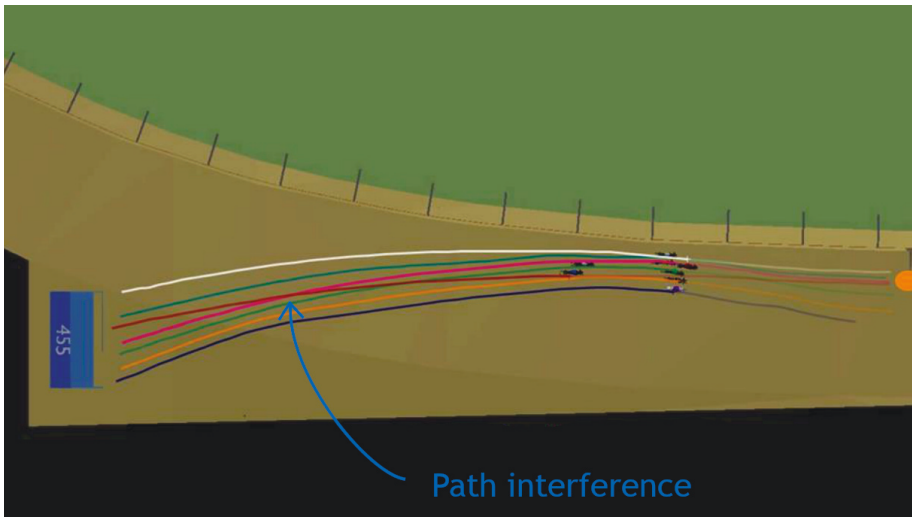

Figure 5.39: Path interference between greyhounds due to natural trajectory outcome by different starting headings from different boxes.

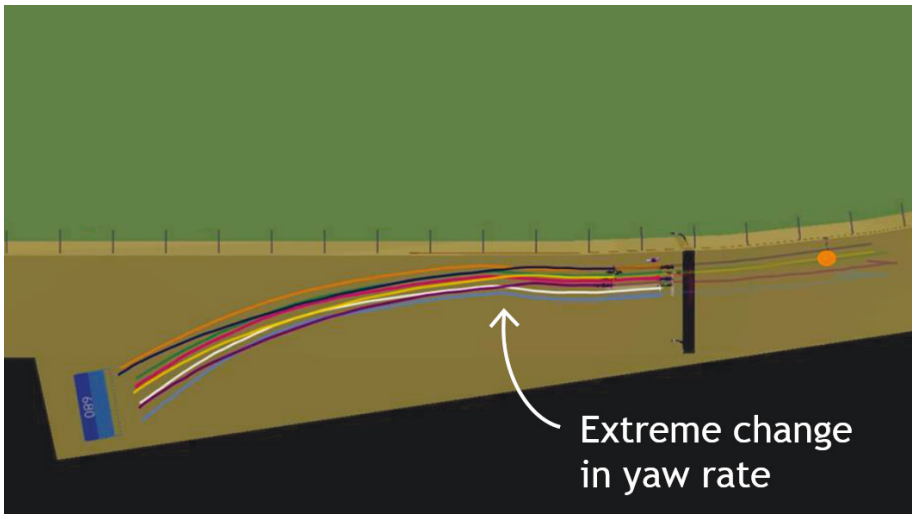

Figure 5.40: Trajectories of greyhounds not bounding to the track dimensions forcing greyhounds to make sudden changes in the yaw rates and headings.

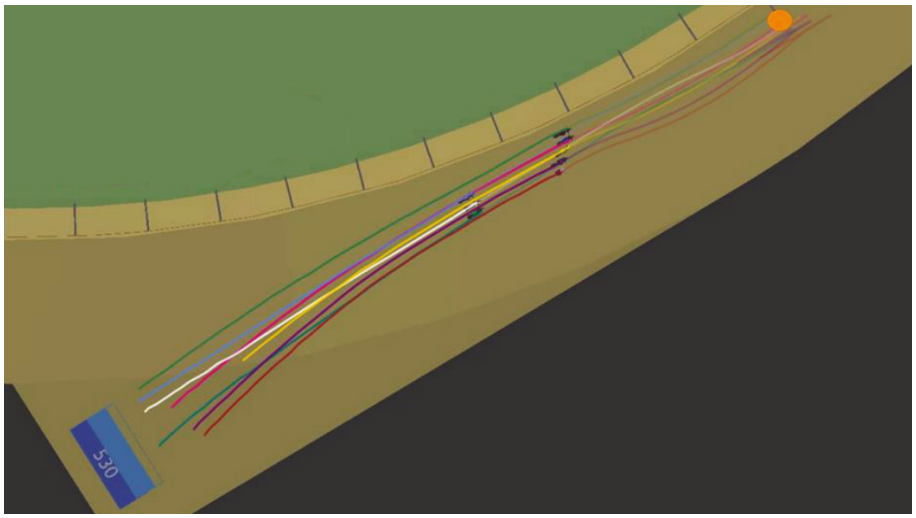

Figure 5.41: Trajectories of greyhounds which are aligned with the track chainage path when the starting boxes are located at a track bend and rotated to be tangent to the track bend radius.

Orientation of starting boxes

Starting box orientation relative to track path can influence trajectory outcomes for quadrupeds and therefore, dynamics of a quadruped. Using a best fit racing line an optimum orientation for starting boxes can be established where the yaw rate of quadrupeds would be minimum and quadrupeds heading into the bend is optimum for the approach. However, in GR an optimum orientation for starting boxes can not be determined entirely from the geometry of a track as the trajectories of greyhounds coming out from the boxes also depend on the lure placement and lure motion during a greyhound's transition to the track. Therefore, an optimum orientation for starting boxes for GR can be designed by knowing lure motion after starting box gate opening, as well as the natural greyhound trajectory response to the lure motion and then optimising the trajectories for an optimum fit racing line.

Figure 5.42, represents an orientation of starting boxes relative to track bend entrance tangent as found in most GRNSW and GRV tracks. Figures 5.43 and 5.44

show two other starting boxes orientation configurations for the same race distance location, shown in Figure 5.42. Yaw rate performance for these three starting box orientation configurations is depicted in Figure 5.45. Configuration 1, which is found in existing GRNSW and GRV tracks, gave a maximum yaw rate value of nearly 1.42 rad/s and took a greyhound more than a 40 m run distance to align with the track chainage path. If the boxes are rotated 4 deg anticlockwise from the orientation Configuration 1 like shown in Figure 5.43, it produced a maximum yaw rate of approximately 1.73 rad/s which allowed the greyhound to merge with the track chainage after a 40 m run distance from the boxes. If the boxes are rotated to 8 deg anticlockwise from the orientation Configuration 1, as shown in Figure 5.44, then the maximum yaw rate from the boxes was reduced to approximately 1.10 rad/s, this also allowed the greyhound to merge with the track chainage within the 40 m run distance. Differences between the yaw rates for Configuration 2 and 3 as well as the yaw rate of Configuration 1 clearly showed that designing of box orientation would require greyhound trajectory and lure speed profile consideration. Furthermore, the best approach to box orientation would also involve designing for an optimum fit racing line while lowering the maximum yaw rate from the boxes.

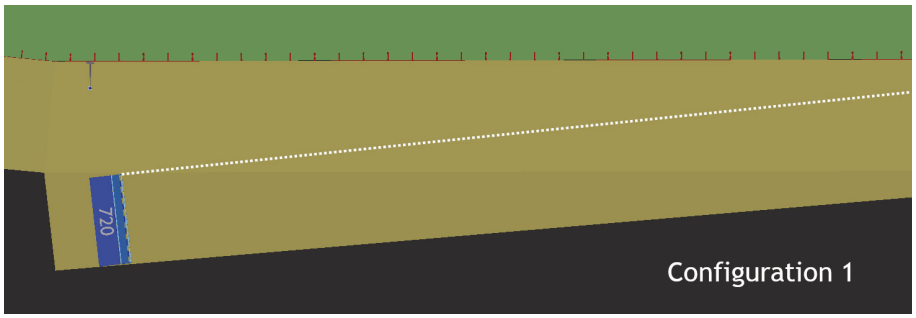

Figure 5.42: Starting boxes which are located off a track's straight and rotated to the tangent of the bend entrance.

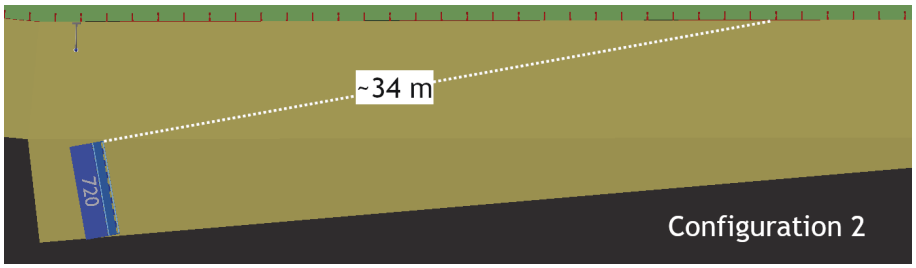

Figure 5.43: Starting boxes which are located off a track's straight and rotated such that it is pointing at the track inside edge from a distance of about 34 m.

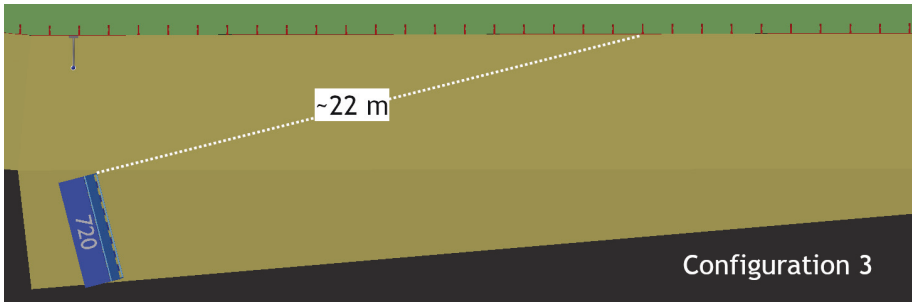

Figure 5.44: Starting boxes which are located off a track's straight and rotated such that it is pointing at the track inside edge from a distance of about 22 m.

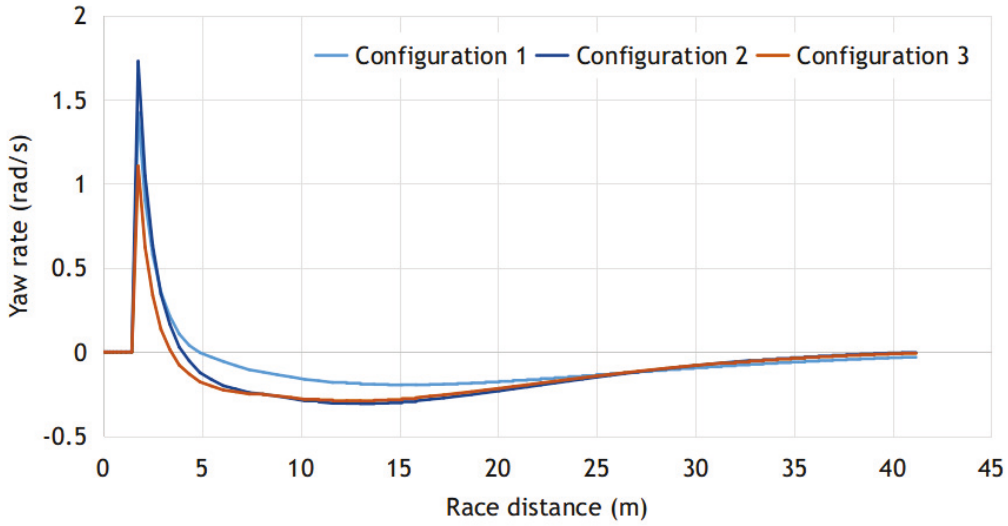

Figure 5.45: Yaw rate performance of a single greyhound for three different starting box orientation configurations.

Heading offset for quadrupeds

The starting boxes arrangements for greyhounds from GRNSW and GRV showed that multiple greyhounds are arranged in a row inside starting boxes, creating a distance bias among greyhounds for box-to-track transitions, as shown in Figure 5.46. The greyhound furthest away from the lure initially has a longer distance to run, as shown in Figure 5.46, because of this bias. To reduce the distance bias and understand the corresponding race dynamics results, race simulations were conducted by providing heading leads to greyhounds further away from a lure. The arrangement resulted from this setting of greyhounds inside the boxes can be seen from Figure 5.47, where red is the greyhound closest to the lure and purple is furthest from the lure. The race dynamics results from these two arrangements of greyhounds are depicted in Figures 5.48 and 5.49. As can be seen from Figure 5.48, the race simulations did not point to any substantial variations in lure driving performances. This is indicated by results for lure separation distance with and without heading offsets in Figure 5.47. This indifference to lure separation distance between the two greyhounds arrangements indicates simulation setup integrity between the two arrangements. Figure 5.49 displays pack density as the inverse of average for greyhounds' distances from pack centroid that showed major congestion and dispersing trends in the races for the two greyhounds arrangements setups. As can be seen from the graph in Figure 5.49 both setups for greyhound's arrangements resulted in a significant drop in congestion five seconds into the races, which occurred immediately after the entrance into the first bend. Also, the inverse of pack density parameter showed congestion was slightly more intense for the no heading lead arrangement setup compared to with heading lead setup after the 5 second event. Likewise, the heading lead arrangements for greyhounds resulted in a relatively smoother lead into the first bend as can be seen from the stable trend in the pack density value compared to no heading lead setup. However, the race simulations predicted slightly

higher peer pressure development in greyhounds with heading lead setup compared to normal setup.

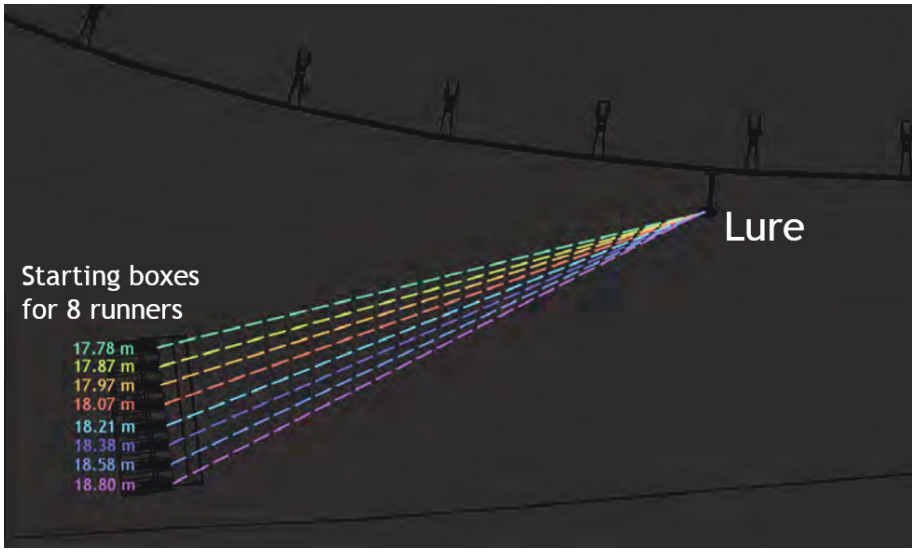

Figure 5.46: Greyhounds' initial distances to a lure at the time of starting boxes gate opening.

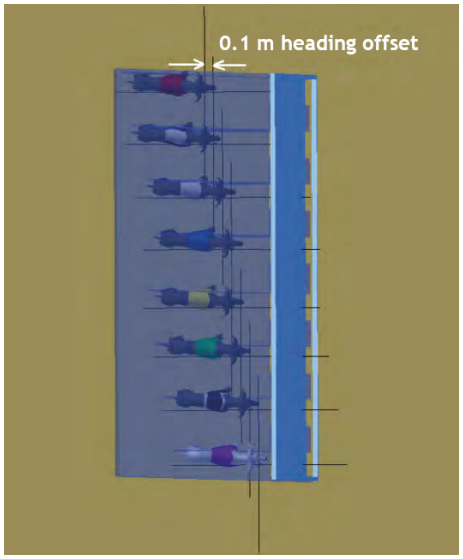

Figure 5.47: Greyhounds which are arranged with a constant distance lead from its neighbouring greyhound.

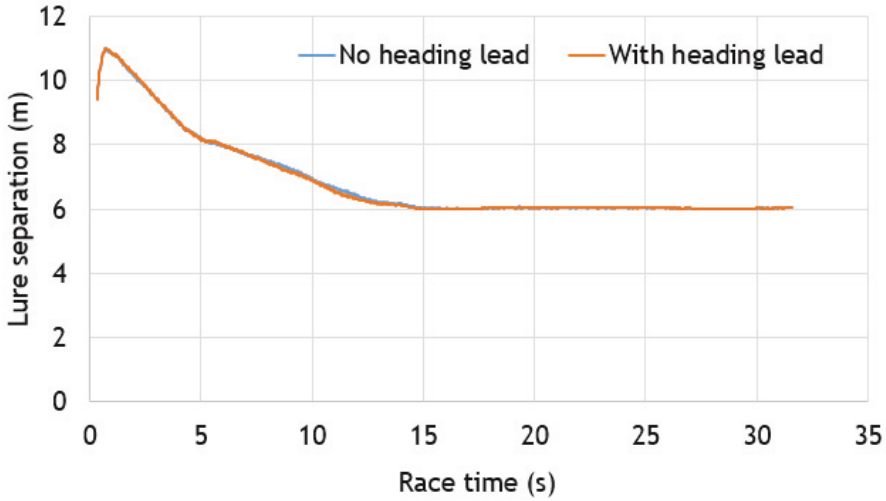

Figure 5.48: Lure separation from the greyhounds during a race for 100 simulated races with and without greyhound heading lead offset.

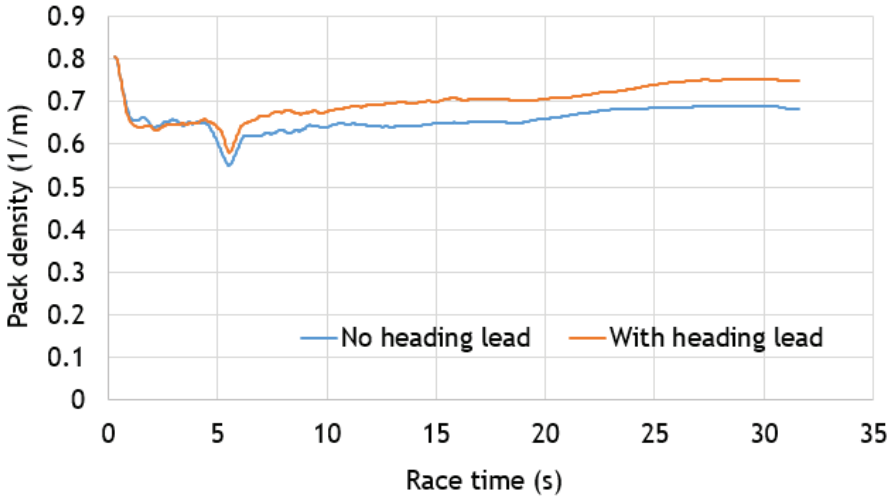

Figure 5.49: Pack density value of 100 simulated races with and without greyhound heading lead offset.

Number of starts for a race

At a GRNSW or GRV track race meeting, it is a commonplace to find eight greyhounds starting for any given race. The effect of altering the number of competing

greyhounds in pack formation was analysed in race simulations by considering six greyhounds instead of eight greyhounds in a race. The results are shown in Figures 5.51 and 5.52 where Figure 5.50 shows lure driving performance in terms of lure separation from greyhounds when number of competing greyhounds was reduced to six greyhounds. As can be seen from Figure 5.50, the lure driving performance outcome between six and eight starts race were almost identical except a slight difference between 100 m and 300 m distance into the race. Furthermore, the lure separation distance gradually came down and reached a low at around 250 m into the race distance and gradually climbed up again for the race with eight greyhounds starts as seen from Figure 5.50. This happened partially due to the presence of a bend at a track. However, no such situation was noticeable for the race with six greyhounds starts as can be seen from Figure 5.50. Figure 5.51 shows that overall pack spacing was slightly higher for the eight greyhounds starts race compared to the six starts race up until 270 m into the race distance as indicated by a lower pack spacing value for the eight starts. As a result, during the six greyhounds starts races greyhounds dispersed slightly more efficiently compared to the eight greyhounds starts. However, another pack spacing parameter, as shown in Figure 5.52 depicted different race dynamics outcomes between the races with six and the eights greyhounds starts. Figure 5.52 shows a pack spacing parameter value evaluation by greyhound clusters consideration which indicated the average distance between a greyhound from a nearby greyhound. The graph in Figure 5.52 shows that the average distance between a greyhound from a nearby greyhound was moderately lower for the six greyhounds starts, indicating a higher peer pressure compared to the eight greyhounds starts races. Consequently, the six greyhounds starts races imposed another sort of challenge for the racing greyhounds compared to the eight greyhounds starts races.

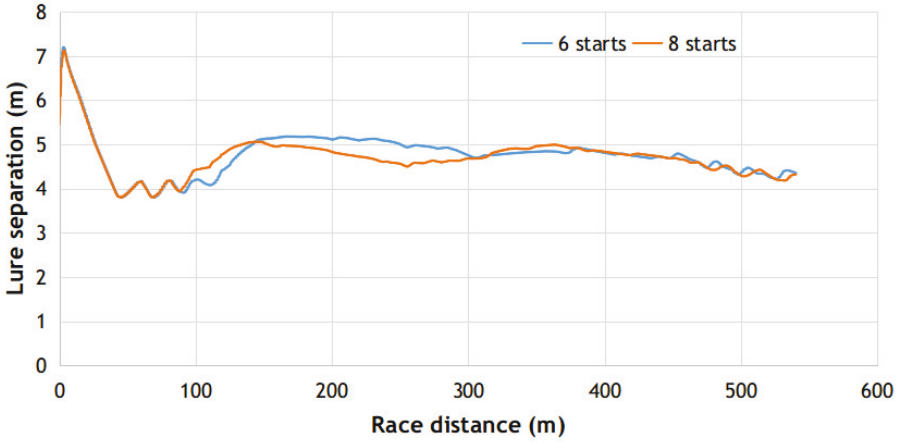

Figure 5.50: Lure separation from the greyhounds for six and eight starts races from the race simulations.

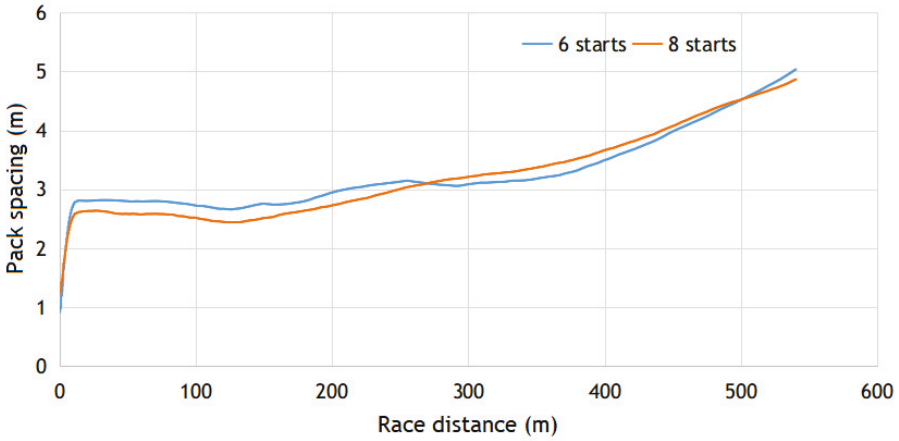

Figure 5.51: Pack spacing calculation using pack centroid to quadruped distance for six and eight greyhound starts simulated races.

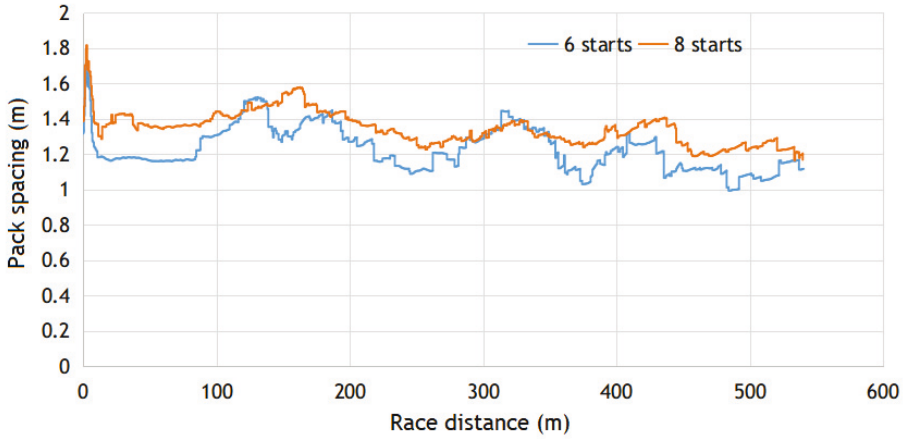

Figure 5.52: Pack spacing calculation using quadruped distance to other quadrupeds present in different clusters for six and eight greyhound starts simulated races.

Normally in a GRNSW and GRV race meeting all the greyhounds are placed side by side in a tightly spaced manner, where the gap between greyhounds are less than the width of one greyhound as shown in Figure 5.53 (top configuration). Race simulations were carried out to find race dynamics results for more spacious arrangements like shown in Figure 5.53 (bottom configuration) where four greyhounds instead of eight starts for a race are deployed. Figures 5.54 and 5.55 depict pack spacing parameterisations by greyhounds distance to pack centroid distance and greyhounds distance to its cluster distance outcomes respectively for both standard eight greyhounds arrangement and spaced four greyhounds arrangement races. As can be seen from Figure 5.54, overall pack spacing value was considerably higher for the standard eight greyhounds race arrangement, which indicated a lower peer pressure for this arrangement compared to the spacious four greyhounds arrangement. Similarly, Figure 5.55 shows that the average distance between the greyhounds was moderately low up until a 120 m distance into the races for the spacious four greyhounds starts arrangement compared to the standard eight greyhounds starts races as indicated by a lower pack spacing value.

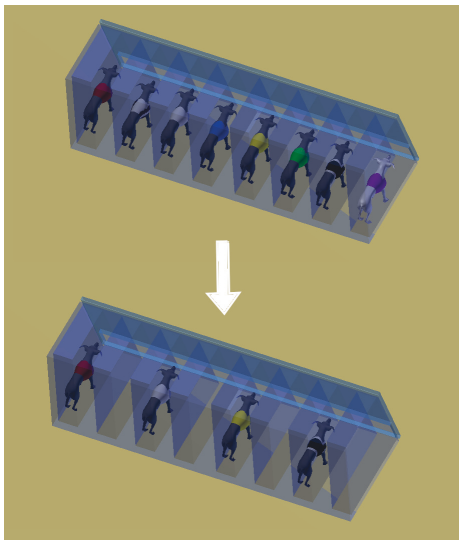

Figure 5.53: Placement of four greyhounds instead of eight for giving more clearance between the greyhounds.

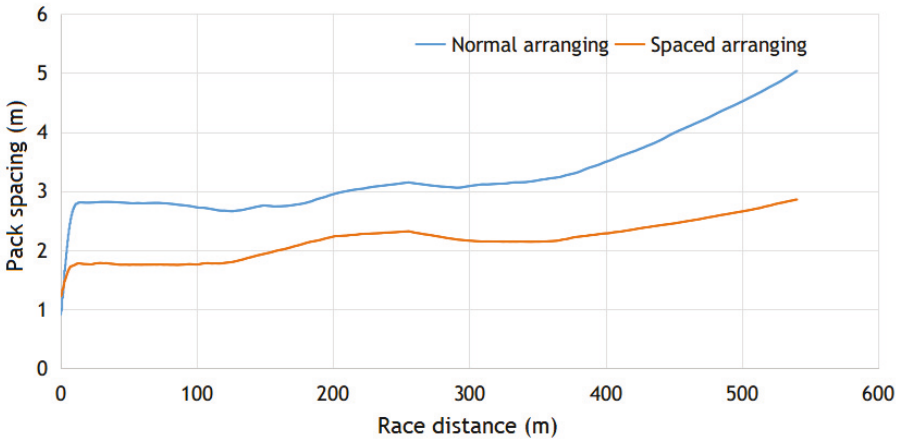

Figure 5.54: Pack spacing calculation using pack centroid to quadruped distance for normal eight and spaced four greyhound starts races from the simulated races.

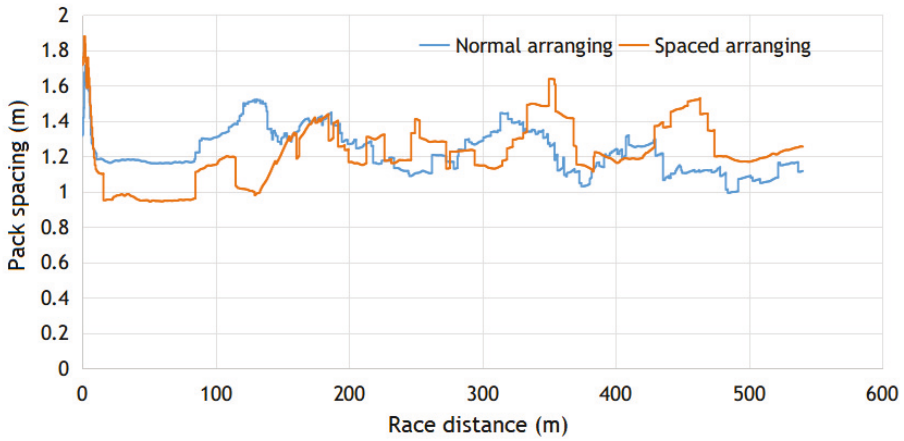

Figure 5.55: Pack spacing calculation using quadruped distance to other quadrupeds present in different clusters for normal eight and spaced four greyhound starts races from the simulated races.

Location of starting boxes

Figure 5.56 shows most common locations for starting boxes around an oval track. In the Transition start arrangement, as shown in Figure 5.56, starting boxes are placed near the transition into the straight from a bend. Some race distances require starting boxes to be placed within the peripheral of a track bend, as shown in the "Bend start" arrangement. Similarly, starting boxes can also be placed on a straight outside the main track, as shown in the Offset start arrangement. Each location configuration of starting boxes as shown in Figure 5.56 exposes different level of alignments for greyhounds trajectories to track path. The locations of starting boxes and corresponding alignment of greyhounds trajectories were compared in race simulations by looking into the yaw rate of a single greyhound running path from the boxes. Figure 5.57 portrays yaw rate results from race simulations for boxes to track transition period. The highest yaw rate occurred for an offset start starting boxes location where it took a maximum distance of approximately 40 m for a greyhound to merge with the track chainage line path as marked by the zero

yaw rate. The starting boxes location for a Transition start resulted in minimum yaw rates among all the locations starts where it required a running distance of approximately 30 m for a greyhound to merge with the track chainage line path. The maximum yaw rate of a Bend start starting boxes location was slightly higher than the Transition start boxes location, but it gave greyhounds from this location start least running distance of approximately 20 m to merge with the track chainage line path.

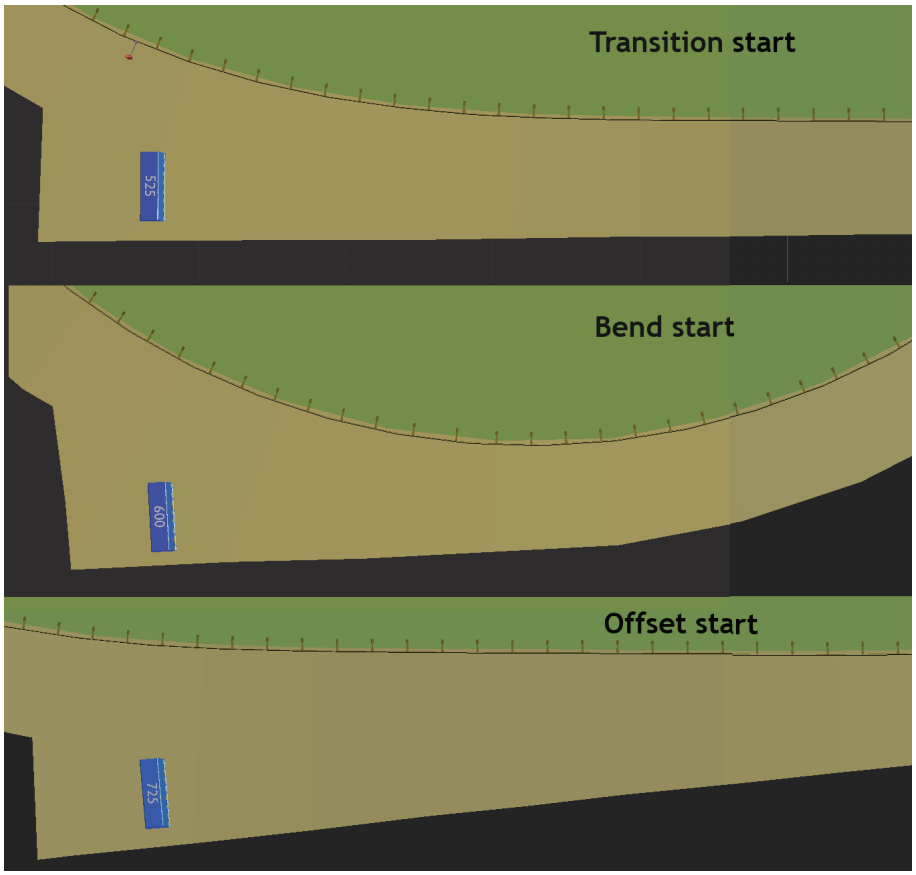

Figure 5.56: Commonly found locations of starting boxes around an oval track.

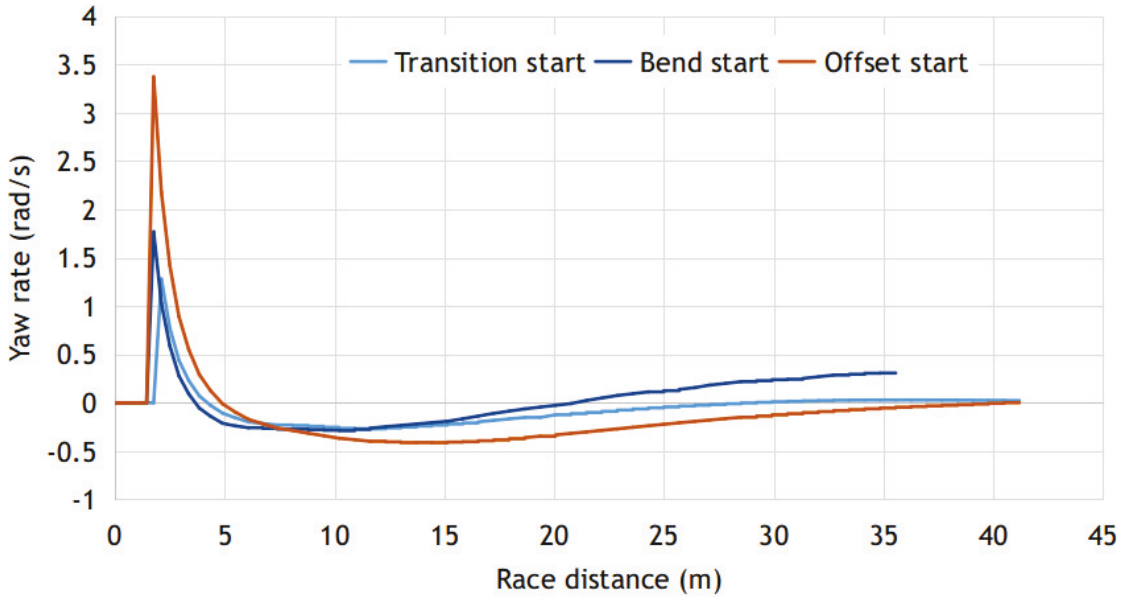

Figure 5.57: Average yaw rate of a single greyhound from race simulations for Transition, Bend, and Offset boxes locations.

5.2.6 Track path modelling for clothoids

Path design variables enumeration for constant radius bend

Every track has a bend radius requirement which is calculated from the real-estate and design goals. If a track requires a 52 m radius bend at the end of the transition then using Equation 4.39 we find the following expected greyhound kinematics and transition design possibilities as can be seen from Table 5.2. It should be noted that there could be a large number of design outcomes for a single target parameter such as design for a specific bend radius. The greyhound yaw rate at the entrance is simply the greyhound angular displacement rate change per stride multiplied by greyhound stride frequency. Also, greyhound racing speed was assumed to be 19.5 m/s and stride frequency to be 3.5 Hz.

Table 5.2: Clothoid transition options for a 52 m radius bend.

Design No.	**Clothoid transition length, T(m)**	***Greyhound yaw rate at the transition entrance (deg/s)**	**Greyhound angular displacement rate change per stride, d (deg/stride^2)**	**Expected constant greyhound stride length, s(m)**
1	75	1.2969	0.393	5.0
2	60	1.6533	0.501	5.0
3	40	2.3825	0.722	4.8
4	60	1.7952	0.544	5.2

As can be seen from the above table, each of the clothoid transition possibilities can be applied at different locations of the track based on the race requirements. For instance, the clothoid transition Design No. 3 can be applied at the home turn bend exit since the greyhound speed, and stride length would be much lower, making it possible for a greyhound to adapt to a higher yaw rate and angular displacement acceleration path navigation.

Path design variables enumeration for constant angular displacement rate change

For racing greyhounds known to have certain angular displacement rate change limits based on greyhound training and health background histories, using Equation 4.39 we can enumerate the possible clothoid design options. For example, if the expected greyhounds have a maximum angular displacement rate change limit of 0.5 $deg/stride^2$ then we can consider following clothoid transition design options as shown in Table 5.3:

Table 5.3: Clothoid transition options for racing greyhounds accelerating with a maximum angular heading turning of 0.5 deg per stride[2].

Design No.	**Clothoid transition length, T(m)**	**Radius of constant bend at the transition end (m)**	**Expected constant greyhound stride length, s(m)**
1	45	71.6	5.00
2	50	70.5	5.25
3	60	52.0	5.00
4	70	53.7	5.50

Modelling centrifugal acceleration jerk dynamics

Since a clothoid has uniform curvature acceleration, the jerk produced by a clothoid remains the same for the entire length of the transition. So, we can find jerk value at any arbitrary location in a clothoid transition to find overall jerk for the transition. For example, if we are interested in the jerk at the end of a clothoid transition first, we would calculate radius value R for both T and $T - s$ segments for the transition. Then, we would calculate corresponding centrifugal acceleration values. Finally, since the jerk is the change in centrifugal acceleration over time, we simply divide the difference of centrifugal accelerations by the time taken for one stride. Table 5.4 presents some example calculations of racing greyhound jerk values for various clothoid transition designs considering instantaneous greyhound speed to be 19.5 m/s:

Table 5.4: Racing greyhounds jerk modelling using Equation 4.39 for clothoid transitions.

Design No.	**Clothoid transition length, T(m)**	**Radius of constant bend at the transition end (m)**	**Expected constant greyhound stride length, s(m)**	**Greyhound angular displacement rate change per stride, d (deg/stride^2)**	**Absolute jerk (m/s^3)**
1	45	71.6	5.0	0.5	2.59
2	50	70.5	5.3	0.5	2.35
3	60	52.0	5.0	0.5	2.59
4	70	53.7	5.5	0.5	2.14

5.2.7 Track path modelling using composite curve transition

Figure 5.58 shows curvature and jerk results for four different composite curves as ideal transitions for racing greyhounds, plotted using the numerical method explained in Section 4.6.4, the configurations for these composite curves are given in Table 5.5.

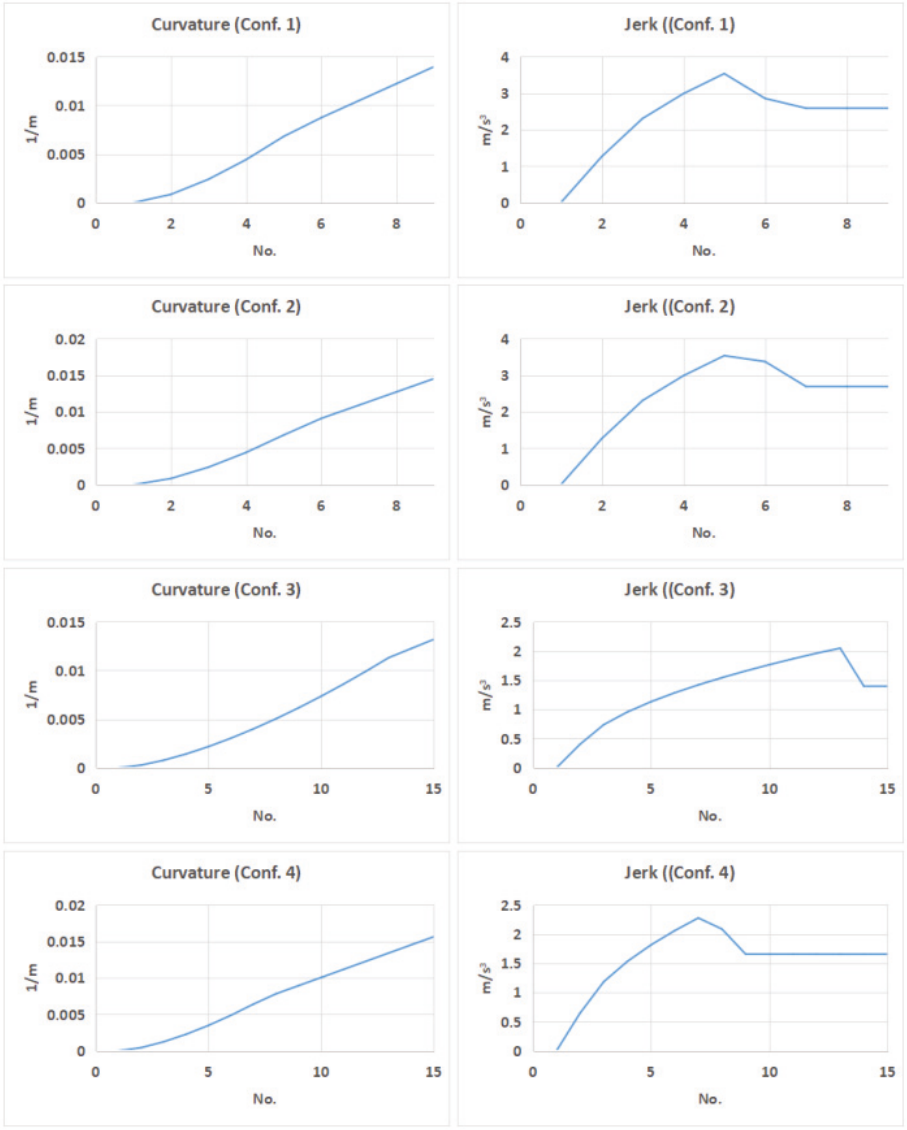

Figure 5.58: Straight to bend curvature and jerk results for four different ideal transition curves for greyhound racing.

Table 5.5: Kinematic and shape properties for four straight to bend composite curve transitions.

Composite curve configuration	**Transition deflection angle acceleration for auxiliary curve (deg)**	**Transition deflection angle acceleration for main clothoid curve (deg)**	**Total transition length No. (m)**	**Transition exit radius (m)**
1	0.39	0.5	45	71.6
2	0.39	0.52	45	68.9
3	0.19	0.27	75	75.8
4	0.25	0.32	75	64.0

As can be seen from Figure 5.58, composite transition curves have strong advantages over pure clothoid transition in terms of curvature and jerk continuities and excellent moderate G3 continuity for the first half of the transition. The overall instantaneous jerk is significantly lower in the composite curve transitions compared to clothoid transitions. This difference in jerk outcome is because the window of jerk initiation is much longer in composite curve transitions. Also, in the composite curve, the development of the jerk was gradual, which on average took 4 transition segments or four greyhound strides compared to just one stride in the clothoid transitions.

5.3 Validating and verifying results

5.3.1 Race simulation

To validate GR simulation, numerical models results greyhound racing data from IsoLynx system was used. Greyhound coordinate data from both simulation results and actual races were used for validating simulation models performances. The races which were selected from both simulation and actual race have identical race setups

to rule out unknown factors affecting the comparisons as well as to find different racing factors general trends. Moreover, simulation and race data were resampled to match greyhound stride duration since greyhound dynamics state is reflected with every stride. Finally, simulations were run with slightly varying lure driving, greyhound maximum acceleration behaviour configurations from nominal values to exaggerate the effects of different racing factors outcomes. The following major greyhound kinematics variables from the simulation results were analysed to verify the models' simulation performance.

Quadruped path following

As quadrupeds race, they follow a specific path in the track. The following graphs show X and Y coordinates of a single greyhound during a race. The graphs show that the shape of greyhound path coordinates from simulation model results closely match with race data. By looking into rate change of coordinates, subtle differences were also analysed. The maximum and minimum percentage differences between simulation and race for X coordinates are 6% and 7% respectively. The maximum and minimum percentage differences between simulation and race for Y coordinates are 4% and 15% respectively. This shows simulated models resulted in a highly accurate path following while percentages differences can be attributed to slightly different race configurations between simulation and actual race and varying nature of each race.

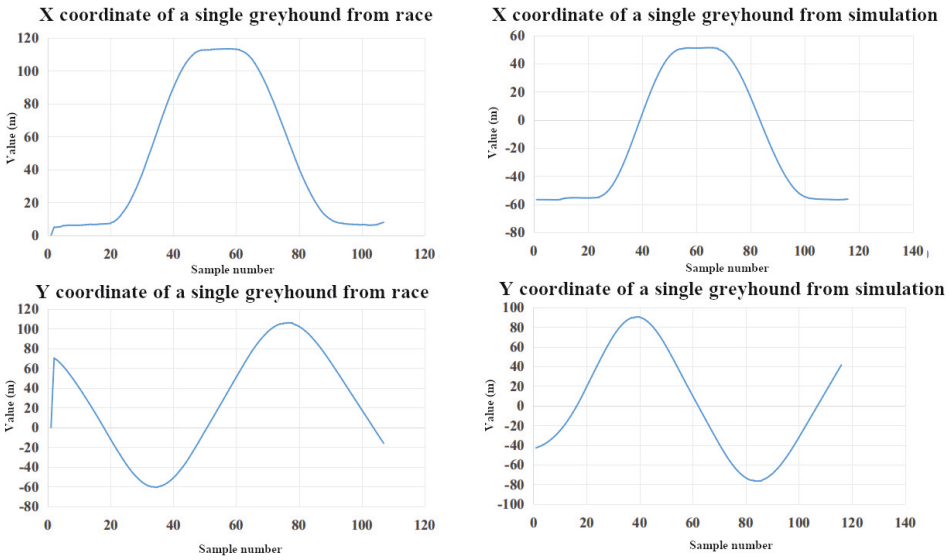

Figure 5.59: A quadruped's coordinate data as extracted from a simulation and an actual race.

Quadruped speed and acceleration

During a race, a greyhound's speed remains variable and has different phases as found from simulation and race data. The following graphs depict the greyhound's instantaneous speeds versus time for both simulated and actual races. As shown in Figures 5.60 and 5.61, the greyhound had an initial high acceleration phase which put a greyhound into its maximum speed limit of roughly 19.5 m/s where the overall duration of this phase depended on race distance, track shape and starting box location in the track. Both simulated and actual race data showed that the initial acceleration lasted for 5 s where the rate change of this initial acceleration was highly variable for actual race whereas for simulation it was fixed as the greyhound model functions use a constant average maximum acceleration for greyhounds. After an initial acceleration phase reaching maximum speed, greyhounds tend to lose speed as time passes, as shown in Figures 5.60 and 5.61. The average deceleration of greyhound in this phase was approximately 0.13 m/s^2 as found from both simulation

and race. Finally, the local fluctuations in greyhounds speed can be attributed to factors including track surface effects, bumping and checking of greyhounds, and specific individual greyhound behaviour.

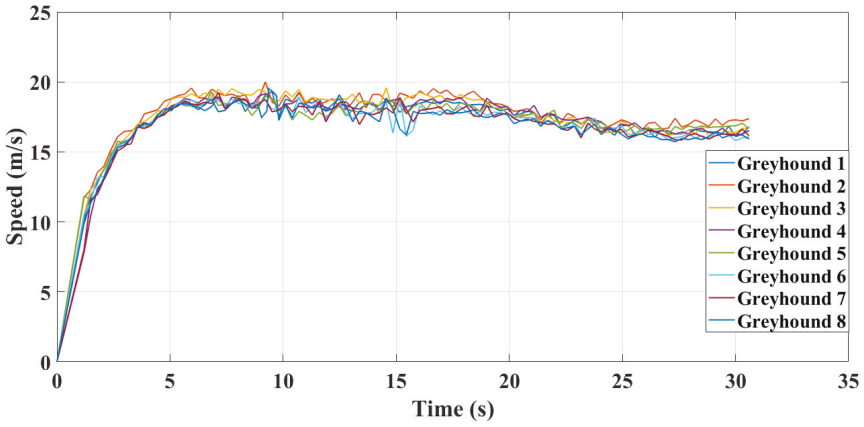

Figure 5.60: Quadrupeds speed during a race.

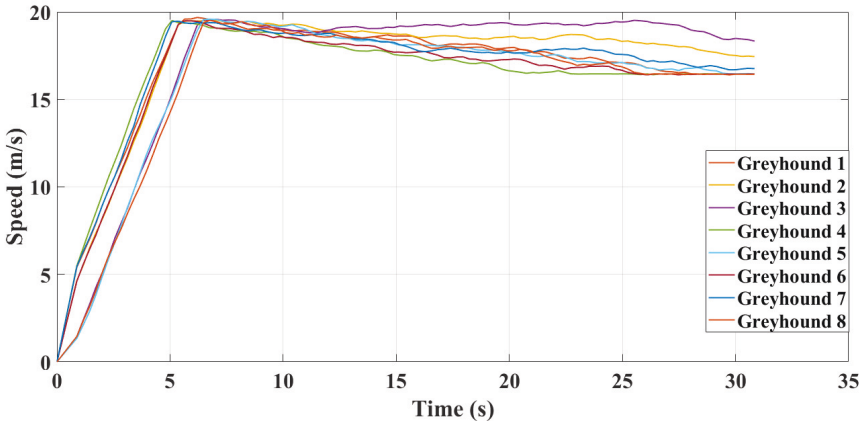

Figure 5.61: Quadrupeds speed during a race simulation.

Quadruped yaw rate

The yaw rate is an important aspect of greyhound kinematics as it defines how quickly a greyhound is turning its heading. Also, veering performance during a race as well as the lateral force magnitude acting on a quadruped can be traced from the

yaw rates. Figures 5.62 and 5.63 illustrate the instantaneous yaw rate of a greyhound as derived from simulated and actual race data, respectively. For the race distance selected, there were two bends of constant radius in the track which are visible in the yaw rates Figure 5.62 (red regions) where a yaw rate of approximately 0.37 rad/s means the greyhound was having a turning radius of roughly 50.5 m while traversing through the bends with a speed roughly 18.8 m/s. Also, it is noticeable there is an initial spike in the yaw rate of about 0.4 rad/s at 2.84 s and 1.49 s for simulation and race data, respectively. This was because the race distance start box location was not perfectly aligned with the track path, which caused the greyhound to make an initial sharp turn for transitioning into the track. The local fluctuations in the yaw rates could have been caused by greyhound path deviation because of bumping and checking or collision avoiding. Overall, the simulated race shows an excellent agreement with the actual race data.

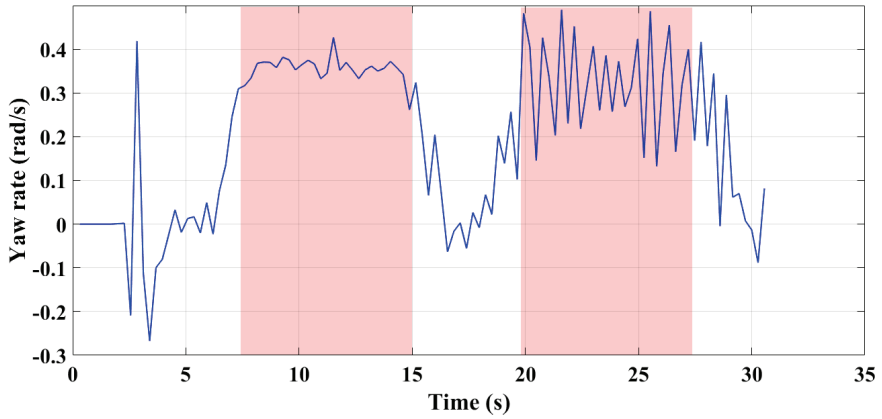

Figure 5.62: A quadruped's yaw rate during a race simulation.

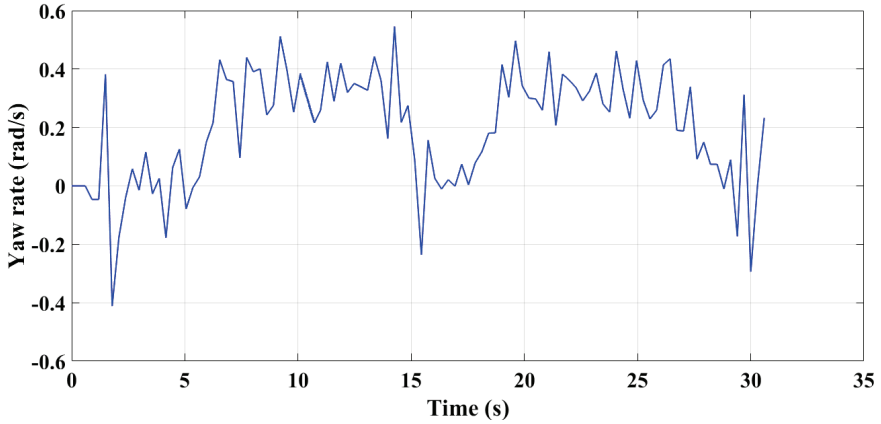

Figure 5.63: A quadruped's yaw rate during a race.

Lure speed

Lure driving condition was analysed between simulation lure model and the actual race. The simulation model yielded better lure driving performance than the actual race, as shown in Figures 5.64 and 5.65. The overall rate change of lure speed was higher in the actual race and lower in the simulation model. Furthermore, in actual race lure speed was affected by track shape. Around the bends, the overall speed was slightly lower, whereas no such trends were noticeable in the simulation model other than fluctuations from overall speed. Finally, it was expected that both the simulation model and actual race lure driving would be slightly different from each other as every race is unique in terms of greyhound kinematics which the lure highly depended on.

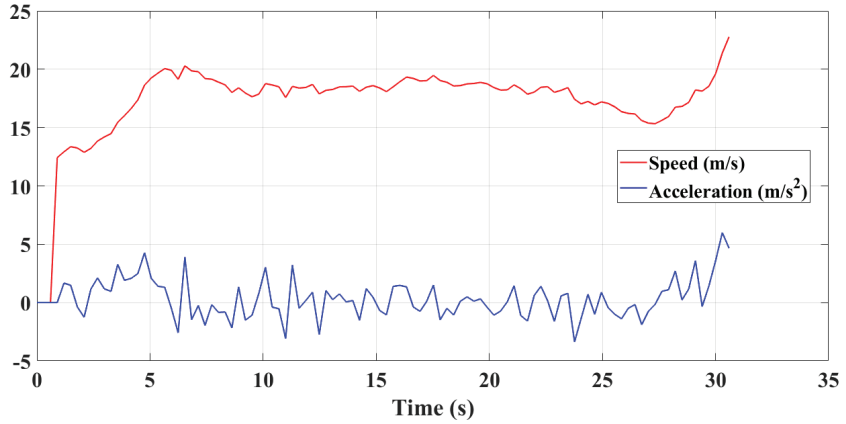

Figure 5.64: Lure driving speed and acceleration during a race.

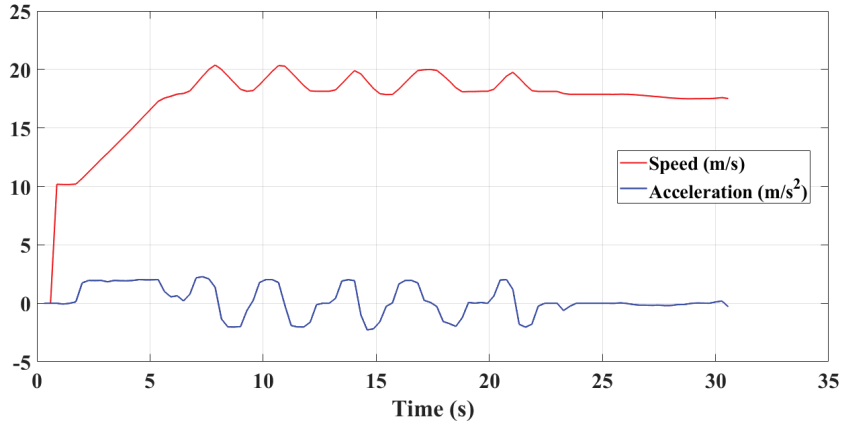

Figure 5.65: Lure driving speed and acceleration during a race simulation.

Lure separation distance

Maintaining a safe and optimal distance of lure from the leading quadruped during a race is also a performance indicator for lure driving conditions. Figures 5.66 and 5.67 show the simulation model and actual race lure separation distance from a leading greyhound during races. As can be seen, in the actual race lure separation distance tend to become gradually lower until 20 s into the race where it was increased and lowered again. Moreover, in actual races, lure separation distance was highly

inconsistent between the races. In the simulation model, lure separation distance is steadier and stable between the races after the initial phase and was increased after approximately 21 s into the race.

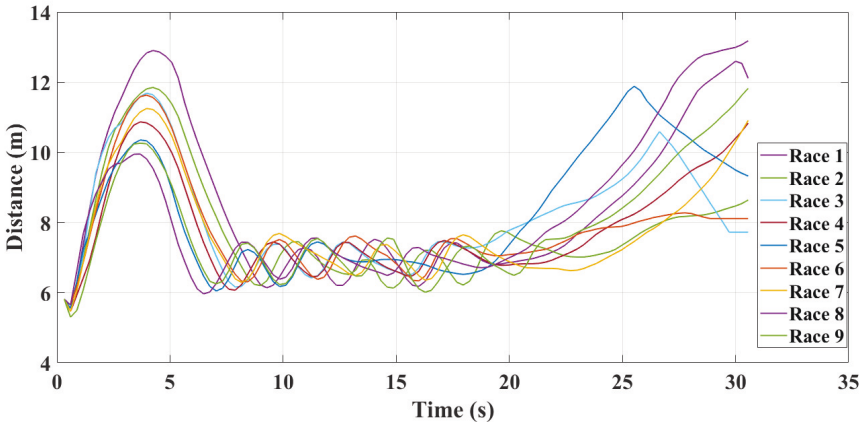

Figure 5.66: Lure to leading quadruped separation during various simulated races for a start distance.

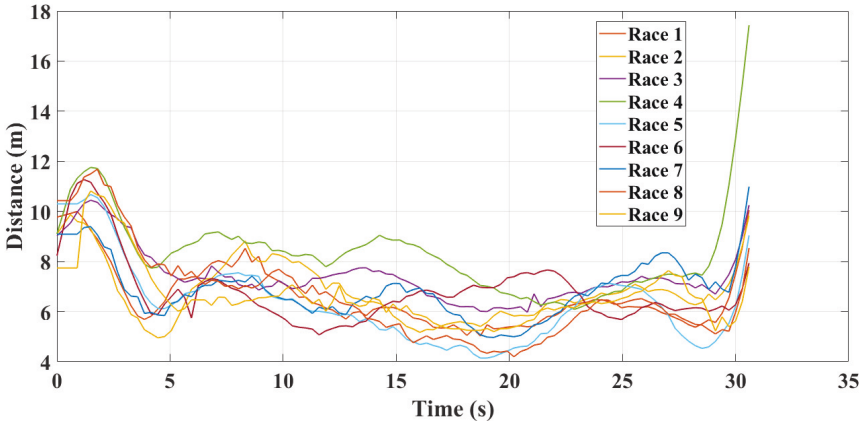

Figure 5.67: Lure to leading quadruped separation during various races for a start distance.

5.3.2 Track path modelling

The track path survey data of greyhound racing tracks from Australia shows that a brief transition is applied, made of an arc spline consisting of one or more circular arcs joined with continuous tangent vectors. This particular design practice leads to multiple discontinuities in track path curvature.

We looked into one particular greyhound racing track which is located in Australia and its two years of racing history. In the first year, it had a track path design with G1 continuity constituting half-circle bends and straights as can be seen from Figure 5.68 (Before). In the second racing year, the track was renovated with clothoid curve transitions into and out of the constant radius bends like shown in Figure 5.68 (After). A 40 m clothoid transition was adjoined between a straight and a constant bend section for four bend and straight intersections. The outcome of this clothoid transition incorporation into the original track path design eases centrifugal acceleration effect on the greyhounds where the centrifugal force is raised gradually from zero to an approximate nominal 240 N. The renovation definitely would have changed centrifugal jerk performance significantly as the clothoid curve joining straights and bends would maintain G2 curvature continuity for the track path. To see whether this resulted in a significant decrease in racing injury rates, injury data for a two year period were analysed containing one-year injury data for before and after renovation. By assuming differences in other contributing factors to injury rates, such as variations in weather, maintaining track conditions, different greyhound breeds and training patterns, race operating conditions between the years are minimal the injury rates should show general trends due to track path renovation changes. We found that before the clothoid intervention at the track the normalised catastrophic and major injury rate per 1000 race starts was about 4.58 whereas after the clothoid intervention it was reduced to 4.22, a 7.9% reduction in this category of injury rates. Typically, this category of injury results from signifi-

cant damage to greyhound physics. However, when we took into account all types of injuries for before and after renovation, the normalised injury rates per 1000 race starts reduced to 26.71 from 44.68 injuries, a 40.2% reduction in overall injuries due to clothoid implementation at the track. Furthermore, under all injury types, the most commonly occurring injury is happening in the greyhound forelegs responsible for assisting turning for dog's navigation. Metacarpal fractures and tibial fractures due to torsional stress occurring in the forelegs indicate navigational work stress on the greyhounds.

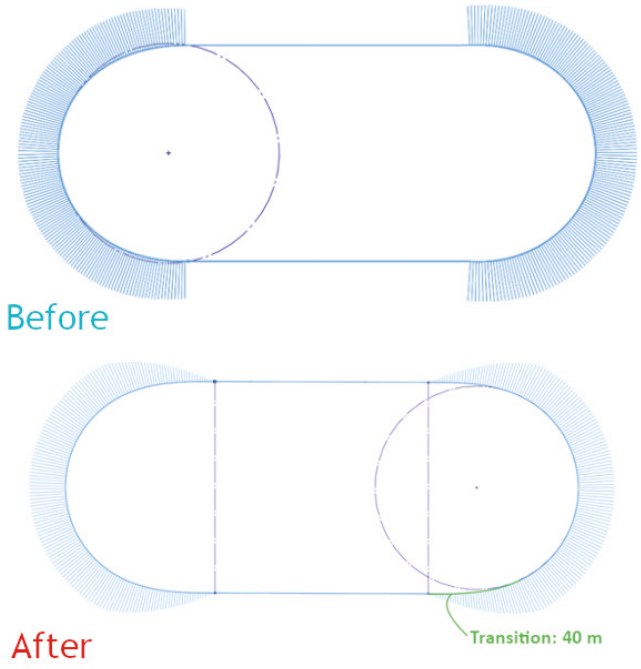

Figure 5.68: Track path curvatures comparison for before and after adding a transition.

Like any path following object, a racing greyhound has limitations on the radius of curvature or extremes of curvature for its running path. Also, when a racing greyhound runs following a track path which has curvature discontinuity or non-optimal transitions, a deviation in the greyhound's position occurs from the projected track

path trajectory. This phenomenon was observed in the greyhound location data in the races. Furthermore, it was also confirmed from the numerical racing greyhound simulations that when a greyhound is following the line of sight to a lure, its yaw rate gradually builds up to the bend for a track shape which is less circular [57]. To see if there is any difference between a racing greyhounds path trajectory to track path, we analysed a racing greyhounds location tracking data for a track which has non-optimal transition length to reduce the jerk magnitude. From the RLT and track survey data, we generated curvature results for both the racing greyhounds' trajectory and the track path like shown in Figure 5.69. The greyhound location data for all greyhounds starts were averaged to plot the results where 10 races or 80 greyhound starts were considered to plot the results below. As can be seen from the curvature plot in Figure 5.69 there is a significant difference between a racing greyhounds trajectory and track path. This indicates racing greyhounds are deviating from the track path to accommodate a more natural trajectory according to their physics. Also, it was observed from the analysis that transitions occurring in racing greyhound trajectory is relatively gradual and longer as indicated by the green dashed marker compared to the black dashed marker for track path.

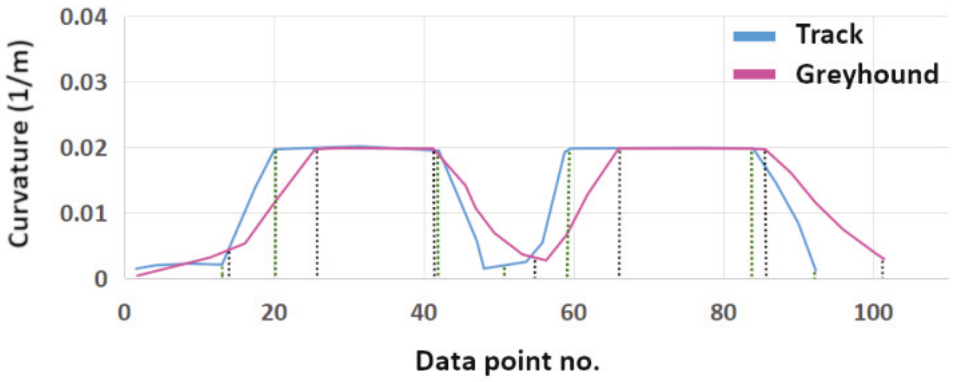

Figure 5.69: Track path and greyhounds' trajectory curvatures comparison.

5.4 Discrepancies

Initially, the simulation and modelling were designed to show various relations between different race variables. However, data gathering from numerous sources enabled cross-verifications to develop refined models to generate results which are close to exact values. Regardless of multiple efforts to minimise the peculiarities in the race simulations, the lack of specific inputs from the industry contributed to restricting simulation inquiry to aspects which are discreet events.

The controller in the simulation that drives the lure around a track was developed to adhere to definite pre-race and race-time conditions such as starting location and, lure separation from greyhounds in a race. However, there are other variables of the lure, such as initial and race-time accelerations, were not available from the industry to tweak the simulation lure controller to match actual race scenarios precisely. This made it challenging to obtain simulation results for verifying and modelling the convergence rate of a greyhounds pack due to lure motion.

Creation of different race scenarios inside race simulations requires planning and setting of multiple initial and race run-time parameters to creating the matching environments. Some parameters need to be consistent across scenarios to detect and find the influences of the distinct variables across races. For instance, the only parameter that is modified between two race scenarios is the lure separation from the greyhounds. However, because of the parameters entanglement, changing the value of the lure separation parameter also modifies the lure speed and acceleration profiles during a race. As a result, identifying one parameter's active involvement in a particular race dynamics becomes a tedious and complicated process.

In the race simulations, the greyhound kinematic model adopted a linear acceleration model. Furthermore, the model was applied to each and every race starting greyhounds. However, in actuality, greyhound acceleration is a non-linear phenomenon.

Also, acceleration function differs from one greyhound to another during a race. Besides, non-linear acceleration model development showed notable divergence in other simulation kinematic models output. Therefore, certain dynamics states such as instantaneous kinetic energy could not be extracted reliably from the simulation results.

Likewise, a single homogeneous veering model was utilised in the race simulations for all greyhounds. This can not be true in actual races as it was witnessed from the races that each greyhound veering is most likely unique where two greyhounds may choose a slightly different approach to heading. For instance, in the real races, some greyhounds maintain an extended offset from the inside track edge. This behaviour of a greyhound can be attributed to several factors, such as individual greyhound preference and also physical capability.

In the simulation, each scenario created presents identical initial conditions of a track for each consecutive race. However, in reality, when multiple races occur at a track, the track condition after each consecutive race varies due to track maintenance procedures after each race. This situation made it hard to track changes in the actual race data and calibrate simulation models more accurately. Also, the cumulative effect of track changes, for instance, the deterioration of the track conditions during multiple races and corresponding effects during the races was not detected in the simulations.

Chapter 6

Conclusions and future work

6.1 Conclusions

This research sought to answer a sophisticated problem which was comprised of multiple factors. The research in this dissertation solves several challenging parameter evaluation problems concerning the dynamics of quadrupedal racing greyhound conditions at the tracks. The main contributions of this are numerous but can be grouped into dynamical path smoothing and safe geometric track design principles and race operating requirements. In this chapter, we summarise the contributions of this dissertation first and then provide relevant future research directions.

6.2 Research output

This research acquired the following results:

1. Identification of factors directly impacting race dynamics at the tracks. This was achieved by designing and implementing a modular and numerical race simulation platform and conducting experiments which required a minimal number of data inputs. The kinematics result generated from the simulations was used to verify factors involvement and relations.

   (a) The contribution of line of sight to the lure in the greyhound path choosing (Chapter 5)

   (b) Greyhound heading preferences for different starting locations (Chapter 5)

(c) Congestion points occurring at the various locations at the tracks (Chapter 5)

(d) Greyhound pack spacing and density nature during a race (Chapter 5)

(e) Factors need optimisations for smooth entry into a bend (Chapter 5)

(f) Lure lateral alignments and corresponding race dynamics outcome (Chapter 5)

(g) Lure driving configuration and corresponding race dynamics outcome (Chapter 5)

(h) Starting box setup and corresponding race dynamics outcome (Chapter 5)

(i) Effect of different number of starting greyhounds (Chapter 5)

2. Validate and determine greyhound galloping gait and race kinematics performance through data analysis and modelling.

(a) Verify through data analysis greyhound galloping aerial and stance phases in the straight (Chapter 3)

(b) Verify through data analysis the location of the centre of gravity of galloping greyhound in the straight (Chapter 3)

(c) Conduct greyhound galloping gait paw tracing analysis to determine paws longitudinal and vertical motions (Chapter 3)

(d) Conduct greyhound galloping gait paw tracing analysis to provide details of instantaneous galloping speed in the straight (Chapter 3)

(e) Calculate galloping stride frequency and length from the proper acceleration data (Chapter 3)

(f) Calculate galloping stride frequency and length from the HFR data (Chapter 3)

(g) Calculate greyhound galloping instantaneous speed from the proper acceleration data (Chapter 3)

(h) Calculate an estimation of paw track surface penetration from the paw motion data analysis (Chapter 3)

(i) Extract racing greyhounds heading speed, acceleration, and yaw rate profiles of different race distances for a track (Chapter 3)

(j) Present tri-axial proper accelerations of a galloping greyhound for a track bend (Chapter 3)

(k) Present galloping greyhound stride length details from the paw print data (Chapter 3)

(l) Present galloping greyhound speed at the tracks from the Radar gun data (Chapter 3)

(m) Present galloping greyhound leaning at the bend for a particular track (Chapter 3)

3. Review existing track path designs and their dynamics performance. And also propose oval track transition curve design options.

(a) Analyse existing greyhound racing track path design components (Chapter 3)

(b) Determine existing track design limitations for galloping greyhound dynamics such as limiting speed, lack of transition, and short straight distance (Chapters 3 and 5)

(c) Formulate theoretical centrifugal acceleration jerk analysis method from track path data and present existing tracks jerk performance (Chapter 3)

(d) Formulate track path transition design requirements and propose smooth jerk transition curves (Chapters 4 and 5)

(e) Propose clothoid transition design options for various greyhound kinematic performance (Chapter 5)

4. And, presents a computationally efficient and simplified approach to model multi factors kinematics through numerical formulation and derives numerical methods to calculate coordinates of smooth jerk transition curves for quadrupeds (Chapters 4)

6.3 Suggestions for future research work

Interesting approaches for future work are presented below:

- Extend simulation capabilities

    1. Create greyhound dynamics health state model to identify defaulted greyhounds during a race; This would also allow benchmarking of tracks based on greyhound dynamics health
    2. Integrate a track condition deterioration model for simulating the cumulative effect of multiple races at a track
    3. Use machine learning algorithms to analyse simulation results
    4. Use discrete event simulation for emulating exact incidents in the simulation
    5. Develop parameter optimisation model required for optimising simulation results

- Design dynamic data-driven models for simulation

    1. Develop data characterisation methods to derive patterns from real-time location tracking data
    2. Integrate different quadruped behaviour models into the greyhound veering model synthesised from the real-time location tracking data

- Model track path camber profile for bends from paw impact force models
- Develop dynamic motion trace methods for quadruped racing performance analysis

Bibliography

[1] Scott, "How to drive the perfect racing line," 2019.

[2] M. W. Hancock and B. Wright, "A policy on geometric design of highways and streets," *American Association of State Highway and Transportation Officials: Washington, DC, USA*, 2013.

[3] R. L. Gillette and T. C. Angle, "Recent developments in canine locomotor analysis: a review," *The Veterinary Journal*, vol. 178, no. 2, pp. 165–176, 2008.

[4] N. S. Poy, C. E. DeCamp, R. L. Bennett, and J. G. Hauptman, "Additional kinematic variables to describe differences in the trot between clinically normal dogs and dogs with hip dysplasia," *American Journal of Veterinary Research*, vol. 61, no. 8, pp. 974–978, 2000.

[5] R. Alexander, "Optimization and gaits in the locomotion of vertebrates," *Physiological reviews*, vol. 69, no. 4, pp. 1199–1227, 1989.

[6] M. Tanase, Y. Ambe, S. Aoi, and F. Matsuno, "A galloping quadruped model using left–right asymmetry in touchdown angles," *Journal of biomechanics*, vol. 48, no. 12, pp. 3383–3389, 2015.

[7] E. Muybridge, "Animals in motion (new york)," 1957.

[8] C. M. Biancardi, C. G. Fabrica, P. Polero, J. F. Loss, and A. E. Minetti, "Biomechanics of octopedal locomotion: kinematic and kinetic analysis of the spider grammostola mollicoma," *Journal of Experimental Biology*, vol. 214, no. 20, pp. 3433–3442, 2011.

[9] D. P. Krasny and D. E. Orin, "Generating high-speed dynamic running gaits in a quadruped robot using an evolutionary search," *IEEE Transactions on Systems, Man, and Cybernetics, Part B (Cybernetics)*, vol. 34, no. 4, pp. 1685–1696, 2004.

[10] R. M. Alexander and A. Jayes, "A dynamic similarity hypothesis for the gaits of quadrupedal mammals," *Journal of zoology*, vol. 201, no. 1, pp. 135–152, 1983.

[11] M. Hildebrand, "Analysis of asymmetrical gaits," *Journal of Mammalogy*, vol. 58, no. 2, pp. 131–156, 1977.

[12] M. Hildebrand, "The quadrupedal gaits of vertebrates," *BioScience*, vol. 39, no. 11, p. 766, 1989.

[13] C. D. Remy, *Optimal exploitation of natural dynamics in legged locomotion*. Thesis, 2011.

[14] D. W. Marhefka, D. E. Orin, J. P. Schmiedeler, and K. J. Waldron, "Intelligent control of quadruped gallops," *IEEE/ASME Transactions On Mechatronics*, vol. 8, no. 4, pp. 446–456, 2003.

[15] C. Biancardi, "Biomechanics of terrestrial locomotion: asymmetric octopedal and quadrupedal gaits," 2012.

[16] C. M. Biancardi and A. E. Minetti, "Biomechanical determinants of transverse and rotary gallop in cursorial mammals," *Journal of Experimental Biology*, vol. 215, no. 23, pp. 4144–4156, 2012.

[17] R. M. Alexander, "Why mammals gallop," *American zoologist*, vol. 28, no. 1, pp. 237–245, 1988.

[18] R. Blickhan, "The spring-mass model for running and hopping," *Journal of biomechanics*, vol. 22, no. 11-12, pp. 1217–1227, 1989.

[19] S. R. Bullimore and J. F. Burn, "Dynamically similar locomotion in horses," *Journal of experimental biology*, vol. 209, no. 3, pp. 455–465, 2006.

[20] S. R. Bullimore and J. F. Burn, "Ability of the planar spring–mass model to predict mechanical parameters in running humans," *Journal of Theoretical Biology*, vol. 248, no. 4, pp. 686–695, 2007.

[21] G. A. Cavagna, N. C. Heglund, and C. R. Taylor, "Mechanical work in terrestrial locomotion: two basic mechanisms for minimizing energy expenditure," *American Journal of Physiology-Regulatory, Integrative and Comparative Physiology*, vol. 233, no. 5, pp. R243–R261, 1977.

[22] R. J. Full and D. E. Koditschek, "Templates and anchors: neuromechanical hypotheses of legged locomotion on land," *Journal of experimental biology*, vol. 202, no. 23, pp. 3325–3332, 1999.

[23] T. A. McMahon and G. C. Cheng, "The mechanics of running: how does stiffness couple with speed?," *Journal of biomechanics*, vol. 23, pp. 65–78, 1990.

[24] A. E. Minetti, "The biomechanics of skipping gaits: a third locomotion paradigm?," *Proceedings of the Royal Society of London. Series B: Biological Sciences*, vol. 265, no. 1402, pp. 1227–1233, 1998.

[25] M. H. Raibert, "Legged robots," *Commun. Acm*, vol. 29, no. 6, pp. 499–514, 1986.

[26] K. J. Waldron, M. Göller, F. Steinhardt, T. Kerscher, J. M. Zöllner, and R. Dillmann, "Robust navigation system based on rfid transponder barriers for the interactive behavior-operated shopping trolley (inbot)," *Industrial Robot: An International Journal*, 2009.

[27] A. N. Lay, C. J. Hass, and R. J. Gregor, "The effects of sloped surfaces on locomotion: a kinematic and kinetic analysis," *Journal of biomechanics*, vol. 39, no. 9, pp. 1621–1628, 2006.

[28] R. J. Gregor, J. L. Smith, D. W. Smith, A. Oliver, and B. I. Prilutsky, "Hindlimb kinetics and neural control during slope walking in the cat: unexpected findings," *Journal of Applied Biomechanics*, vol. 17, no. 4, pp. 277–286, 2001.

[29] J. L. Smith and P. Carlson-Kuhta, "Unexpected motor patterns for hindlimb muscles during slope walking in the cat," *Journal of Neurophysiology*, vol. 74, no. 5, pp. 2211–2215, 1995.

[30] N. C. Heglund and C. R. Taylor, "Speed, stride frequency and energy cost per stride: how do they change with body size and gait?," *Journal of Experimental Biology*, vol. 138, no. 1, pp. 301–318, 1988.

[31] S. Williams, J. Usherwood, and A. Wilson, "Acceleration in the racing greyhound," *Comparative Biochemistry and Physiology, Part A*, vol. 4, no. 146, p. S110, 2007.

[32] L. Jaramillo, F. Gadau, M. Lin, and B. Thompson, "Race track optimization," 2015.

[33] I. Fredricson, G. Dalin, S. Drevemo, G. Hjerten, G. Nilsson, and L. Alm, "Ergonomic aspects of poor racetrack design," *Equine Veterinary Journal*, vol. 7, no. 2, pp. 63–65, 1975.

[34] I. Fredricson, G. Dalin, S. Drevemo, G. Hjertén, and L. O. Alm, "A biotechnical approach to the geometric design of racetracks," *Equine Veterinary Journal*, vol. 7, no. 2, pp. 91–96, 1975.

[35] A. K. Stubbs, *Racetrack Design and Performance*. Canberra, Australia: RIRDC, 2004.

[36] J. Symons, D. Hawkins, D. Fyhrie, S. Upadhyaya, and S. Stover, "Modelling the interaction between racehorse limb and race surface," *Procedia engineering*, vol. 147, pp. 175–180, 2016.

[37] L. Cardamone, D. Loiacono, P. L. Lanzi, and A. P. Bardelli, "Searching for the optimal racing line using genetic algorithms," in *Proceedings of the 2010 IEEE Conference on Computational Intelligence and Games*, pp. 388–394, IEEE, 2010.

[38] F. Beltman, "Optimization of ideal racing line," 2008.

[39] G. K. Sicard, K. Short, and P. A. Manley, "A survey of injuries at five greyhound racing tracks," *J Small Anim Pract*, vol. 40, no. 9, pp. 428–32, 1999.

[40] J. Iddon, R. Lockyer, and S. Frean, "The effect of season and track condition on injury rate in racing greyhounds," *journal of small animal practice*, vol. 55, no. 8, pp. 399–404, 2014.

[41] J. Hickman, "Greyhound injuries," *Journal of small animal practice*, vol. 16, no. 1-12, pp. 455–460, 1975.

[42] A. Gibbesch and B. Schafer, "Multibody system modelling and simulation of planetary rover mobility on soft terrain," in *8th International Symposium on Artificial Intelligence, Robotics and Automation in Space (i-SAIRAS 2005), Munich, Germany, September*, pp. 5–8, Citeseer, 2005.

[43] T. Y. Park, K. H. Han, and B. K. Choi, "An object-oriented modelling framework for automated manufacturing system," *International Journal of Computer Integrated Manufacturing*, vol. 10, no. 5, pp. 324–334, 1997.

[44] M. I. Hossain, D. Eager, and P. Walker, "Simulation of racing greyhound kinematics," in *Proceedings of the 9th International Conference on Simulation and Modeling Methodologies, Technologies and Applications*, pp. 47–56, SCITEPRESS-Science and Technology Publications, Lda, 2019.

[45] H. Hayati, D. Eager, and P. Walker, "A slip model to predict the dynamics of rapid tetrapod locomotion during hind-leg single support," in *International Society of Biomechanics Conference*, 2019.

[46] J. S. Respondek, "Numerical simulation in the partial differential equation controllability analysis with physically meaningful constraints," *Mathematics and Computers in Simulation*, vol. 81, no. 1, pp. 120–132, 2010.

[47] J. Respondek, "Controllability of dynamical systems with constraints," *Systems & Control Letters*, vol. 54, no. 4, pp. 293–314, 2005.

[48] G. Maier, "Optimal arc spline approximation," *Computer Aided Geometric Design*, vol. 31, no. 5, pp. 211–226, 2014.

[49] K. Yeh and K. Kwan, "A comparison of numerical integrating algorithms by trapezoidal, lagrange, and spline approximation," *Journal of pharmacokinetics and biopharmaceutics*, vol. 6, no. 1, pp. 79–98, 1978.

[50] D. Eager, A. M. Pendrill, and N. Reistad, "Beyond velocity and acceleration: jerk, snap and higher derivatives," *European Journal of Physics*, vol. 37, 2016.

[51] J. Powell and R. Palacín, "Passenger stability within moving railway vehicles: limits on maximum longitudinal acceleration," *Urban Rail Transit*, vol. 1, no. 2, pp. 95–103, 2015.

[52] S. Manuwa, "Evaluation of soil/material interface friction and adhesion of akure sandy clay loam soils in southwestern nigeria," *Advances in Natural Science*, vol. 5, no. 1, pp. 41–46, 2012.

[53] J. G. De Jalon and E. Bayo, *Kinematic and dynamic simulation of multibody systems: the real-time challenge*. Springer Science & Business Media, 2012.

[54] S. Reich, "Numerical simulation in molecular dynamics: Numerics, algorithms, parallelization, applications," *SIAM Review*, vol. 52, no. 1, p. 213, 2010.

[55] L. M. Beer, "A study of injuries in victorian racing greyhounds 2006-2011," 2014.

[56] H. Hayati, D. Eager, R. Stephenson, T. Brown, and E. Arnott, "The impact of track related parameters on catastrophic injury rate of racing greyhounds," in *9th Australasian Congress on Applied Mechanics (ACAM9)*, p. 311, Engineers Australia, 2017.

[57] F. Mahdavi, M. I. Hossain, H. Hayati, D. Eager, and P. Kennedy, "Track shape, resulting dynamics and injury rates of greyhounds," in *ASME 2018 International Mechanical Engineering Congress and Exposition*, vol. Volume 13: Design, Reliability, Safety, and Risk, (V013T05A018), 2018.

[58] T. V. Mathew and K. K. Rao, "Introduction to transportation engineering," 2006.

[59] D. K. Wilde, "Computing clothoid segments for trajectory generation," in *2009 IEEE/RSJ International Conference on Intelligent Robots and Systems*, pp. 2440–2445, 2009.

[60] M. E. Vázquez-Méndez and G. Casal, "The clothoid computation: A simple and efficient numerical algorithm," in *Journal of Surveying Engineering*, vol. 142, American Society of Civil Engineers, 2016.

[61] H. Delingette, M. Hebert, and K. Ikeuchi, "Trajectory generation with curvature constraint based on energy minimization," in *Proceedings IROS*

'91:IEEE/RSJ International Workshop on Intelligent Robots and Systems '91, pp. 206–211 vol.1, 1991.

[62] R. C. Hibbeler, *Engineering Mechanics: Dynamics (13th Edition)*. Prentice Hall, 2012.

[63] Sampson, "Surface continuity," 2018.

[64] D. S. Meek and D. J. Walton, "An arc spline approximation to a clothoid," *Journal of Computational and Applied Mathematics*, vol. 170, no. 1, pp. 59–77, 2004.

[65] H. Banzhaf, N. Berinpanathan, D. Nienhüser, and J. M. Zöllner, "From g 2 to g 3 continuity: Continuous curvature rate steering functions for sampling-based nonholonomic motion planning," in *2018 IEEE Intelligent Vehicles Symposium (IV)*, pp. 326–333, IEEE, 2018.

[66] A. Ahmad and J. M. Ali, "G3 transition curve between two straight lines," in *2008 Fifth International Conference on Computer Graphics, Imaging and Visualisation*, pp. 154–159, IEEE, 2008.

[67] D. S. Meek and D. J. Walton, "A note on finding clothoids," *Journal of Computational and Applied Mathematics*, vol. 170, no. 2, pp. 433–453, 2004.

[68] F. Bertails-Descoubes, "Super-clothoids," *Computer Graphics Forum*, vol. 31, no. 2pt2, pp. 509–518, 2012.

[69] L. Z. Wang, K. T. Miura, E. Nakamae, T. Yamamoto, and T. J. Wang, "An approximation approach of the clothoid curve defined in the interval [0, /2] and its offset by free-form curves," *Computer-Aided Design*, vol. 33, no. 14, pp. 1049–1058, 2001.

[70] J. Sánchez-Reyes and J. M. Chacón, "Polynomial approximation to clothoids via s-power series," *Computer-Aided Design*, vol. 35, no. 14, pp. 1305–1313, 2003.

Appendices

Appendix A: Data acquisition devices

6.3.1 Yost IMU device details

Software:

`https://yostlabs.com/yost-labs-3-space-sensor-software-suite/`

System summery:

Installed SD card capacity: 1.86 GB

Led status:

Blue pulse = communicating with the computer

Blue = Power on and no data-logging session in progress

Green = logging sensors data

Green pulse = Battery is fully charged

Red = data medium error

Red pulse = Low battery

Yellow pulse = Battery is actively charging

Buttons actions:

Left button: start logging sensors data (configurable)

Right button: stop logging sensors data (configurable)

*Vertical acceleration for stationary position $+1g$

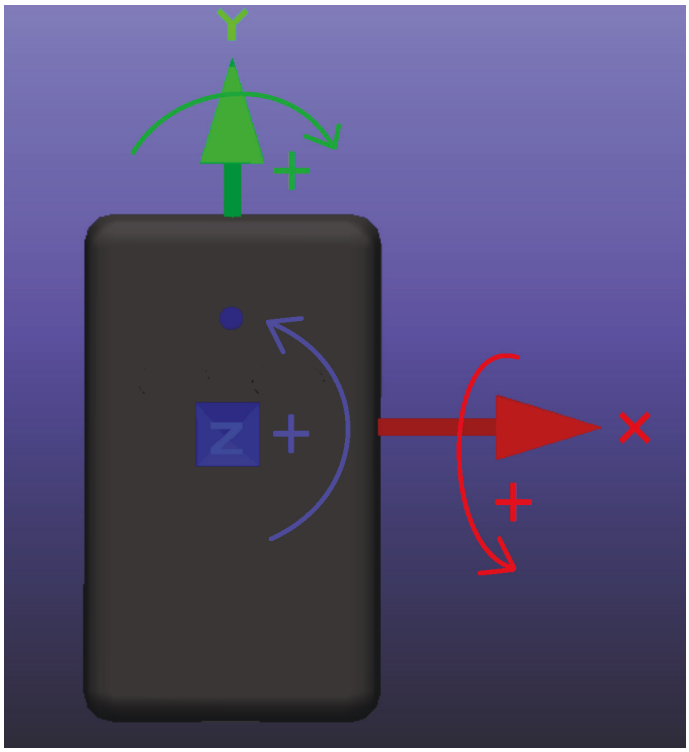

Figure 6.1: Yost Labs 3-Space data logger coordinate system.

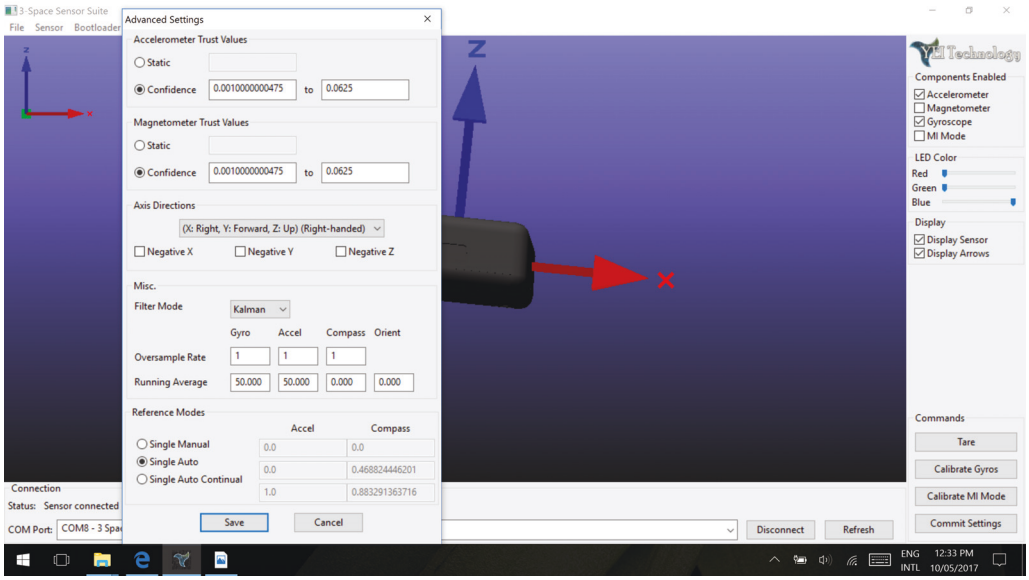

Figure 6.2: Yost Labs 3-Space data logger configuration for data acquisition.

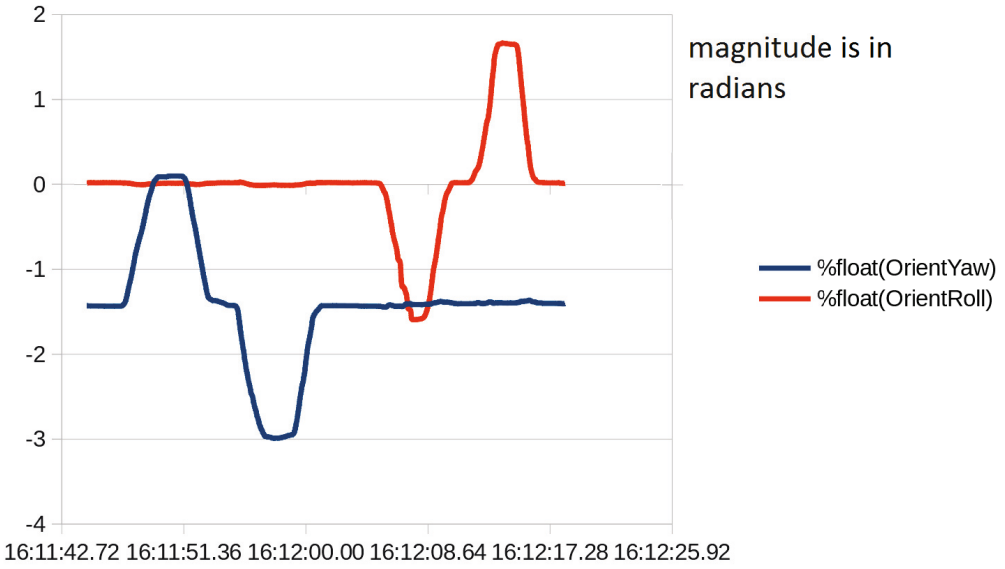

Figure 6.3: Yost Labs 3-Space data logger calibration by turning and rolling on the table.

6.3.2 Radar gun details

Specification:

Product type: Stationary Doppler Radar

Speed range: 5 - 150 MPH

Accuracy: ±3% of reading

Max. clocking distances: 300 feet with unobstructed view

Operating frequency: 24.125 GHz (K-Band) +/- 50 MHz

Polarization: Circular Polarization

3 db beam width: 14 Degrees (nominal) (15 Degrees Maximum)

Microwave source: Gunn-Effect diode

Receive type: Schottky Barrier Mixer Diode

Power output: 10 Milliwatts (nominal)

Computer processor: Digital Signal Processor(DSP)

Display type: Liquid crystal

Operating temperatures: -20F to +120F

Storage temperatures: -40F to +140F

Figure 6.4: Stalker Sport 2 Radar Gun.

Appendix B: Simulation

Table 6.1: Greyhound race simulations settings and default race configuration.

Parameter	**Value**
Lure initial speed	72.0 km/h
Maintained separation between lure and leading greyhound	5.0 ± 1.8 m
Lure and greyhound separation distance stabilising period	7.0 ± 1.0 s
Maximum greyhound speed	72.0 km/h
Minimum greyhound speed	59.4 km/h
Simulation timestamp	0.04 s
Lure arm length	1.2 m

Figure 6.5: Greyhound collision detection using spheres was used in the race simulations.

Figure 6.6: Greyhound sight from behind the leading group showing the lure is obscured by the greyhounds ahead as generated from race simulation.

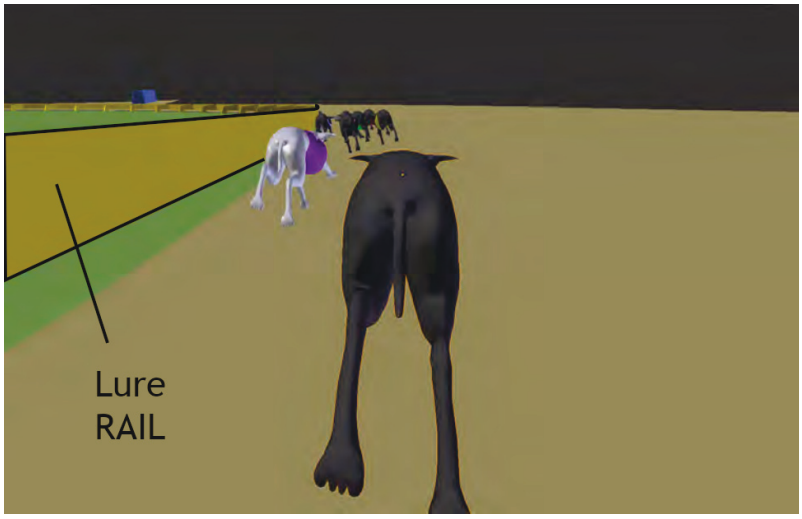

Figure 6.7: Greyhound sight from the very back of the pack showing the lure is obscured by the greyhounds ahead as generated from race simulation.

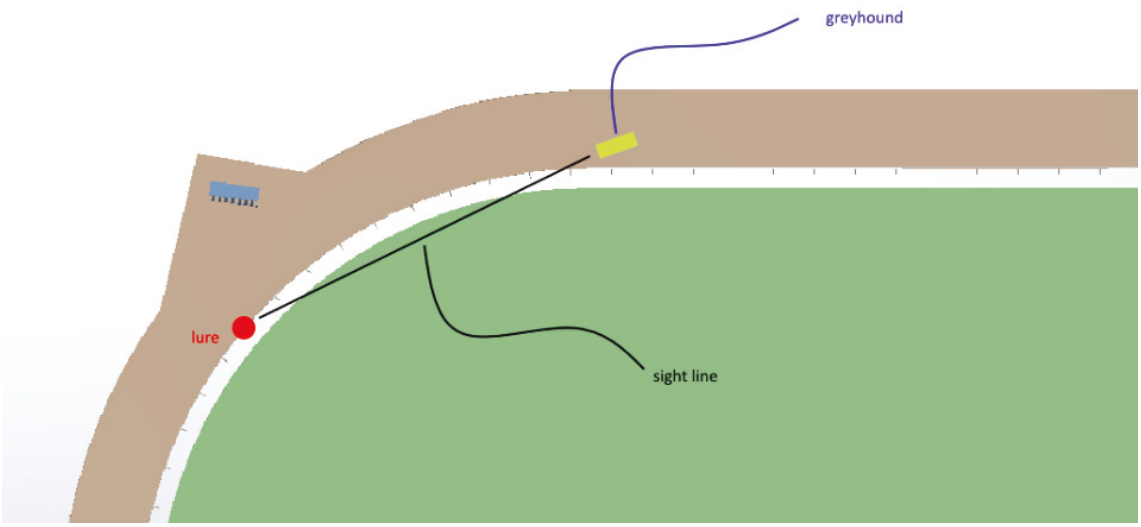

Figure 6.8: A lure that is located too far is obscured by the track inside edge.

Following are race simulations for different lure alignments on the track:

Lure 0.3 m: `http://bit.ly/2OarmDo`

Lure 1.2 m: `http://bit.ly/2Gwm8hb`

Following are race simulations for six and eight greyhounds races:

Six greyhounds: `http://bit.ly/2GyCuWx`

Eight greyhounds: `http://bit.ly/2U3KTZY`

Appendix C: Miscellaneous

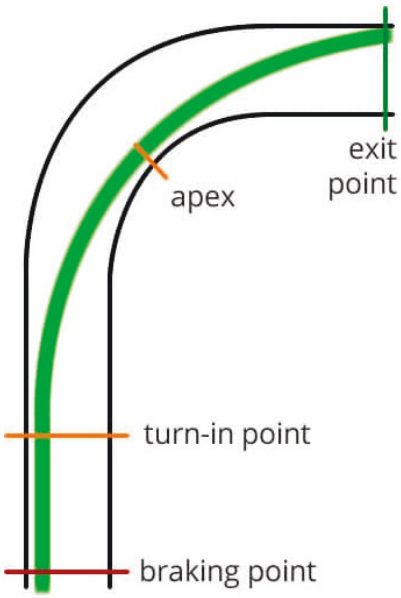

Figure 6.9: A typical racing line for a given corner apex [1].

Table 6.2: The recommended safe minimum radius of curvature of a bend for highway designs when superelevation is the lowest [2].

Design Speed (km/h)	**Minimum curve radius (m)**
15	4
20	8
30	22
40	47
50	86
60	135
70	203
80	280
90	375
100	492

Table 6.3: Expected length of a spiral curve transition [2].

Design Speed (km/h)	**Spiral length (m)**
20	11
30	17
40	22
50	28
60	33
70	39
80	44
90	50
100	56
110	61
120	67
130	72